ANALYSIS OF A MAGNETICALLY ACTIVE REGENERATOR

by

Gregory R. Gallagher

B.S.M.E., University of Rhode Island

1984

SUBMITTED IN PARTIAL FULFILLMENT
OF THE REQUIREMENTS OF THE
DEGREE OF

MASTER OF SCIENCE
IN MECHANICAL ENGINEERING

at the

MASSACHUSETTS INSTITUTE OF TECHNOLOGY

September 1986

Signature of Author _____
Department of Mechanical Engineering
September 1986

Certified by _____
Yukikazu Iwasa
Thesis Supervisor

Certified by _____
Joseph L. Smith, Jr.
Thesis Supervisor

Accepted by _____
Ain A. Sonin
Chairman, Departmental Committee on Graduate Students

ANALYSIS OF A MAGNETICALLY ACTIVE REGENERATOR

by

Gregory R. Gallagher

Submitted to the Department of Mechanical Engineering
on September 8, 1986 in partial fulfillment of the
requirements for the Degree of Master of Science in
Mechanical Engineering

ABSTRACT

This thesis presents an analysis of the magnetically active regenerator used in the magnetic refrigeration project at the Cryogenic Engineering Laboratory at MIT. The purpose of the project is to evaluate an experimental regenerator operating in a Carnot cycle over the temperature range of 4.2K to 10 K. This thesis examines the performance of the device both analytically and numerically and compares experimental results with those predicted by the analysis.

The paramagnetic salt used in the regenerator was $Gd_3Ga_5O_{12}$ (GGG). As part of the analysis, the experimental magnetization and specific heat data of GGG found in the literature were studied in detail and closed-form expressions were derived. Based on these expressions, an entropy function of GGG was obtained and used for numerical analysis of the system.

Thesis Supervisor: Dr. Yukikazu Iwasa
Title: Senior Research Engineer, Francis Bitter National Magnet Laboratory

Thesis Supervisor: Professor Joseph L. Smith, Jr.
Title: Professor of Mechanical Engineering

Acknowledgments

I would like to thank Dr. Yuki Iwasa and Professor Joseph L. Smith for their support, as well as for their contributions to the work presented in this thesis. I would like to express special thanks to Carl Taussig. It has been a great pleasure to work with him and his contributions to my work and experience at MIT have proven to be invaluable. I am also grateful for the often sought after advice and encouragement from Jim Chafe, Al Kornhauser, Fred Cogswell, and everyone at the Cryogenics Lab. Warm thanks are expressed to Nancy Ferrari, who has managed to put up with me during the worst of times, and whose help in the production of this thesis is warmly appreciated.

This thesis is dedicated to my mother, Lucille Gallagher, who has always given me the love, support, and encouragement to set high standards for myself and to strive for my goals.

Table of Contents

Chapter 1 Introduction

1.1 History of Magnetic Refrigeration

The idea of magnetic cooling was first presented by Giauque and Debye independently in 1926.[1] Their method involves first the isothermal magnetization and then the adiabatic demagnetization of a paramagnetic salt. During the isothermal magnetization, magnetic work is performed on the salt while it is in thermal contact with a reservoir of constant temperature. Thus, heat is driven out of the salt and into the reservoir. Once the salt is magnetized, it is then isolated from the reservoir and demagnetized adiabatically. As work is removed from the salt adiabatically, its temperature decreases. Figure 1.1 illustrates the processes on a T–s diagram, with process 1 being the isothermal magnetization, and process 2 being the adiabatic demagnetization. Giauque and MacDougall experimentally produced temperature swings from 3.5 K to 0.5 K using this cooling method in 1933.[2] It is now common for temperatures as low as 1 mK to be produced through adiabatic demagnetization.

The method of cooling by adiabatic demagnetization is a "one shot process," and any cooling effect is short term. The history of continuous magnetic refrigeration is fairly young. In 1954, Heer, Barnes, and Daunt built a continuous refrigerator that produced 7μW at 0.26 K.[3] Van Geuns proposed a regenerative magnetic Ericcson cycle in 1966 that operates between 4 K and 15 K. His calculated performance showed that this type of cycle should attain 60–70% of the Carnot efficiency.[4]

The majority of magnetic refrigeration research has been performed during the past decade. Lacaze *et al.* constructed a double acting reciprocating magnetic Carnot refrigerator operating between 1.8 K and 4.2 K that provided 0.36 W of refrigeration at 2.1 K with an efficiency of 24% of the Carnot efficiency.[5] After improvements were made on the device, it produced 0.24 W of refrigeration at 2.1 K with an efficiency of 65% of Carnot.[6] Barclay *et al.* constructed a regenerative rotating magnetic refrigerator, which when operating between 4 K and 15 K produced 0.9 W with an efficiency of about 20% of Carnot (ignoring drive motor mechanism

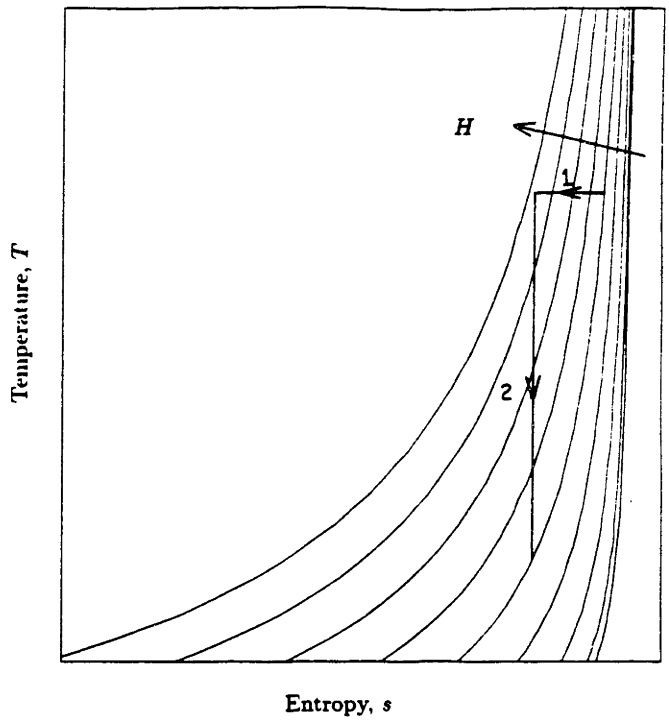

Figure 1.1 Magnetic cooling processes shown on a T-s diagram.

losses).[7] Nakagome *et al.* produced a magnetic refrigerator operating between 4.2 K and 16 K using a pulsed magnet with a stationary salt. Ignoring the large magnet losses, their device operated at 50% of the Carnot efficiency.[8] Brown has demonstrated that with the use of ferri- or ferromagnetic materials, regenerative magnetic refrigeration cycles can operate effectively between 4.2 K and room temperature.[9]

The major loss mechanisms in the devices described above include frictional losses (in the devices with moving parts), seal leakage, heat transfer over finite temperature differences, effects of entrained helium, and magnet losses (for the pulsed magnet).

1.2 Magnetic Materials

For the temperature range of 15 K and below, several surveys of magnetic refrigerants are found in the literature.[10-13] For magnetic refrigerants to be useful below 15 K, their characteristics must include the ability to undergo large work interactions when the applied field is swept, high thermal conductivity, low lattice specific heat capacity, and commercial availability. The category of materials that fulfill these requirements well are the rare-earth garnets, and in particular, gadolinium-gallium-garnet ($Gd_3Ga_5O_{12}$ or GGG). GGG is a paramagnetic salt, and although it does not obey the Curie-Weiss law below 6 K, it does exhibit the important characteristics of magnetic refrigerants.[14] GGG has been chosen as the magnetic refrigerant for the MIT device.

1.3 Thermodynamics of the Magneto-Caloric Effect

Altering the thermodynamic state of a magnetic material by performing heat and magnetic work processes has become known as the "magneto-caloric effect." The "magneto-caloric effect" is essentially the application of the first and second laws of thermodynamics to a magnetic system. The thermodynamic analysis of a magnetic system is shown below.

Consider the magnetic system in Fig. 1.2. It consists of a magnetic material of mass m undergoing a differential magnetic work process and a differential reversible heat process. If a control volume is drawn around the system and an energy balance is performed, the result is

$$dU + dW_{mag} = dQ \tag{1.1}$$

where dU is the differential change in the internal energy of the material, dW_{mag} is the work performed by the material, and dQ is the heat transferred into the material at temperature T. Performing an entropy balance on the control volume for the reversible process gives

$$m\,ds = \frac{dQ}{T} \tag{1.2}$$

where $m\,ds$ is the differential change in the total entropy of the material at temperature T. Substituting Eq. (1.2) into (1.1) and dividing by the mass of the system m results in the equation

$$du = T\,ds - dw_{mag} \tag{1.3}$$

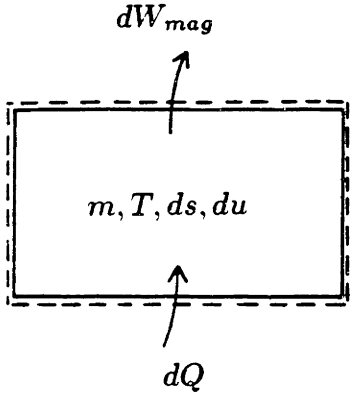

Fig. 1.2. Magnetic material undergoing differential work and heat processes.

The specific differential magnetic work performed by a magnetic material is

$$dw_{mag} = -\mu_0 v H\,d\mathcal{M} \tag{1.4}$$

where μ_0 is the permeability of free space, v is the specific volume of the magnetic material, H is the applied field, and $d\mathcal{M}$ is the differential change in magnetization. Substituting (1.4) into (1.3) gives

$$du = T\,ds + \mu_0 v H\,d\mathcal{M} \tag{1.5}$$

which is the combined first and second law for a magnetic system.

Equation (1.5) is very similar to its corresponding equation in a p-v system,

$$du = T\,ds - p\,dv \tag{1.6}$$

where $p\,dv$ is analogous to $-\mu_0 v H\,d\mathcal{M}$. The fundamental difference between Eqs. (1.5) and (1.6) is the method by which work enters and exits the system. It is the efficiency and simplicity of the magnetic cooling process at low temperatures that makes it attractive.

1.4 Paramagnetic Materials as Refrigerants

Equation (1.4) shows that in order to perform a magnetic work interaction, the magnetization of the material must change in some applied field. In practice, we alter the applied field to change the magnetization. Materials able to attain high degrees of magnetic ordering when a field is applied and to then return to a state of no magnetization when the field is removed (no residual magnetization) are ideal for magnetic refrigeration. At low temperatures (below 20 K), paramagnetic materials such as GGG and gadolinium sulphate octahydrate ($Gd_2(SO_4)_3 \cdot 8H_2O$)) behave in this manner. Ideally, paramagnetic materials have a magnetization given by the Curie-Weiss law

$$\mathcal{M} = \frac{CH}{T + \theta} \tag{1.7}$$

where C is the Curie constant and θ is the Curie temperature. C and θ are material properties.

Both GGG and gadolinium sulphate octahydrate have been used as magnetic refrigerants and both obey the Curie-Weiss law fairly well at temperatures above 6 K and at reasonably low fields (< 4 T). While equation (1.7) suggests that $\mathcal{M}$ increases infinitely as the ratio $H/(T + \theta)$ increases, real paramagnetic materials begin to saturate when the ratio gets too large. Once all of the magnetic dipoles in the material are aligned, no further magnetic work can be performed on the material.

1.5 Magnetic Refrigeration with Ideal Paramagnetic Materials

The magnetic cooling process of Section 1.1 is a "one-shot" process. While low temperatures are achieved through the isothermal magnetization followed by the isentropic demagnetization, the process is not very useful for maintaining cold temperatures. Instead, a refrigeration cycle composed of several processes is required. The magnetic cooling process described in section 1.1 is essentially half of a magnetic Carnot cycle. By adding an isothermal demagnetization process and an

isentropic magnetization process to the isothermal magnetization and the isentropic demagnetization processes, a complete Carnot cycle can be created.

Figure 1.3 shows a Carnot cycle on an H-$\mathcal{M}$ diagram constructed from a Curie-Weiss law. Process 1 is an isentropic demagnetization, process 2 is an isothermal demagnetization, process 3 is an isentropic magnetization, and process 4 is an isothermal magnetization. Because the magnetic work done per cycle by the system is $w_{cycle} = -\oint \mu_0 v H \, d\mathcal{M}$, the refrigeration cycle moves in a clockwise direction.

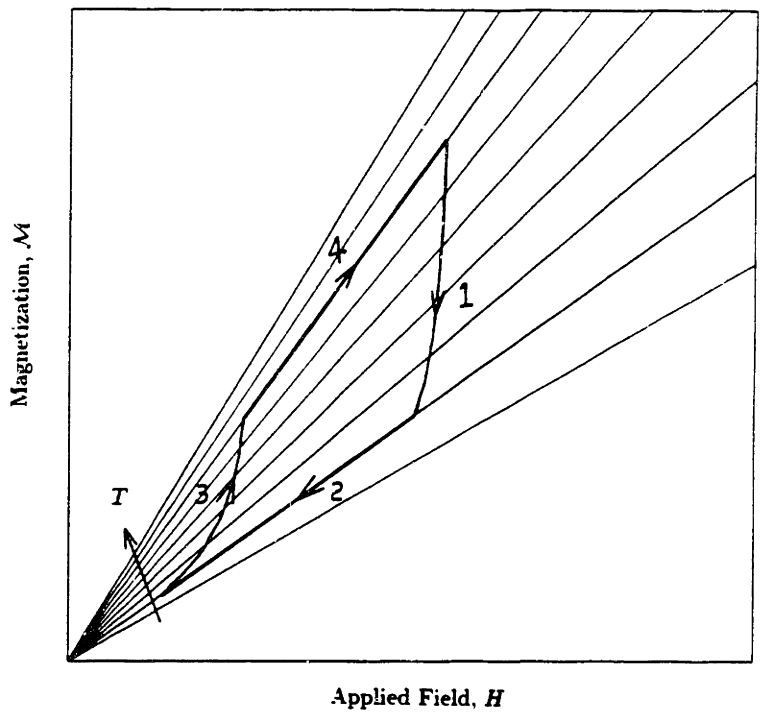

Fig. 1.3. Carnot cycle on an H-$\mathcal{M}$ diagram for a Curie-Weiss material.

The same cycle can be shown on a T-s diagram, but first it is necessary to obtain an entropy function of temperature and applied field. If we assume a function $s = s(T, H)$ and take its exact differential, we get

$$ds = \left(\frac{\partial s}{\partial T}\right)_H dT + \left(\frac{\partial s}{\partial H}\right)_T dH \tag{1.8}$$

The specific heat at constant applied field is defined as

$$c_H \equiv T\left(\frac{\partial s}{\partial T}\right)_H \tag{1.9}$$

If the Maxwell relations for a magnetic system are derived (Appendix A), one is found with the quantity $(\partial s/\partial H)_T$. The relation is

$$\left(\frac{\partial s}{\partial H}\right)_T = \mu_0 v\left(\frac{\partial \mathcal{M}}{\partial T}\right)_H \tag{1.10}$$

Substituting Eqs. (1.9) and (1.10) into Eq. (1.8) gives

$$ds = \frac{c_H(T)}{T}\,dT + \mu_0 v\left(\frac{\partial \mathcal{M}}{\partial T}\right)_H dH \tag{1.11}$$

For a Curie-Weiss material, $(\partial M/\partial T)_H$ is obtained by differentiating Eq. (1.7). Substituting the result into Eq. (1.11) gives

$$ds = \frac{c_H}{T}\,dT - \frac{\mu_0 v C H}{(T+\theta)^2}\,dH \tag{1.12}$$

Given the specific heat as a function of temperature at the zero field (obtained from experimental data), Eq. (1.12) can be integrated along the zero field and then along any constant temperature path to obtain the entropy at any value of T and H. The value of the entropy $s(T,H)$ is

$$s(T,H) = s_0 + \int_{T_0}^{T} \frac{c_{H=0}}{T}\,dT - \frac{\mu_0 v C H^2}{2(T+\theta)^2} \tag{1.13}$$

where s_0 is the reference entropy at $T = T_0$ and $H = 0$. The T-s diagram that results from Eq. (1.13) resembles that of Fig. 1.4.

A Carnot cycle is also shown in the T-s diagram of Fig. 1.4. Process 1 is an isentropic demagnetization, process 2 is an isothermal demagnetization, process 3 is an isentropic magnetization, and process 4 is an isothermal magnetization. The work per cycle done by the system is $\oint T\,ds$.

The shape of the magnetic refrigeration cycle is arbitrary. A Carnot cycle was shown here, but any type of cycle can be devised, provided it is possible to produce the heat and work processes necessary for the individual processes that compose the cycle.

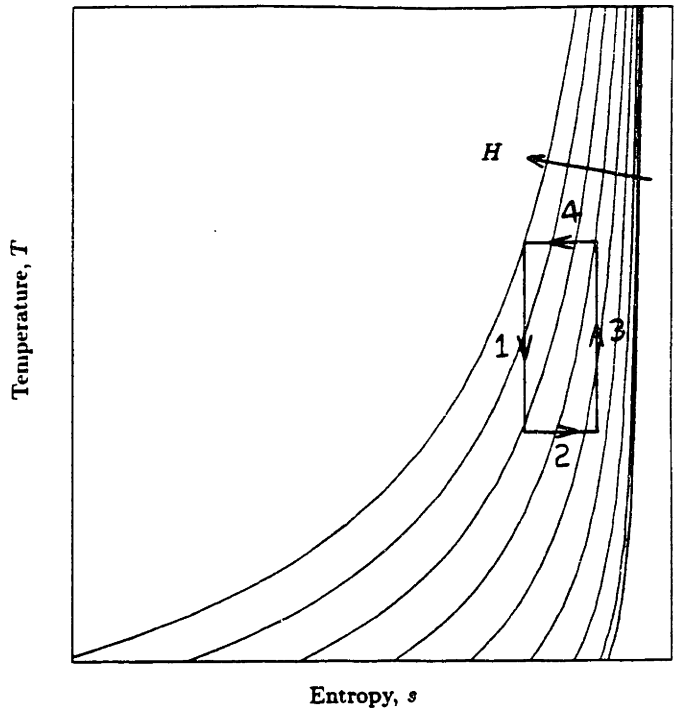

Fig. 1.4. Carnot cycle on a T-s diagram for a Curie-Weiss material.

Chapter 2 Magnetically Active Regenerator

2.1 Experimental Device at MIT

The device implemented at the Cryogenic Engineering Laboratory at MIT is being used to investigate a regenerative Carnot cycle, operating between a 4.2-K reservoir and a 10-K reservoir. The regenerator is composed of the paramagnetic material gadolinium gallium garnet (GGG), and has been given the name "magnetically active regenerator," because work enters and exits the system via magnetizations and demagnetizations of the regenerator core material. Thus the regenerator is active, unlike most passive regenerators which work only as capacitive elements. GGG is used because it undergoes large changes in magnetization at the applied fields and temperatures chosen for the cycle. The magnetic flux densities chosen for the cycle range from 0 to 4 T.

Figure 2.1 shows a schematic of the device. It consists of a displacer, a 10-K temperature controller (hot reservoir), the regenerator, a 4.2-K temperature controller (cold reservoir), a pressure compensator, and a superconducting magnet. The working fluid is 3 atm supercritical helium, and the pressure is held constant by the compensator, which consists of a weighted free piston. The flow is driven by the displacer, and the temperature of the helium entering the hot and cold ends of the regenerator is maintained at 10 K and 4.2 K, respectively, by the temperature controllers. The regenerator is housed in a vacuum-insulated stainless-steel tube that rests inside the bore of an AC superconducting magnet. The magnet and regenerator housing are placed in a 4.2-K liquid helium bath.

The regenerator core was designed by Taussig[15] to minimize the losses resulting from axial conduction, fluid friction, irreversible heat transfer, and helium entrainment, within the constraints imposed by manufacturing limitations. The resulting design is shown in Fig. 2.2. The core consists of 120 cylindrical disks, each having a gross diameter of 38 mm and a thickness of 2.5 mm. The stack of GGG disks is laminated together with a thin layer (0.1 mm) of epoxy, which serves as a thermal barrier to axial conduction. The laminated stack is cut into longitudinal strips

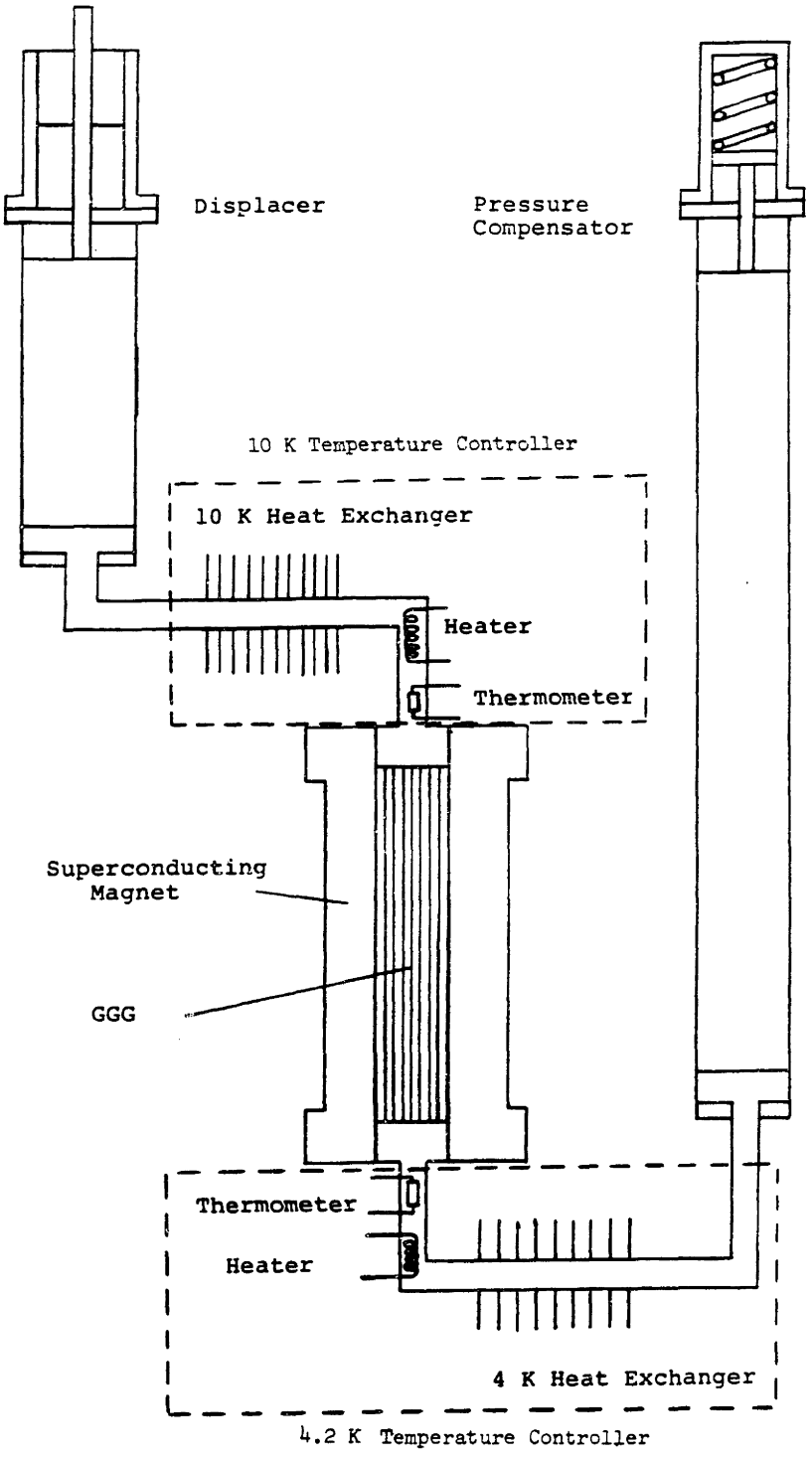

Fig. 2.1. Schematic of the MIT device.

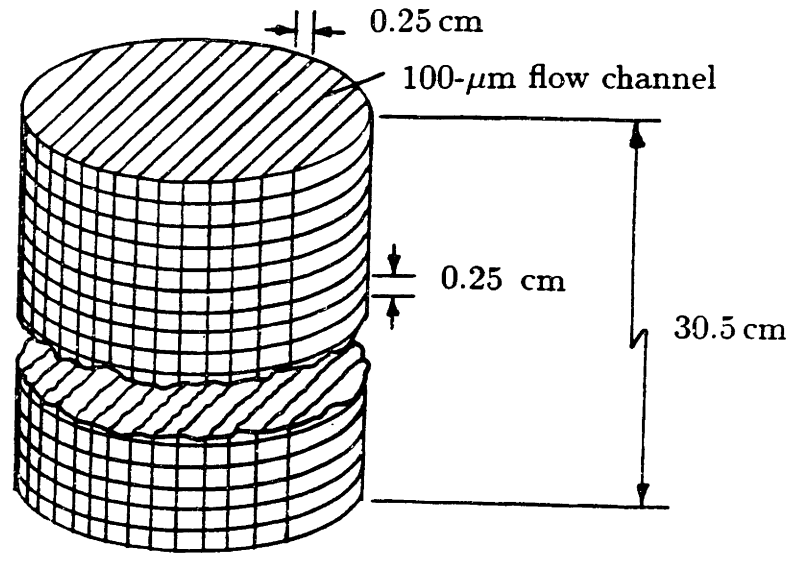

Fig. 2.2. Regenerator core design.

2.5 mm wide, and reassembled with 100-μm spacers between them to form the axial flow passages. The entire assembly is potted into the vacuum-insulated housing that isolates the core from the 4.2-K bath and the superconducting magnet.

A superconducting solenoid with an axially uniform field was built for the initial experiments. It has a 38 mm bore and an active length of 300 mm over which the field is uniform within 5%. The magnet is constructed from NbTi superconductor and can be swept with a triangular waveform to generate a dB/dt sweep rate of 0.5 $\mathrm{T\,s^{-1}}$ between 1 and 4 T.

2.2 Analysis of a Regenerator with Ideal Properties

The Carnot cycle for a reversible regenerator with ideal helium and regenerator thermodynamic properties begins with an isothermal magnetization flow process, where work is performed on the regenerator core while helium is forced to flow from the cold reservoir to the hot reservoir. During the magnetization flow process, the

regenerator transfers heat to the helium flow by forced convection. The temperature of the helium increases as it flows through the regenerator until the helium emerges out of the hot end with a temperature higher than that of the reservoir, thus providing heat rejection. For the ideal magnetization flow process, the temperature profile in the regenerator remains fixed.

The second process is an isentropic demagnetization. During this process, the helium flow is stopped while the core is adiabatically demagnetized. Because work is removed from the system during this process, and because there are no heat interactions between the GGG and the helium (assuming no entrainment effects), the temperature profile of the regenerator shifts downward. Ideally, this process is reversible. The regenerator temperature profile at the end of the process assumes that of the isothermal demagnetization flow process that follows.

The isothermal demagnetization process is similar to the isothermal magnetization process, except that the helium flows from the hot end to the cold end of the regenerator, and the field is swept in the opposite direction. The helium transfers heat to the regenerator in the process and emerges out of the cold end at a temperature less than that of the cold reservoir.

An isentropic magnetization process occurs next and closes the cycle. In this process, the flow is stopped while the core is magnetized. As work is done on the regenerator, its temperature profile shifts to a higher value. The temperature profile at the end of the process is that of the next isothermal magnetization process.

The ideal regenerative cycle can be identified as a series of Carnot cycle refrigerators as shown in Fig. 2.3. In one cycle, a mass of helium, M_{he}, flows from the cold reservoir at temperature T_{cold}, and is heated as it flows across the tops of the heat pumps until it reaches the hot reservoir with a temperature greater than T_{hot}. An equal mass of helium flows from the hot reservoir and is cooled as it passes along the bottom of the heat pumps until it reaches the cold reservoir with a temperature less than T_{cold}, thus providing refrigeration to the cold bath. Figure 2.4 shows idealized temperature profiles for the cycle. The temperature distribution $T_h(x)$ is that of the stream being heated and $T_c(x)$ is that of the stream being cooled. Figure 2.5

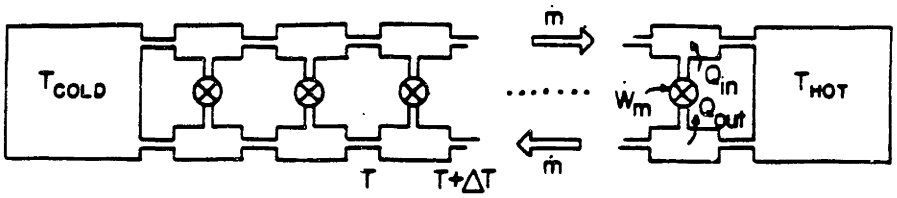

Fig. 2.3 Cascaded series of Carnot cycle magnetic refrigerators.

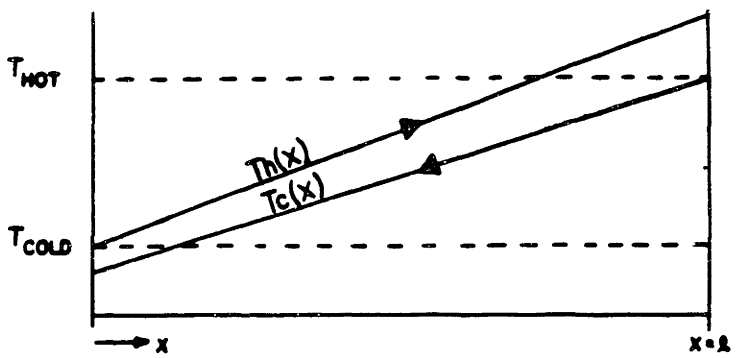

Fig. 2.4 Ideal temperature profiles.

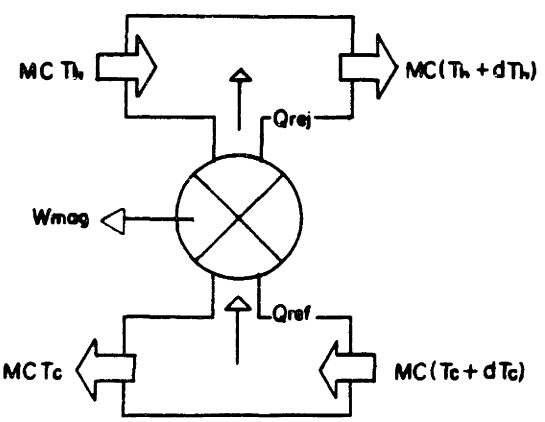

Fig. 2.5 Single heat pump removed from an arbitrary location.

shows a single heat pump removed from an arbitrary location.

The energy balance for the single Carnot refrigerator of Fig. 2.5 is:

$$dW_{mag} = dQ_{ref} - dQ_{rej} \tag{2.1}$$

where

$$dQ_{rej} = M_{he} c_{he}\, dT_h \tag{2.2}$$

and

$$dQ_{ref} = M_{he} c_{he}\, dT_c \tag{2.3}$$

dW_{mag} is the magnetic work done by the salt; c_{he} is the specific heat capacity of helium, and is assumed constant. The entropy balance, assuming a reversible process is

$$\frac{c_{he}\, dT_h}{T_h} = \frac{c_{he}\, dT_c}{T_c} \tag{2.4}$$

Integration of Eq. (2.4) gives

$$\frac{T_h(x)}{T_c(x)} = \text{constant} = k \tag{2.5}$$

For a reversible process with constant specific heat, the temperatures of the heated and cooled streams must be proportional at all locations. Equation (2.5) does not specify the shape of the temperature profiles. They are determined by the magnetic work input as a function of location. If the temperature distributions are specified *a priori*, then the magnetic field profiles in space and time can be determined by an energy balance.

The overall efficiency of the ideal cycle is measured by the coefficient of performance ($C.O.P.$), defined as the refrigeration per cycle divided by the total work into a cycle.

$$C.O.P. = -\frac{Q_{ref}}{W_{mag}} = \frac{Q_{ref}}{Q_{rej} - Q_{ref}} \tag{2.6}$$

The refrigeration per cycle, Q_{ref}, can be written in terms of the enthalpy output of the cold reservoir.

$$\begin{aligned} Q_{ref} &= M_{he} c_{he} (T_{cold} - T_c(x = 0)) \\ &= M_{he} c_{he} \left(1 - \frac{1}{k}\right) T_{cold} \end{aligned} \tag{2.7}$$

Similarly, the heat rejected, Q_{rej}, can be written as

$$\begin{aligned} Q_{rej} &= M_{he} c_{he} (T_h(x = L) - T_{hot}) \\ &= M_{he} c_{he} (k - 1) T_{hot} \end{aligned} \tag{2.8}$$

The $C.O.P.$ can then be expressed as

$$C.O.P. = \frac{1}{k(T_{hot}/T_{cold}) - 1} \tag{2.9}$$

This quantity differs from the $C.O.P.$ of an ideal Carnot cycle by the presence of k in the denominator. As the value of k increases, the the refrigeration power increases. However, the efficiency decreases because of the irreversibility associated with thermal mixing in the reservoirs.

Chapter 3 Analysis of the Regenerator with Actual Properties

This chapter contains a derivation of the differential equations describing the flow and nonflow processes of the regenerator, considering the actual thermodynamic properties of GGG and 3 atm supercritical helium. The flow and nonflow processes are treated separately, and each is preceeded by a list of assumptions and variables used in the derivation.

3.1 Analysis of the Flow Processes

The assumptions used in the derivation of the governing equations for the flow processes (isothermal processes) are as follows:

1) The salt core is divided into 120 segments (disks), with one uniform temperature throughout each segment.
2) The thermal barriers between segments have zero conductivity; there is no conduction between segments.
3) All heat interactions in the regenerator are between the GGG segments and the supercritical helium; there is zero heat leak through the regenerator casing.
4) There is no axial heat conduction through the supercritical helium.
5) There are no pressure losses in the regenerator.
6) Magnetic work interactions with GGG are reversible.

Assumptions 1, 2, and 4 are discussed in Appendix C.

The following variables, given in SI units, are used in the analysis:

x: Spatial variable in the axial direction, (m).

t: Time variable, (s).

L: Axial length of a regenerator segment, (m).

v: Specific volume of GGG, ($m^3\,kg^{-1}$).

M: Mass of a single regenerator segment, (kg).

V_{seg}: Volume of a regenerator segment, (m^3).

$\dot{m}$: Mass flow rate of supercritical helium through the regenerator, ($kg\,s^{-1}$).

m_{he} or $m_{He}(x,t)$: Mass of entrained helium in a flow channel, (kg).

ρ_{He}: Density of entrained helium in a flow channel, ($\mathrm{kg\,m^{-3}}$)

T_s or $T_s(t)$: Temperature of a regenerator segment, (K).

T_{in} or $T_{in}(t)$: Temperature of the helium entering a regenerator segment, (K).

T_{out} or $T_{out}(t)$: Temperature of the helium exiting a regenerator segment, (K).

u_s or $u_s(t)$: Specific internal energy of the regenerator segment, ($\mathrm{J\,kg^{-1}}$).

h_{in} or $h_{in}(t)$: Specific enthalpy of the entering helium, ($\mathrm{J\,kg^{-1}}$).

h_{out} or $h_{out}(t)$: Specific enthalpy of the exiting helium, ($\mathrm{J\,kg^{-1}}$).

s_s or $s_s(t)$: Specific entropy of a regenerator segment, ($\mathrm{J\,kg^{-1}\,K^{-1}}$).

c_p: Specific heat capacity at constant pressure of helium, ($\mathrm{J\,kg^{-1}}$).

$\dot{Q}$: Heat flux from the regenerator to the helium in a regenerator segment, (W).

W_{mag}: Magnetic work done by a regenerator segment, (W).

w_{mag}: Specific magnetic work done by a regenerator segment, ($\mathrm{W\,kg^{-1}}$).

T_{He} or $T_{He}(x,t)$: Helium temperature at location x and time t, (K).

h_{He} or $h_{He}(x,t)$: Specific enthalpy of helium at location x and time t, ($\mathrm{J\,kg^{-1}}$).

u_{He} or $u_{He}(x,t)$: Specific internal energy of helium at location x and time t.

c_v of $c_v(x,t)$: Specific heat capacity of constant volume of helium at x and t.

$\hbar$: Heat transfer coefficient, ($\mathrm{W\,m^{-2}\,K^{-1}}$).

k_{He}: Thermal conductivity of helium, ($\mathrm{W\,m^{-1}\,K^{-1}}$).

P: Heat transfer area per unit length, (m).

H: Magnetic field intensity, ($\mathrm{A\,m^{-1}}$). (Magnetic flux density, B is in T.)*

$\mathcal{M}$: Magnetization, ($\mathrm{A\,m^{-1}}$).*

Figure 3.1 shows a simplified view of a regenerator segment. Helium flows in and out of the segment while it undergoes a reversible work process.

---

* In SI units, H and $\mathcal{M}$ have units of $\mathrm{A\,m^{-1}}$, and the magnetic flux density B (T) is defined by $B = \mu_0(H + \mathcal{M})$. μ_0 is the permeability of free space ($4\pi\times10^{-7}$ $\mathrm{H\,m^{-1}}$). In electromagnetic units (emu), B (Gauss) is defined by $B = H + 4\pi\mathcal{M}$, where H has units of Oersted, while $\mathcal{M}$ has units of magnetic moment $\mathrm{cm^{-3}}$. Oersted, magnetic moment $\mathrm{cm^{-3}}$, and Gauss are all equivalent to $\mathrm{g^{1/2}\,cm^{-1/2}\,s^{-1}}$. In both sets of units there is a tendency to use H and B interchangeably. It is very common to see the field H expressed in T when the correct units are $\mathrm{A\,m^{-1}}$. Note that in air, $B \approx \mu_0 H$ (in SI units).

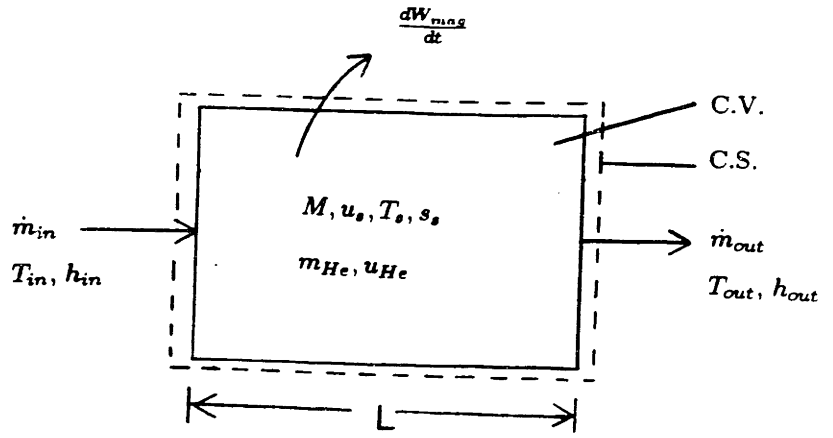

Fig. 3.1. Simplified view of a single regenerator segment.

From assumption 1, the regenerator segment temperature T_s is a function of time only. The segment has mass M, entropy s_s, and internal energy u_s. Helium enters with a temperature of T_{in} and an enthalpy of h_{in}, and exits with a temperature of T_{out} and an enthalpy of h_{out}. If a control volume is drawn around the regenerator segment of Fig. 3.1 and an energy balance is performed, the resulting equation is

$$\frac{d}{dt}\int_0^L \left[\left(\frac{\partial m_{He}}{\partial x}dx\right)u_{He}\right] + \dot{m}_{out}h_{out} - \dot{m}_{in}h_{in} + M\frac{du_s}{dt} + \frac{dW_{mag}}{dt} = 0 \qquad (3.1)$$

The first term of Eq. (3.1) represents the rate at which the internal energy of the control volume changes with time.

It is assumed that the rate of change of helium mass per unit time in a segment is much smaller than the mass flow rate of helium entering a segment; i.e., $\left|\frac{d}{dt}\int_0^L [(\frac{\partial m_{He}}{dx}dx)u_{He}]\right| \ll \dot{m}_{in}$. This assumption is reasonable when the large mass flow rates and small porosity of the regenerator are considered. Equation (3.1) is simplified if the helium mass flow rate is assumed to be a function of time only; i.e., $\dot{m}_{in} = \dot{m}_{out} = \dot{m}(t)$. Substituting $\dot{m} = \dot{m}_{in} = \dot{m}_{out}$ into Eq. (3.1) gives

$$\frac{d}{dt}\int_0^L \left[\left(\frac{\partial m_{He}}{\partial x}dx\right)u_{He}\right] + \dot{m}(h_{out} - h_{in}) + M\frac{du_s}{dt} + \frac{dW_{mag}}{dt} = 0 \qquad (3.2)$$

If $\left|\frac{d}{dt}\int_0^L[(\frac{\partial m_{He}}{dx}dx)u_{He}]\right| \neq 0$, but is small compared to $\dot{m}$, then continuity is slightly violated. The constant mass flow assumption should be very accurate in general, and it greatly simplifies the analysis by eliminating the need to solve the continuity equation.

For the sake of simplicity, the quantity $\int_0^L(\frac{\partial m_{He}}{\partial x}dx)u_{He}$ can be roughly approximated by assuming that the helium properties do not change with x. This approximation gives the result, $\int_0^L(\frac{\partial m_{He}}{\partial x}dx)u_{He} \approx \epsilon\rho_{He}V_{seg}c_vT_{in}$, where ϵ is the regenerator porosity, ρ_{He} is the helium density, V_{seg} is the volume of a segment, c_v is the helium specific heat capacity at constant volume, and T_{in} is the temperature of the helium entering a segment. If we also assume that $\frac{\partial\rho_{He}}{\partial t} = \frac{\partial c_v}{\partial t} = 0$, then $\frac{d}{dt}\left[\int_0^L(\frac{\partial m_{He}}{\partial x}dx)u_{He}\right] \approx \epsilon\rho_{He}V_{seg}c_v\frac{dT_{in}}{dt}$. Finally, if we assume that $\frac{dT_{He}}{dt} \approx \frac{dT_s}{dt}$, then $\frac{d}{dt}\left[\int_0^L(\frac{\partial m_{He}}{\partial x}dx)u_{He}\right] \approx \epsilon\rho_{He}V_{seg}c_v\frac{dT_s}{dt}$

The differential magnetic work per unit mass done by a regenerator segment is

$$dw_{mag} = -\mu_0 v H\, d\mathcal{M} \tag{3.3}$$

The combined first and second law for a control system consisting of a magnetic material undergoing a differential reversible heat and magnetic work process was derived in Chapter 2, and is

$$\begin{aligned} T_s\, ds_s &= du_s + dw_{mag} \\ &= du_s - \mu_0 v H\, d\mathcal{M} \end{aligned} \tag{3.4}$$

Likewise, the combined first and second law per unit time for the heat and reversible magnetic work process is

$$T_s\frac{ds_s}{dt} = \frac{du_s}{dt} + \frac{dw_{mag}}{dt} \tag{3.5}$$

Combining Eqs. (3.2) and (3.5) and substituting $\epsilon\rho_{He}V_{seg}c_v\frac{dT_s}{dt}$ for the quantity $\frac{d}{dt}\left[\int_0^L(\frac{\partial m_{He}}{\partial x}dx)u_{He}\right]$ gives

$$\epsilon\rho_{He}V_{seg}c_v\frac{dT_s}{dt} + \dot{m}(h_{out} - h_{in}) + MT_s\frac{ds_s}{dt} = 0 \tag{3.6}$$

Figure 3.2 shows a regenerator segment flow passage. (For simplicity, the segment in Fig. 3.2 shows only one flow passage.) The convective heat transfer from

the GGG to the helium is given by

$$\frac{\partial \dot{Q}}{\partial x} = \hbar P(T_s - T_{He}) \tag{3.7}$$

where $\hbar$ is the heat transfer coefficient and P is the surface area per unit length. The heat transfer process is modeled as forced convection between infinite plates with a laminar flow. Rohsenow[16] gives as a heat transfer coefficient

$$\hbar = \frac{3.8\, k_{He}}{d} \tag{3.8}$$

where k_{He} is the thermal conductivity of helium and d is the distance between the plates (the width of the flow channels).

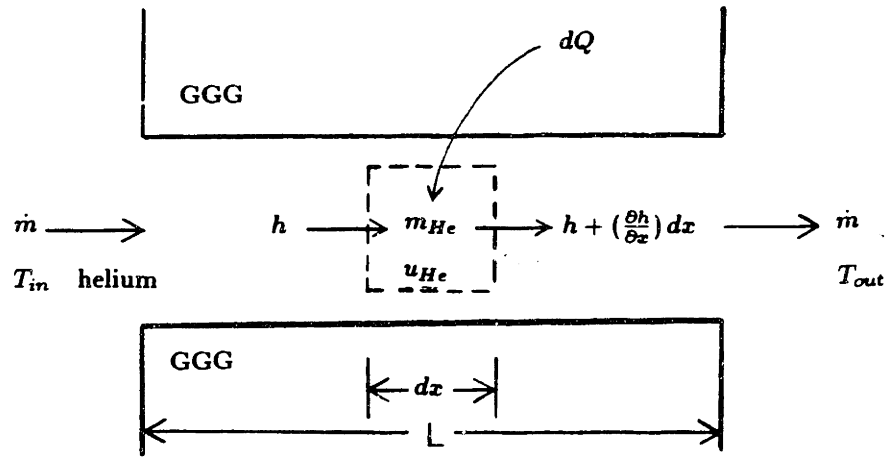

Fig. 3.2. A differential slice of a regenerator flow channel.

A control volume containing a differential slice of the segment flow channel is shown in Fig. 3.2. An energy balance of the control volume gives

$$\frac{\partial \dot{Q}}{dx} dx = \dot{m} \frac{\partial h_{He}}{dx} dx + \frac{\partial}{\partial t}\left[\left(\frac{\partial m_{He}}{\partial x} dx\right) u_{He}\right] \tag{3.9}$$

It is assumed that second term on the right-hand side of Eq. (3.9) is much smaller than the first term. (It is zero for the isothermal process.) Neglecting the second

term reduces Eq. (3.9) to a much simpler equation,

$$\frac{\partial \dot{Q}}{\partial x} = \dot{m}\frac{\partial h_{He}}{\partial x} = \dot{m}\frac{\partial (c_p T_{He})}{\partial x} \tag{3.10}$$

Equating (3.7) and (3.10) gives

$$\dot{m}\frac{\partial (c_p T_{He})}{\partial x} = \hbar P(T_s - T_{He}) \tag{3.11}$$

Since it was assumed that $\partial T_s/\partial x = 0$ for any particular regenerator segment, Eq. (3.11) can be integrated easily over a regenerator segment. If c_p is assumed constant over the interval $0 \leq x \leq L$, the integral of Eq. (3.11) is

$$T_{out}(t) = T_s(t) + [T_{in}(t) - T_s(t)]e^{-(\hbar PL/\dot{m}c_p)} \tag{3.12}$$

Equation (3.12) gives the exiting helium temperature at any instant of time as a function of the entering helium temperature, the GGG temperature, and the heat transfer rate. Note that the equation allows for the exiting helium temperature T_{out} to change instantaneously with time.

The governing equations for the magnetization and demagnetization flow processes are Eqs. (3.6), (3.8), and (3.12) along with the following equations

$$s_s = s_s(T_s, H) \tag{3.13}$$

$$h_{He} = h_{He}(p = 3 \text{ atm}, T_{He}) \tag{3.14}$$

$$k_{He} = k_{He}(p = 3 \text{ atm}, T_{He}) \tag{3.15}$$

$$c_p = c_p(p = 3 \text{ atm}, T_{He}) \tag{3.16}$$

$$H = H(t) \tag{3.17}$$

Equation (3.13) contains the necessary GGG thermodynamic properties, while Eqs. (3.14)–(3.16) contain the necessary helium thermodynamic and transport properties. Equation (3.17) is simply the applied field as a function of time. The superconducting magnet in the device was designed such that, for the magnetization processes,

$$\mu_0 \frac{dH}{dt} = 0.5 \text{ T s}^{-1} \tag{3.18}$$

and during the demagnetization processes,

$$\mu_0 \frac{dH}{dt} = -0.5 \text{ T s}^{-1} \tag{3.19}$$

Equation (3.6) is much simpler to solve if its derivative ds_s/dt is expanded using the chain rule:

$$\frac{ds_s}{dt} = \left(\frac{\partial s_s}{\partial T_s}\right)_H \frac{dT_s}{dt} + \left(\frac{\partial s_s}{\partial H}\right)_{T_s} \frac{dH}{dt} \tag{3.20}$$

Combining Eqs. (3.6) and (3.20), we obtain the first-order differential equation,

$$\frac{dT_s}{dt} = -\left[\frac{\dot{m}(h_{out} - h_{in}) + MT_s\left(\frac{\partial s_s}{\partial H}\right)_{T_s} \frac{dH}{dt}}{\epsilon\rho_{He}V_{seg}c_v + MT_s\left(\frac{\partial s_s}{\partial T_s}\right)_H}\right] \tag{3.21}$$

The partial derivatives $(\partial s_s/\partial H)_{T_s}$ and $(\partial s_s/\partial T_s)_H$ are the derivatives of Eq. (3.13), and are both functions of H and T_s; dH/dt is the derivative of Eq. (3.17). Equation (3.21) describes the diffusion of heat into and out of a regenerator segment in the presence of a changing field. It has one boundary condition, which is the temperature of the helium entering the regenerator segment. Namely,

$$T_{in} = T_{in}(t) \tag{3.22}$$

In order to solve the unsteady flow process, T_s must have an initial condition,

$$T_s(t = 0) = T_{s,initial} \tag{3.23}$$

A summary of the equations necessary to solve the regenerator magnetization and demagnetization flow processes is shown below.

$$\frac{dT_s}{dt} = -\left[\frac{\dot{m}(h_{out} - h_{in}) + MT_s\left(\frac{\partial s_s}{\partial H}\right)_{T_s} \frac{dH}{dt}}{\epsilon\rho_{He}V_{seg}c_v + MT_s\left(\frac{\partial s_s}{\partial T_s}\right)_H}\right] \tag{3.21}$$

$$T_{in} = T_{in}(t) \tag{3.22}$$

$$T_s(t = 0) = T_{s,initial} \tag{3.23}$$

$$H = H(t) \tag{3.17}$$

$$T_{out} = T_s + (T_{in} - T_s)\epsilon^{-(\hbar PL/\dot{m}c_p)} \tag{3.12}$$

$$\hbar = \frac{3.8\, k_{He}}{d} \tag{3.8}$$

$$s_s = s_s(T_s, H) \tag{3.13}$$

$$h_{He} = h_{He}(p = 3 \text{ atm}, T_{He}) \tag{3.14}$$

$$k_{He} = k_{He}(p = 3 \text{ atm}, T_{He}) \tag{3.15}$$

$$c_p = c_p(p = 3 \text{ atm}, T_{He}) \tag{3.16}$$

The quantities that are known include $\dot{m}$, M, P, L, and d. The above equations are sufficient to solve $T_s(t)$.

Computation of $T_s(t)$ for each of the 120 segments begins by solving T_s for Segment 1, bounded at one of the reservoirs; i.e., $T_{in} = T_{reservoir}$, and proceeding onto Segment 2 with its boundary condition being the exiting helium state of Segment 1, and so forth, until T_s is solved for all 120 segments. During the magnetization flow process, the flow originates from the cold reservoir (4.2 K) and the applied field sweep is positive ($\mu_0\, dH/dt = +0.5\ \mathrm{T\,s^{-1}}$). During the demagnetization flow process, the flow originates from the hot reservoir (10 K) and the applied field sweep is negative ($\mu_0\, dH/dt = -0.5\ \mathrm{T\,s^{-1}}$).

3.2 Analysis of the Nonflow Processes

The assumptions used in the derivation of the governing equations for the nonflow processes (adiabatic processes) are as follows:

1) The salt core is divided into 120 segments (disks), with one uniform temperature throughout each segment.
2) The thermal barriers between segments have zero conductivity; there is no conduction between segments.
3) All heat interactions in the regenerator are between the GGG segments and the supercritical helium; there is zero heat leak through the regenerator casing.
4) There is no axial heat conduction through the supercritical helium.

5) Magnetic work interactions with GGG are reversible.

Assumptions 1, 2, and 4 are discussed in Appendix C.

The following variables, given in SI units, are used in the analysis:

x: Spatial variable in the axial direction, (m).

t: Time variable, (s).

L: Axial length of a regenerator segment, (m).

M: Mass of a single regenerator segment, (kg).

m_{He}: Mass of entrained helium in a single regenerator segment, (kg).

T_s or $T_s(t)$: Temperature of a regenerator segment, (K).

T_{He} or $T_{He}(t)$: Entrained helium temperature for a single regenerator segment, (K).

s_s or $s_s(t)$: Specific entropy of the GGG in a regenerator segment, ($\mathrm{J\,kg^{-1}\,K^{-1}}$).

s_{He} or $s_{He}(t)$: Specific entropy of entrained helium in a segment, ($\mathrm{J\,kg^{-1}\,K^{-1}}$).

w_{mag}: Specific magnetic work done by a regenerator segment, ($\mathrm{W\,kg^{-1}}$).

ϵ: Regenerator porosity (fraction of entrained helium by volume), (dimensionless).

ρ_{He}: Density of helium, ($\mathrm{kg\,m^{-3}}$).

V_{seg}: Volume of a regenerator segment, ($\mathrm{m^3}$).

A simple model of the adiabatic nonflow processes assumes a reversible process in which there is thermal equilibrium between the GGG and helium; i.e., $T_s(t) = T_{He}(x,t)$ for a single segment. This assumption allows the nonflow process to be solved simply as a relaxation process. Figure 3.3 is a simplified view of a regenerator segment, again showing one flow channel for reasons of simplicity. If a control volume is drawn around the segment shown in Fig. 3.3 and an entropy balance is performed for a nonflow process, the result is

$$\left(\frac{dS}{dt}\right)_{C.V.} = M\,\frac{ds_s}{dt} + \frac{d}{dt}(m_{He}s_{He}) = 0 \qquad (3.24)$$

where $M\frac{ds_s}{dt}$ is rate at which the entropy of the GGG segment changes with time, and $\frac{d}{dt}(m_{He}s_{He})$ is the rate at which the entropy of the entrained helium in a segment changes with time.

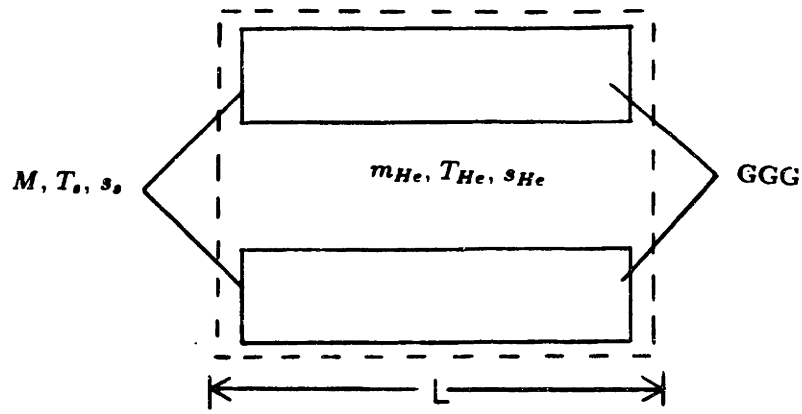

Fig. 3.3. Simplified view of a regenerator segment during the nonflow process.

If the helium mass in a segment is assumed to remain constant throughout the nonflow process (for reasons of simplicity,) then we can integrate Eq. (3.24) over the nonflow process time interval. The result is

$$\begin{aligned} Ms_s(t_{ad,i}) + m_{He}s_{He}(t_{ad,i}) &= Ms_s(t_{ad,f}) + m_{He}s_{He}(t_{ad,f}) \\ &= \text{constant} \end{aligned} \tag{3.25}$$

where $t_{ad,i}$ is the time at the start of the process and $t_{ad,f}$ is the time at the end of the process. The total entropy of a segment at the end of the nonflow process is equal to the total entropy at the start of the process. m_{He} is approximated by the relation

$$m_{He} = \epsilon \rho_{He} V_{seg} \tag{3.26}$$

where ϵ is the porosity of the regenerator, ρ_{He} is the density of the helium at the start of the process, and V_{seg} is the volume of a regenerator segment. Equations (3.25) and (3.26) can be solved to determine the temperature of all the regenerator segments at the end of the nonflow processes.

It should be noted that typically at the end of a flow process, there exists a nonconstant helium temperature profile in a segment. Because it was assumed that the helium temperature at the start of a nonflow process was constant throughout

the segment and equal to the GGG temperature, there is a violation of the first law of thermodynamics during the transition of a flow process to a nonflow process. In reality, the helium temperature cannot change instantaneously, but because the porosity of the regenerator is small (~4%), the violation of the first law should be small compared to the enthalpy fluxes through the regenerator during a flow process. A slight violation of the first law also exists during the transition of a nonflow process to a flow process.

A simpler model of the nonflow processes neglects the effects of the entrained helium, and causes Eq. (3.24) to become

$$MT_s\frac{ds_s}{dt} = 0 \tag{3.27}$$

Since M and T_s are nonzero, Eq. (3.27) reduces to

$$s_s(t_{ad,i}) = s_s(t_{ad,f}) = \text{constant} \tag{3.28}$$

The numerical analysis incorporates both models, so that the effects of entrained helium can be quantified.

Chapter 4 Thermodynamic Properties of GGG

In order to solve the governing differential equations presented in Chapter 3, the entropy of GGG as a function of temperature and applied field must be known. This chapter presents the results of a survey of the literature for thermodynamic properties of GGG, as well as an empirical formulation of the entropy based on experimental magnetization and specific heat data.

4.1 Derivation of Entropy as a Function of Temperature and Applied Field

A derivation of entropy as a function of temperature and applied field for a Curie-Weiss material was presented in Chapter 2. By expressing the entropy s as an exact differential of temperature T and applied field H, defining the specific heat at constant field $c_H \equiv T(\partial s/\partial T)_H$, and using a Maxwell relation, Eq. (2.12) was derived and is shown below.

$$ds = \frac{c_H(T)}{T}\,dT + \mu_0 v\left(\frac{\partial \mathcal{M}}{\partial T}\right)_H dH \tag{2.12}$$

Equation (2.12) is valid for all magnetic materials and is analogous to the equation

$$ds = \frac{c_p(T)}{T}\,dT - \left(\frac{\partial v}{\partial T}\right)_p dp \tag{4.1}$$

which is valid for p-v systems. If $c_H(T)$ is known for a value of H, preferably $H = 0$, and the magnetization is known for all values of temperature and applied fields, *i.e.*, $\mathcal{M} = \mathcal{M}(T, H)$, then it is possible to integrate Eq. (2.12) to determine $s = s(T, H)$. If it is $c_{H=0}(T)$ that is known, the integration occurs from T_0 to T along the constant-field path ($H = 0$), and then along an isothermal path from $H = 0$ to $H = H$. Equation (2.12) becomes

$$s(T,H) = s_0 + \int_{T_0}^{T} \frac{c_{H=0}(T)}{T}\,dT + \mu_0 v \int_0^H \left[\left(\frac{\partial \mathcal{M}}{\partial T}\right)_H\right]_T dH \tag{4.2}$$

where s_0 is the reference entropy at $T = T_0$ and $H = 0$. Because of the large numbers associated with expressing H in SI units, it is much more convenient for Eq. (4.2) to be in the form

$$s(T,H) = s_0 + \int_{T_0}^{T} \frac{c_{H=0}(T)}{T}\,dT + \int_0^{\mu_0 H} v\left[\left(\frac{\partial \mathcal{M}}{\partial T}\right)_H\right]_T d(\mu_0 H) \tag{4.3}$$

where $\mu_0 H$ is in the unit of Tesla (T).

4.2 Experimental Magnetization Data

The only experimental data found for GGG in the temperature range and applied field range of interest are shown in Fig. 4.1. Figure 4.1 shows the product of the specific volume and magnetization $v\mathcal{M}$ vs. temperature. (Fisher *et al.*[17] measured v and found it to be $0.140\,\mathrm{cm}^{-1}$.) Because magnetization data are usually found in the literature in the form $v\mathcal{M}$ (and often labeled simply as $\mathcal{M}$), the data is presented in this form. It is also more convenient to deal with $v\mathcal{M}$ rather than $\mathcal{M}$, because of the large numbers associated with $\mathcal{M}$ expressed in SI units.

The low temperature data ($T \leq 4.2\,\mathrm{K}$) were obtained from the experimental data of Brodale *et al.*,[18,19,20] and the high temperature data ($T \leq 4\,\mathrm{K}$) were obtained from the experimental data of Hashimoto.[21] Unfortunately one observes from Fig. 4.1 that there exists discontinuity between the two sets of experimental data. The reason for the discontinuity is unclear, and because these were the only data available, it would be very difficult to determine which data might be in error. Any model that describes the magnetization will at best disagree with some of the data in the region of discontinuity.

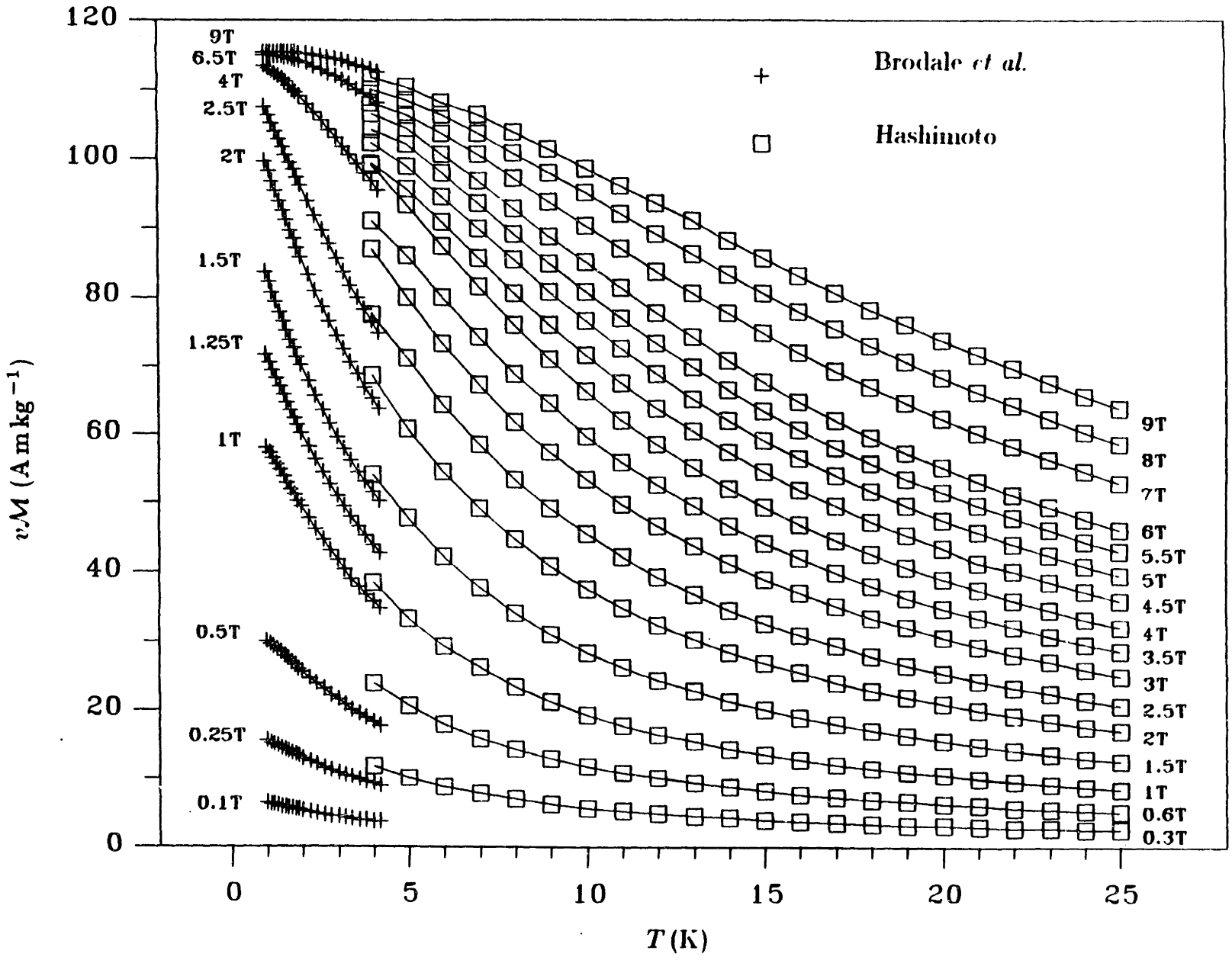

Fig. 4.1 Experimental Magnetization Data For GGG.

The simplest magnetization function found in the literature was the Curie-Weiss law. Wolf *et al.*[22] found that GGG obeys a Curie-Weiss law at high temperatures. They determined the molar Curie constant to be 7.82 g·mol Gd^{3+} emu^{-1} K^{-1} and the Curie temperature to be 2.3 K. Converting the molar Curie constant into SI units, the Curie-Weiss law, with all the quantities expressed in the SI units, is given by

$$\mathcal{M} = \frac{(1.899)\,H}{T + 2.3} \tag{4.4}$$

Figure 4.2 shows the magnetization curves (solid lines) given by Eq. (4.4) and, for comparison, experimental data of Fig. 5.1. Figure 4.2 shows that the Curie-Weiss law is valid at high temperatures and low applied fields where GGG is well out of the magnetic saturation region. While the Curie-Weiss law predicts that the magnetization increases with H, the experimental data show the effect of saturation. Because the Curie-Weiss law incorrectly describes the behavior of GGG in the temperature range and applied field range of interest, it should not be used to derive the entropy function needed for the analysis.

A magnetization function that accounts for saturation effects is found in most quantum mechanics texts and is given by

$$\mathcal{M} = Ng\beta J B_J(x) \tag{4.5a}$$

where

$$B_J(x) = \frac{2J+1}{2J}\coth\left(\frac{2J+1}{2J}x\right) - \frac{1}{2J}\coth\left(\frac{1}{2J}x\right) \tag{4.5b}$$

is the Brillouin function, and

$$x = \frac{g\beta J\mu_0 H}{kT} \tag{4.5c}$$

N is the number of magnetic ions per unit volume, g is the gyromagnetic ratio ($g = 2$), β is the Bohr magneton ($9.274078 \times 10^{-24}\,\mathrm{J\,T^{-1}}$), J is the electron spin number (7/2 for Gd^{3+}), μ_0 is the permeability of free space ($4\pi \times 10^{-7}\,\mathrm{H\,m^{-1}}$), k is the Boltzmann constant ($1.380662 \times 10^{-23}\,\mathrm{J\,K^{-1}}$), H is the applied field, and T

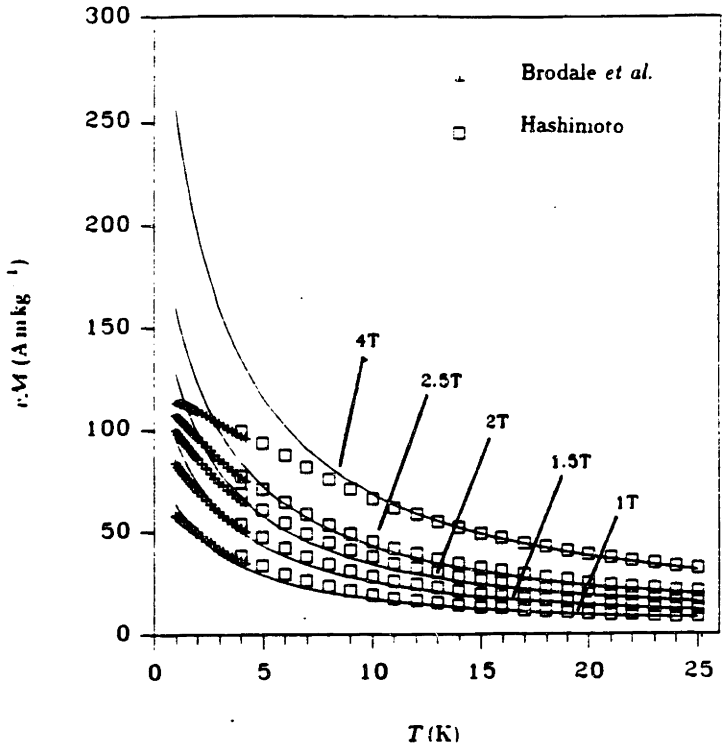

Fig. 4.2. Magnetization calculated from Curie-Weiss law.

is the temperature. A slightly different formulation is given by Bleany[23] where

$$\mathcal{M} = Ng\beta JB_J(x) \tag{4.6a}$$

$$B_J(x) = \frac{2J+1}{2J}\coth\left(\frac{2J+1}{2J}x\right) - \frac{1}{2J}\coth\left(\frac{1}{2J}x\right) \tag{4.6b}$$

and

$$x = \frac{g\beta J\mu_0(H+\mathcal{M})}{kT} \tag{4.6c}$$

Equations (4.6a)–(4.6c) have a disadvantage in that $\mathcal{M}$ cannot be solved explicitly.

It is important to note that the magnetization functions (4.5) and (4.6) are derived using an assumption that each magnetic ion (Gd^{3+} in our case) in the crystal lattice acts as an isolated magnetic dipole and is not influenced by the presence of any neighboring ions. The magnetization per ion is then calculated and multiplied by the number of ions per unit volume of the crystal to give the magnetization of the material. This assumption is valid for some materials such as gadolinium sulphate octahydrate ($Gd_2(SO_4)\cdot 8H_2O$) for which Eqs. (4.6a)–(4.6c) do indeed describe the magnetization very well.[24]

To evaluate Eqs. (4.5) and (4.6), the number of Gd^{3+} ions per unit volume N must be known.

$$\begin{aligned} N &= \frac{\text{no. of } Gd^{3+} \text{ ions}}{\text{unit volume}} \\ &= \left(\frac{3\,\text{mol. } Gd^{3+}}{\text{mol. GGG}}\right)\left(\frac{\text{Avagadro's No.}}{\text{Mol. wt. of GGG}}\right)(\rho_{GGG}) \\ &= \left(\frac{3\,\text{mol. } Gd^{3+}}{\text{mol. GGG}}\right)\left(\frac{6.022 \times 10^{23}\,(\text{mol. } Gd^{3-})^{-1}}{1.01235\,\text{kg}\,(\text{mol. GGG})^{-1}}\right)(7140\,\text{kg m}^{-3}) \\ &= 1.274 \times 10^{28}\,\text{m}^{-3} \end{aligned} \tag{4.7}$$

Because the Brillouin function has a maximum value of 1, the quantity NgB_J from Eqs. (4.5a) and (4.6a) represents the saturated magnetization. For GGG,

$$\begin{aligned} Ng\beta J &= (1.274 \times 10^{28}\,\text{m}^{-3})(2)(9.274078 \times 10^{-2}\,\text{J T}^{-1})(7/2) \\ &= 8.272 \times 10^{5}\,\text{A m}^{-1} \end{aligned} \tag{4.8}$$

Fisher *et al.*[25] experimentally determined the saturated magnetization to be $8.305 \times 10^5\,\text{A m,}^{-1}$, which agrees very well with Eq. (4.8).

Figure 4.3a shows the magnetization calculated from Eqs. (4.5a)–(4.5c), and Fig. 4.3b shows the magnetization calculated from Eqs. (4.6a)–(4.6c). Both figures also show some of the experimental values. Figures 4.3a and 4.3b show that the simple quantum mechanical formulations of magnetization do not fit the data well, suggesting that the assumption of isolated dipoles is not a good one.

To handle the nonideal behavior of GGG, Barclay and Steyert[26] formulated a function modeling the magnetization as a function of the applied field minus the magnetization. Their magnetization function is

$$\mathcal{M} = \frac{3kT_N}{\mu_0 g\beta(J+1)} B_J\left(\frac{g\beta J\mu_0(H-\mathcal{M})}{kT}\right) \tag{4.9}$$

where B_J is the Brillouin function and T_N is the Neel temperature, which they chose to be 2 K. The magnetization calculated from Eq. (4.9) is shown in Fig. 4.4 and is compared to some of the experimental data. Although the function formulated by Barclay and Steyert is much more accurate than the Curie-Weiss law and the quantum mechanical formulations used, it is not very accurate at low fields and temperatures.

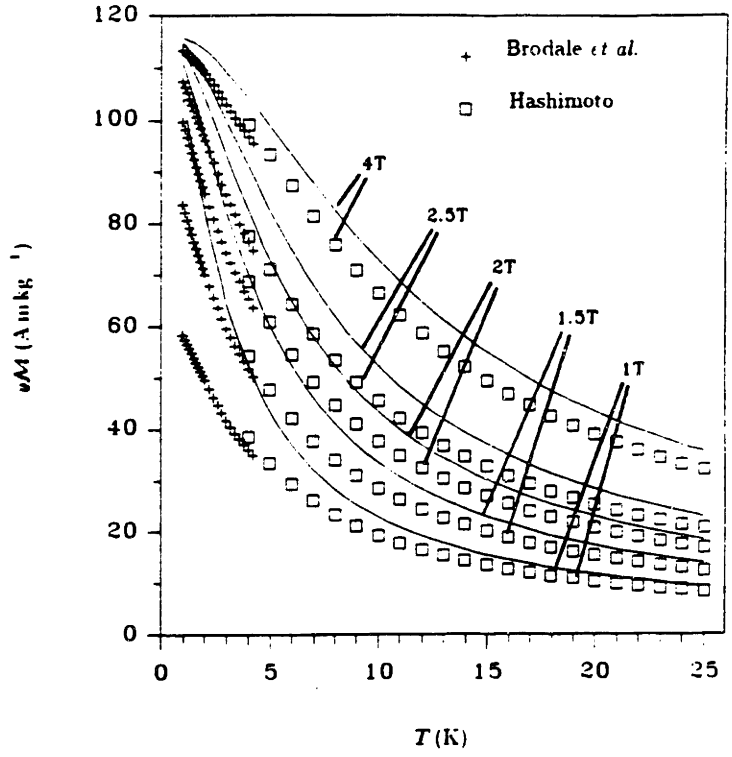

Fig. 4.3a Magnetization calculated from Eqs. (4.5a)–(4.5c).

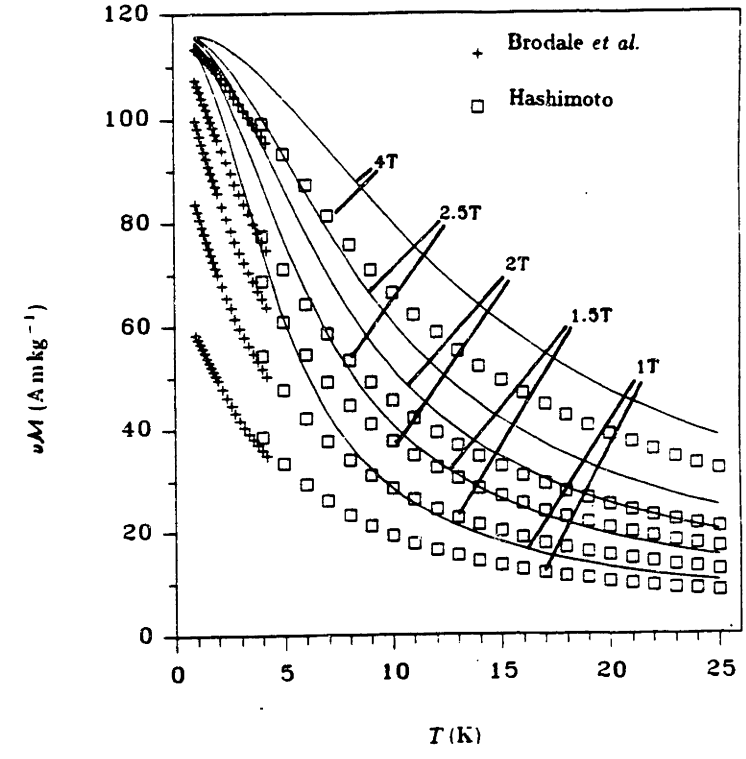

Fig. 4.3b Magnetization calculated from Eqs. (4.6a)–(4.6c).

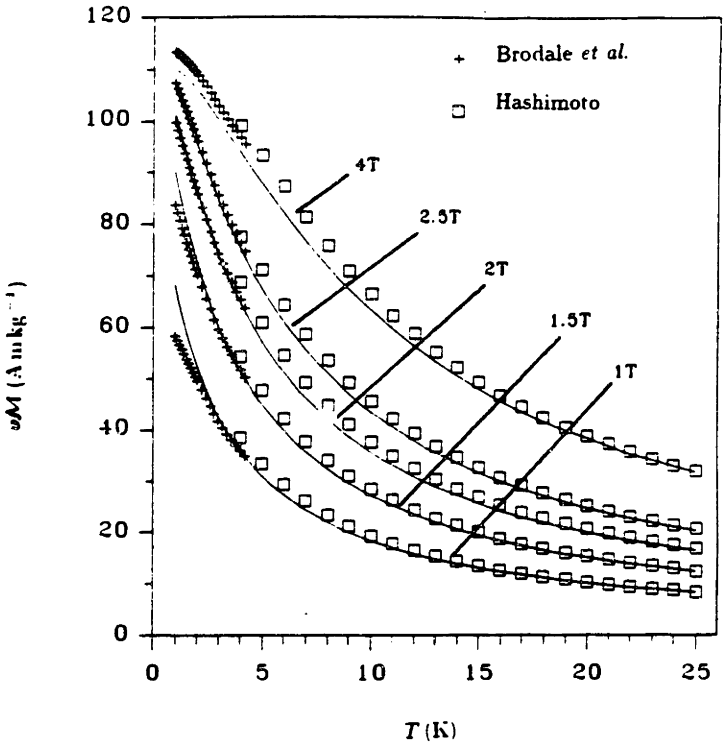

Fig. 4.4 Magnetization calculated from Eq. (4.9).

4.4 Empirical Formulation of Magnetization Function

Because a satisfactory magnetization function for GGG could not be found in the literature, an empirical magnetization function was formulated. Although a function based on physical principles would be elegant, the goal is to obtain a function that describes the magnetization accurately, especially at low temperatures, where the derivative $(\partial\mathcal{M}/\partial T)_H$ is large and where saturation effects are present.

The method of formulation involved plotting different combinations of variables from the experimental data against one another, and relating the combinations by a least squares polynominal curvefit. The method was one of trial and error, with many trials and many errors. The combination of variables that seem to work the best are $\mu_0 H/v\mathcal{M}$ vs. $\mu_0 H$ for constant values of T.

It was found that $\mu_0 H/v\mathcal{M}$ could be fit to a fourth-degree polynomial of $\mu_0 H$ very well. Curvefits were created for 43 different temperatures ranging from 1 K to

25 K, each of the form

$$\frac{\mu_0 H}{v\mathcal{M}} = c_0 + c_1\mu_0 H + c_2(\mu_0 H)^2 + c_3(\mu_0 H)^3 + c_4(\mu_0 H)^4 \tag{4.10}$$

The coefficients c_0, c_1, c_2, c_3, and c_4 from the 43 resulting equations were each curvefit as a function of T, producing a general equation

$$\begin{aligned}\frac{\mu_0 H}{v\mathcal{M}(T,H)} =& c_0(T) + \mu_0 H c_1(T) + (\mu_0 H)^2 c_2(T) \\ &+ (\mu_0 H)^3 c_3(T) + (\mu_0 H)^4 c_4(T)\end{aligned} \tag{4.11}$$

which describes $\mu_0 H/v\mathcal{M}$ over the range of 0–9 T and 1–25 K. (The curvefits of $\mu_0 H/v\mathcal{M}$ vs. $\mu_0 H$ at different temperatures and the curvefits of coefficients c_0, c_1, c_2, c_3, and c_4 as functions of T are shown graphically in Appendix D.) Equation (4.11) can be rearranged to express $\mathcal{M} = \mathcal{M}(H,T)$ as

$$v\mathcal{M} = \frac{\mu_0 H}{c_0(T) + \mu_0 H c_1(T) + (\mu_0 H)^2 c_2(T) + (\mu_0 H)^3 c_3(T) + (\mu_0 H)^4 c_4(T)} \tag{4.12}$$

The functions $c_0(T)$, $c_1(T)$, $c_2(T)$, $c_3(T)$, and $c_4(T)$ are

$$\begin{aligned}c_0(T) =& 13.67388 + 2.718523\,T + 0.1278728\,T^2 \\ &- 2.5072373 \times 10^{-3}\,T^3\end{aligned} \tag{5.13a}$$

$$\begin{aligned}c_1(T) =& -2.980799 + 0.9144735\,T - 7.3461875 \times 10^{-2}\,T^2 \\ &+ 1.1088194 \times 10^{-3}\,T^3 + 9.8684995 \times 10^{-6}\,T^4\end{aligned} \tag{5.13b}$$

$$\begin{aligned}c_2(T) =& 3.166695 - 0.6364962\,T + 4.8334930 \times 10^{-2}\,T^2 \\ &- 1.0840200 \times 10^{-3}\,T^3 + 4.3787923 \times 10^{-6}\,T^4\end{aligned} \tag{5.13c}$$

$$\begin{aligned}c_3(T) =& -0.3461423 + 9.0944469 \times 10^{-2}\,T - 6.9979527 \times 10^{-3}\,T^2 \\ &+ 1.3868879 \times 10^{-4}\,T^3\end{aligned} \tag{5.13d}$$

$$\begin{aligned}c_4(T) =& 1.3560383 \times 10^{-2} - 4.1968897 \times 10^{-3}\,T + 3.3840450 \times 10^{-4}\,T^2 \\ &- 6.8436516 \times 10^{-6} T^3\end{aligned} \tag{5.13e}$$

where $c_0(T)$ has units of $\mathrm{T\,A^{-1}\,m^{-1}\,g}$, $c_1(T)$ has units of $\mathrm{A^{-1}\,m^{-1}\,g}$, $c_2(T)$ has units of $\mathrm{T^{-1}\,A^{-1}\,m^{-1}\,g}$, $c_3(T)$ has units of $\mathrm{T^{-2}\,A^{-1}\,m^{-1}\,g}$, and $c_4(T)$ has units of $\mathrm{T^{-3}\,A^{-1}\,m^{-1}\,g}$,

Figure 4.5 shows values of $v\mathcal{M}$ vs. T calculated from (4.12) as compared to the same experimental data that were compared earlier to the Curie-Weiss law, the quantum mechanical formulations, and the formulation of Barclay and Steyert. Equation (4.12) appears to be much more accurate than the other magnetization functions. The magnetization values of Eq. (4.12) are compared to all the experimental data in Figs. 4.6a and 4.6b, and appear to be inaccurate for temperatures below 4 K at fields above 7 T. The region of discontinuity 4–5 K seems to have been handled very well by the empirical formulation.

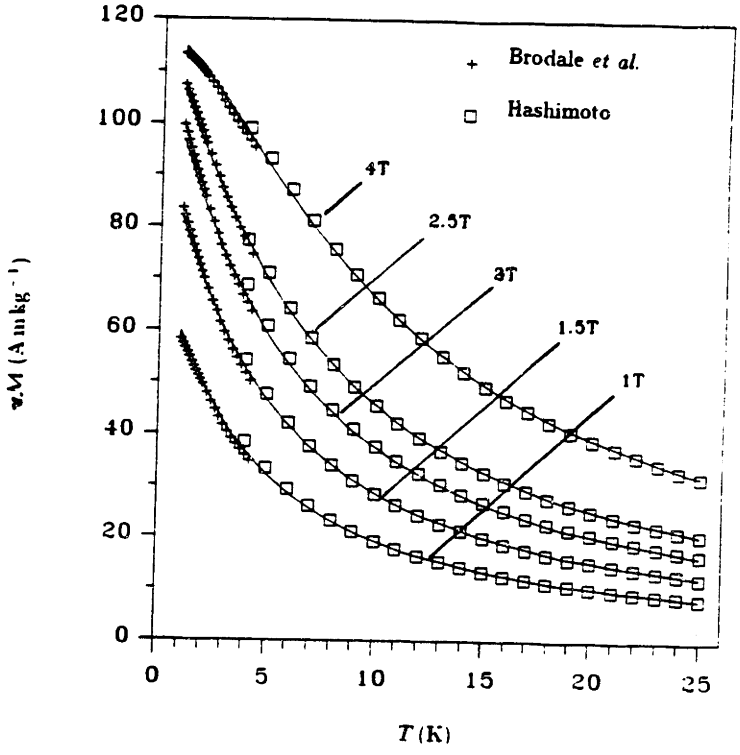

Fig. 4.5 Magnetization calculated from Eq. (4.12).

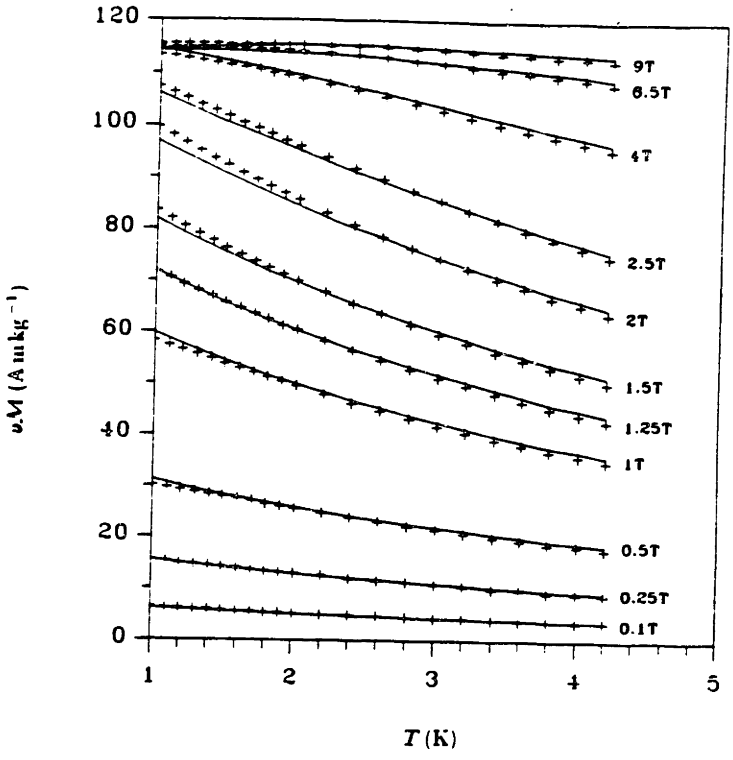

Fig. 4.6a Equation (4.12) compared to all of the low temperature data.

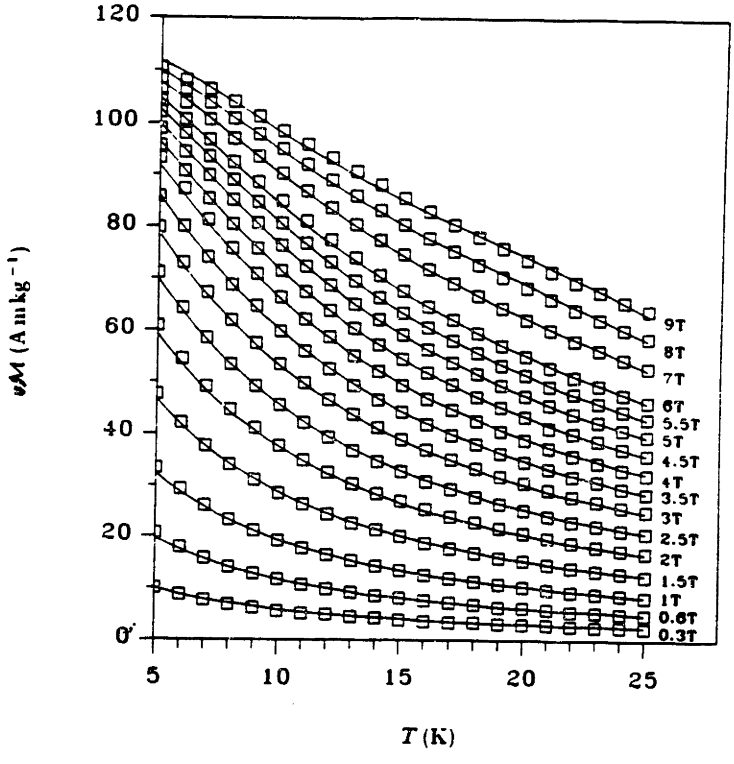

Fig. 4.6b Equation (4.12) compared to all of the high temperature data.

The thermodynamic properties of GGG needed to solve the differential equations derived in Chapter 3 are s, $(\partial s/\partial H)_T$ and $(\partial s/\partial T)_H$, each a function of T and H. To calculate the entropy form Eq. 4.3, we need to know $v(\partial \mathcal{M}/\partial T)_H$. Differentiating Eq. (4.12) with respect to temperature gives

$$v\left(\frac{\partial \mathcal{M}}{\partial T}\right)_H = \frac{\partial}{\partial T}\left(\frac{\mu_0 H}{D(T,H)}\right)_H = -\frac{\mu_0 H(\frac{\partial D(T,H)}{\partial T})_H}{[D(T,H)]^2} \tag{4.14}$$

where $D(T,H) = c_0(T) + \mu_0 H c_1(T) + (\mu_0 H)^2 c_2(T) + (\mu_0 H)^3 c_3(T) + (\mu_0 H)^4 c_4(T)$. The polynomial functions c_0, c_1, c_2, c_3, and c_4 are given by Eqs. (4.13a)–(4.13d).

The entropy s is calculated from Eq. (4.3).

$$s(T,H) = s_0 + \int_{T_0}^{T} \frac{c_{H=0}(T)}{T}\,dT + \int_0^{\mu_0 H} v\left[\left(\frac{\partial \mathcal{M}}{\partial T}\right)_H\right]_T d(\mu_0 H) \tag{4.3}$$

The specific heat at $H = 0$ is needed to evaluate (4.3), and is given by Fisher *et al.*[27] as

$$c_{H=0}(T) = 6.900 \times 10^{-7}\,\mathrm{J\,g^{-1}\,K^{-4}}\,T^3 + \frac{6.385 \times 10^{-2}\,\mathrm{J\,g^{-1}\,K}}{T^2} - \frac{5.096 \times 10^{-2}\,\mathrm{J\,g^{-1}\,K^2}}{T^3} \tag{4.15}$$

Equation (4.15) is accurate to 1% for temperatures between 2 K and 4.2 K. Barclay has found that the lattice specific heat term $6.900 \times 10^{-7}\mathrm{Jg^{-1}K^{-4}T^3}$ is accurate to within experimental error for temperatures up to 20 K.[28] The reference entropy, $s_0(T = T_0, H = 0)$ is arbitrary, so we can set it to any convenient value. We will set $s_0 = 0$ at $T_0 = 1\,\mathrm{K}$. Equation (4.3) now becomes

$$s = \int_{1\,\mathrm{K}}^{T} \frac{c_{H=0}(T)}{T}\,dT + \int_0^{\mu_0 H} v\left[\left(\frac{\partial \mathcal{M}}{\partial T}\right)_H\right]_T d(\mu_0 H) \tag{4.16}$$

The quantity $v(\partial \mathcal{M}/\partial T)_H$, given by Eq. (4.14), cannot be integrated in closed form with respect to $\mu_0 H$. We need to rely on a numerical method to solve the definite integral $\int_0^{\mu_0 H} v[(\frac{\partial \mathcal{M}}{\partial T})_H]_T\,d(\mu_0 H)$.

It was decided that Gauss-Legendre quadrature would be used, since it is a simple method that produces very accurate results. The method is described by Hornbeck.[29] The integration is performed in the following way:

$$\int_0^{\mu_0 H} v\left[\left(\frac{\partial \mathcal{M}}{\partial T}\right)_H\right]_T d(\mu_0 H) \approx \frac{\mu_0 H}{2} \sum_{k=1}^{m} w_k v\left(\frac{\partial \mathcal{M}(T, x_k)}{\partial T}\right)_H \tag{4.17}$$

where $x_k = (1 - \xi_k)\mu_0 H/2$. ξ_k are the m zeros of the m^{th} degree Legendre polynomial and w_k are the corresponding weighting factors. Tabulated values for ξ_k and w_k are found in ref. 29. By trying successively smaller values of m in Eq. (4.17), it was found that $m = 12$ was a good selection that gave accurate results. Table 4.1 shows values for ξ_k and w_k for $m = 12$. Substituting Eq. (4.17) into (4.16) for $m = 12$, we get the resulting entropy function

$$s(T, H) = \int_{1\,\mathrm{K}}^{T} \frac{c_{H=0}(T)}{T} dT + \frac{\mu_0 H}{2} \sum_{k=1}^{10} w_k v\left(\frac{\partial \mathcal{M}(T, x_k)}{\partial T}\right)_H \tag{4.18}$$

where $c_{H=0}(T)$ is given by Eq. (4.15), $v(\partial \mathcal{M}/\partial T)_H$ is given by Eq. (4.14), $x_k = (1 - \xi_k)\mu_0 H/2$, and ξ_k and w_k are given in Table 4.1.

Table 4.1 Zeros and Weights for Gauss-Legendre Quadrature

k	ξ_k	w_k	k	ξ_k	w_k
1	0.12523341	0.24914705	6	-0.12523341	0.24914705
2	0.36783150	0.23349254	7	-0.36783150	0.23349254
3	0.58731795	0.20316743	8	-0.58731795	0.20316743
4	0.76990267	0.16007833	9	-0.76990267	0.16007833
5	0.90411726	0.10693933	10	-0.90411726	0.10693933
11	0.98156063	0.04717534	12	-0.98156063	0.04717534

$(\partial s/\partial T)_H$ is calculated from the partial derivative with respect to T of Eq. (4.18).

$$\left(\frac{\partial s(T, H)}{\partial T}\right)_H = \frac{c_{H=0}(T)}{T} + \frac{\mu_0 H}{2} \sum_{k=1}^{10} w_k v\left(\frac{\partial^2 \mathcal{M}(T, x_k)}{\partial T^2}\right)_H \tag{4.19}$$

where $v(\partial^2\mathcal{M}/\partial T^2)_H$ is the partial derivative with respect to T of Eq. (4.14).

$$v\left(\frac{\partial^2\mathcal{M}}{\partial T^2}\right)_H = \frac{\mu_0 H[2(\frac{\partial D}{\partial T})^2 - D(\frac{\partial^2 D}{\partial T^2})]}{D^3} \tag{4.20}$$

Equations (4.14), (4.18), and (4.19) are believed to be the most accurate functions of $(\partial s/\partial H)_T$, s, and $(\partial s/\partial T)_H$ for GGG, and these equations are used in the analysis. Appendix E contains the tables of the thermodynamic properties of GGG based on the empirical formulation, as well as graphs of $v\mathcal{M}$ vs. T, $\mu_0 H$ vs. $v\mathcal{M}$, s vs. T, and T vs. s.

Chapter 5 Optimal Temperature and Field Ranges for GGG as a Magnetic Refrigerant

Based on the thermodynamic properties of GGG derived in Chapter 4 and the governing equations for the regenerator process derived in Chapter 3, it is possible to determine the optimal temperature and field range for the use of GGG as a magnetic refrigerant.

The governing differential equation for the flow processes in a single regenerator segment was given by Eq. (3.6),

$$\frac{d}{dt}(m_{He}u_{He}) + \dot{m}(h_{out} - h_{in}) + MT_s\frac{ds_s}{dt} = 0 \qquad (3.6)$$

where $\frac{d}{dt}(m_{He}u_{He})$ is the rate of energy storage in the entrained helium, $\dot{m}$ is the helium mass flow through the segment, h_{out} is the exiting helium enthalpy, h_{in} is the entering helium enthalpy, M is the mass of GGG in the segment, T_s is the temperature of the GGG, and ds_s/dt is the derivative of GGG entropy with respect to time. If we expand Eq. (3.6) through the use of the chain rule ($s_s = s_s(H, T_s)$), Eq. (3.6) becomes

$$\frac{d}{dt}(m_{He}u_{He}) + \dot{m}(h_{out} - h_{in}) + MT_s\left[\left(\frac{\partial s_s}{\partial H}\right)_{T_s}\frac{dH}{dt} + \left(\frac{\partial s_s}{\partial T_s}\right)_{H}\frac{dT_s}{dt}\right] = 0 \quad (5.1)$$

The independent variables in Eq. (5.1) are $\dot{m}$ and dH/dt, since these are the quantities with which we control the regenerator flow process experimentally. A boundary condition determines h_{in}; h_{out} is found by solving (5.1) with the heat rate equation. The thermodynamic properties of GGG that influence the regenerator performance are the specific heat capacity at constant field c_H or $T_s(\partial s_s/\partial T_s)_H$, and the quantity $T_s(\partial s_s/\partial H)_{T_s}$.

For an isothermal flow process, it can be easily shown that a large value of $T_s(\partial s_s/\partial H)_{T_s}$ is desirable. Equation (5.1) reduces to

$$\dot{m}(h_{out} - h_{in}) + MT_s\left(\frac{\partial s_s}{\partial H}\right)_{T_s}\frac{dH}{dt} = 0 \qquad (5.2)$$

for an isothermal flow process. Since it is desirable that the magnitude of the enthalpy difference $\dot{m}(h_{out} - h_{in})$ be as large as possible, Eq. 5.2 shows that the quantity $T_s(\partial s_s/\partial H)_{T_s}$ must be large.

The specific heat capacity at constant field, however, should be as small as possible. The detrimental effects of a large value of c_H during an adiabatic nonflow process are easily shown by looking at a simple cyclical relation. A mathematical relationship which is derived in the calculus of several variables is the cyclical relation. Given a function $z = z(x, y)$, the product $(\frac{\partial x}{\partial y})_z(\frac{\partial y}{\partial z})_x(\frac{\partial z}{\partial x})_y = -1$. Since $s_s = s_s(T_s, H)$, it follows that

$$\left(\frac{\partial T_s}{\partial H}\right)_{s_s}\left(\frac{\partial H}{\partial s_s}\right)_{T_s}\left(\frac{\partial s_s}{\partial T_s}\right)_H = -1 \tag{5.3}$$

Solving Eq. (5.3) for $(\frac{\partial T_s}{\partial H})_{s_s}$ gives

$$\begin{aligned}\left(\frac{\partial T_s}{\partial H}\right)_{s_s} &= -\frac{1}{(\partial s_s/\partial T_s)_H}\left(\frac{\partial s_s}{\partial H}\right)_{T_s} \\ &= -\frac{T_s}{c_H}\left(\frac{\partial s_s}{\partial H}\right)_{T_s}\end{aligned} \tag{5.4}$$

The purpose of an adiabatic nonflow processes is to shift the temperature profile of the regenerator. Equation (5.4) shows that large isentropic changes in temperature with field occur when c_H is small and $(\frac{\partial s_s}{\partial H})_{T_s}$ is large. If c_H is large, the GGG requires a large amount of energy input to raise its temperature and a large amount of energy removal output to decrease its temperature. The regenerator becomes sluggish, and a great deal of energy is expended in thermally cycling the GGG instead of refrigerating the helium.

Figure 5.1 is a plot of c_H vs. T created from the thermodynamic properties formulated in chapter 4.. It shows that the specific heat c_H is a much stronger function of field than of temperature and appears to be fairly linear with field in the range of 2–25 K and 0–7 T, except for the region where magnetic saturation effects are present (above 4 T and below 6 K).

Between 20 and 25 K, the slopes of the c_H vs. T curves increase sharply. This effect is due to the lattice specific heat component, which is a function of T^3. It is undesirable to operate a GGG regenerator at temperatures above 20 K, because the large lattice specific heat hampers the regenerator performance.

For temperatures below 20 K, c_H tends to increase largely with field. Although this may appear undesirable, the increase in specific heat is due to magnetization

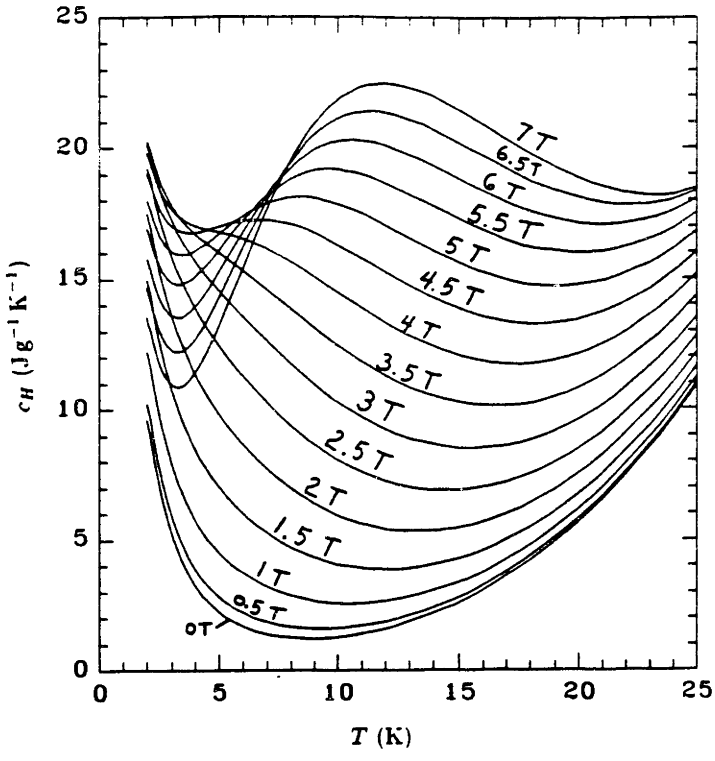

Fig. 5.1 Specific heat at constant field vs. temperature for GGG.

effects which also increase the value of $T_s(\partial s_s/\partial \mu_0 H)_{T_s}$. The specific heat capacity happens to be large in the regions of temperature and field where magnetic work interactions per unit field sweep are large. This is unlike the high-temperature regions where the lattice heat capacity effects are large and magnetic work interactions are small.

Figure 5.2 shows $T_s(\partial s_s/\partial \mu_0 H)_{T_s}$ vs. T_s for various fields. Three important characteristics of GGG are exhibited in Fig. 5.2. The first is the sudden decrease in the magnitude of $T_s(\partial s_s/\partial \mu_0 H)_{T_s}$ as temperature decreases or as field increases to the point where the GGG is suffering from the effects of saturation. As the field increases, the effects of saturation begin at higher temperatures. At fields approaching 7 T, magnetic saturation effects occur at temperatures as high as 20 K. For 4 T, magnetic saturation effects are present at temperatures below 10 K.

The second GGG characteristic shown in Fig. 5.2 is the steady decrease in the magnitude of $T_s(\partial s_s/\partial \mu_0 H)_{T_s}$ as temperature increases. This effect applies to the region where saturation effects are present. The decrease in the magnitude of

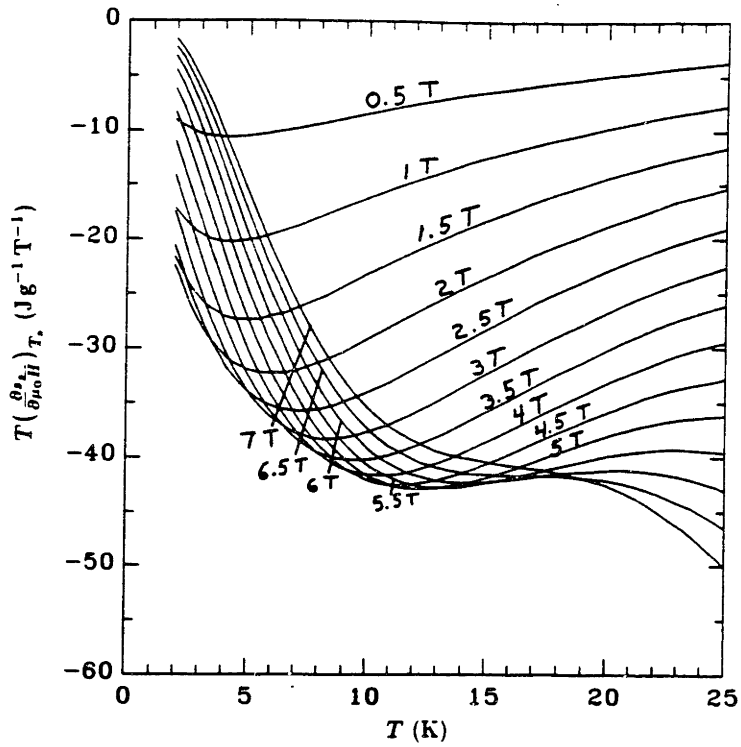

Fig. 5.2 $T_s(\partial s_s/\partial \mu_0 H)_{T_s}$ vs. temperature for GGG.

$T_s(\partial s_s/\partial \mu_0 H)_{T_s}$ as temperature increases is a characteristic of Curie-Weiss materials, since for the Curie-Weiss law,

$$T_s \frac{\partial s_s}{\partial \mu_0 H} = v T_s \left(\frac{\partial \mathcal{M}}{\partial T} \right)_H = v T_s \frac{CH}{(T_s + \theta)^2} \tag{6.1}$$

where C is the Curie constant, and θ is the Curie temperature. For GGG, the magnitude of $T_s(\partial s_s/\partial \mu_0 H)_{T_s}$ at 20 K is about 30% smaller than the magnitude of $T_s(\partial s_s/\partial \mu_0 H)_{T_s}$ at 10 K for fields in the range of 1–4 T.

The third GGG characteristic exhibited in Fig. 5.2 is the strong relationship between $T_s(\partial s_s/\partial \mu_0 H)_{T_s}$ and $\mu_0 H$. This is better shown in the curves of $T_s(\partial s_s/\partial \mu_0 H)_{T_s}$ vs. $\mu_0 H$ of Fig. 5.3. While in the region where magnetic saturation has no effects, $T_s(\partial s_s/\partial \mu_0 H)_{T_s}$ varies linearly with $\mu_0 H$. This effect is also true for Curie-Weiss materials and is shown in Eq. (6.1). It is not desirable to ever operate the regenerator through the zero field, because $T_s(\partial s_s/\partial \mu_0 H)_{T_s} \rightarrow 0$

as $\mu_0 H \rightarrow 0$. At the zero field, the rate of magnetic work done on or by the regenerator is always zero.

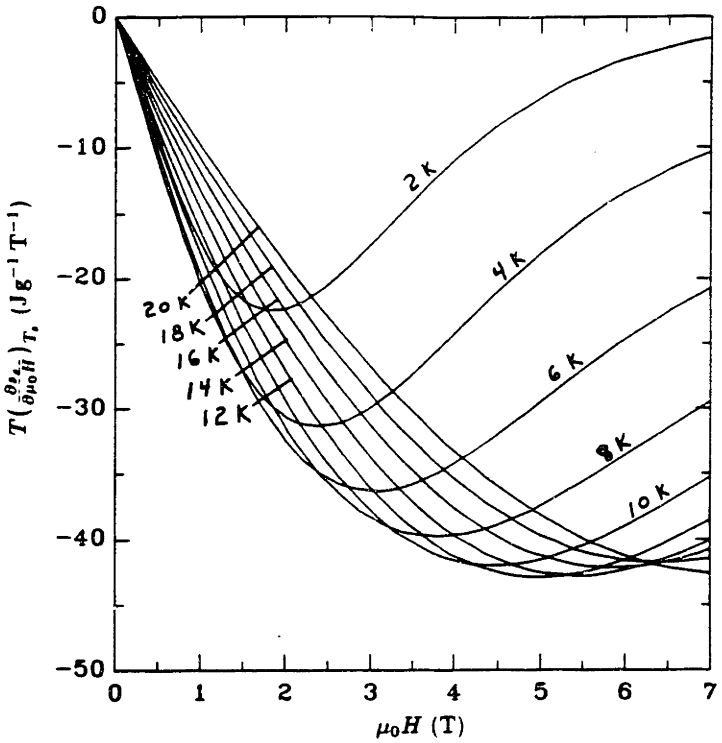

Fig. 5.3 $T_s(\partial s_s/\partial \mu_0 H)_{T_s}$ vs. $\mu_0 H$ for GGG.

When considering the decrease in the magnitude of $T_s(\partial s_s/\partial \mu_0 H)_{T_s}$ as $\mu_0 H$ approaches zero, or as $\mu_0 H$ increases at high applied fields in the saturation region, it seems that the optimal field range for the regenerator composed of GGG is between 1 T and 4 T, or perhaps 1 T and 5 T. Below 1 T and above 5 T, magnetic work interactions are very small for temperatures below 15 K.

Chapter 6 Computer Algorithm and Results

6.1 Computer Algorithm

A computer algorithm was designed and implemented to solve the equations derived in Chapter 3. The first-order differential equation governing the flow processes is solved as an initial-value problem using a Runge-Kutta algorithm. Second-order and fourth-order Runge-Kutta methods were investigated for several timestep sizes and results of a sample cycle were compared. A second-order method with 150 timesteps for a flow process of 3.5 s (23.3 ms timesteps) appeared to yield accurate results.

The governing equation for the flow processes has the form

$$\frac{dT_s}{dt} = f(T_s, t) \tag{6.1a}$$

where $f(T_s, t)$ consists of several equations solved simultaneously (see Chapter 3). The second-order Runge-Kutta method involves dividing a flow process into a number of timesteps and solving T_s for a particular timestep using the equations

$$T_{s,j+1} = T_{s,j} + \Delta t\, f(T^*_{s,j+1/2}, t_{j+1/2}) \tag{6.1b}$$

where

$$T^*_{s,j+1/2} = T_{s,j} + \frac{\Delta t}{2} f(T_{s,j}, t_j) \tag{6.1c}$$

$$t_{s,j+1/2} = t_j + \frac{\Delta t}{2} \tag{6.1d}$$

$$t_{s,j} = t_j + \Delta t \tag{6.1e}$$

The timestep size is Δt, and $T_{s,j}$ refers to T_s at the j^{th} timestep. During the first timestep, $T_{s,j}$ is given by an initial value, which is the final value of T_s from the previous process. The function $f(T_s, t)$ is Eq. (3.21) solved simultaneously with Eqs. (3.8), (3.12), (3.13), (3.14), (3.15), (3.16), (3.17), and (3.22). Each of the 120 regenerator segments is solved in a marching method in the downstream direction.

The helium input conditions for a segment are the helium output conditions for the adjacent segment upstream. The first segment in the marching process has input conditions from a reservoir.

The computer algorithm solves the adiabatic processes by solving implicitly Eqs. (3.25) and (3.26), using a simple bisection technique. The computer program models the helium entrainment effects, but assumes that the helium mass in a segment remains constant throughout the process and that there are no convection effects. The model also assumes that the helium and GGG remain in thermal equilibrium throughout the process.

Subroutines evaluate the thermodynamic properties of GGG and the thermodynamic and transport properties of 3 atm supercritical helium. The GGG properties are evaluated based on the equations formulated in Chapter 4. The helium properties are evaluated from a helium properties computer program between 2.14 K and 10 K, and at intervals of 0.05 K between 10 K and 20 K. The properties generated by the program have agreed well with the tabulated helium properties found in *NBS Technical Note 631; Thermophysical Properties of Helium-4 from 2 to 1500 K with Pressures to 1000 Atmospheres* (National Bureau of Standards, 1972). Interpolation between property values is performed by evaluating cubic spline functions formulated for all the helium properties. The cubic spline technique is discussed in Appendix F.

The computer programs that were created to evaluate the regenerator processes are contained in Appendix G. A flow chart of the computer algorithm is shown at the beginning of the appendix.

6.2 Entrainment Effects During Nonflow Processes

The governing equations derived in Chapter 3 for the adiabatic nonflow processes were solved to evaluate adiabatic magnetization and adiabatic demagnetization processes for several values of helium porosity, where the porosity ϵ is defined as the volume fraction of helium in the regenerator. (The porosity in the experimental regenerator is about 4%.) The results are summarized in Tables 6.1 and 6.2.

Table 6.1 Temperature Swings during an Adiabatic Magnetization

T_{start} (K)	T_{end}(K) after 1 T to 1.75 T Field Sweep				
	$\epsilon = 0$	$\epsilon = 0.04$	$\epsilon = 0.06$	$\epsilon = 0.08$	$\epsilon = 0.10$
4	7.23	5.56	5.40	5.26	5.15
5	8.79	6.12	5.82	5.70	5.63
6	10.16	8.76	8.37	8.05	7.80
7	11.36	10.41	10.10	9.83	9.59
8	12.40	11.64	11.37	11.16	10.92
9	13.31	12.71	12.50	12.23	12.10
10	14.13	13.61	13.48	13.29	13.09

Table 6.2 Temperature Swings During an Adiabatic Demagnetization

T_{start} (K)	T_{end}(K) after 1 T to 1.75 T Field Sweep				
	$\epsilon = 0$	$\epsilon = 0.04$	$\epsilon = 0.06$	$\epsilon = 0.08$	$\epsilon = 0.10$
4	2.98	3.08	3.12	3.16	3.20
5	3.72	3.89	3.97	4.03	4.09
6	4.49	4.74	4.85	4.96	5.06
7	5.28	5.49	5.56	5.62	5.67
8	6.10	6.21	6.26	6.30	6.34
9	6.94	7.03	7.07	7.11	7.15
10	7.80	7.88	7.91	7.95	7.98

Tables 6.1 and 6.2 show that helium entrainment associated with high regenerator porosity is very significant in limiting the temperature swing of the adiabatic magnetization and demagnetization processes. This is due to the high specific heat capacity of helium compared to that of the GGG. At low values of field where

the specific heat capacity of GGG is very small, the regenerator tends to be very susceptable to the effects of entrained helium.

In the actual system, there are no adiabatic processes. The helium density is a very strong function of temperature between 4 K and 10 K, and in that temperature range, the density changes as much as 50% when the temperature is altered by 1 K. During nonflow magnetization processes, the change in density at constant pressure results in an expansion of the helium. Helium at temperatures below 4 K is more dense and less compressible, and tends to remain stationary while the less dense and more compressible helium above 4 K has the tendency to move upward. A natural convection process results, and the hot end of the regenerator core is actually cooled by the helium moving upward from the cold end. During nonflow demagnetization processes, density changes at constant pressure results in a helium contraction. Helium from the hot end flows toward the cold end and the cold end tends to be warmed by the helium. In both cases, the convection process is coupled to a magnetic work process. It is likely that, because of the convection process, the temperature swings for nonzero porosities are actually smaller than as shown in Tables 6.1 and 6.2. The convection effect during nonflow processes is a topic that should be investigated further.

6.3 Comparison of Numerical and Experimental Results

The computer algorithm described in Chapter 5 was set up to solve the regenerator processes for the field profile, mass flow, and the entering and exiting helium temperatures that were measured during one of the experiments. The measured mass flow, field, and helium temperatures for the experimental run are shown in Appendix H. The last three cycles of the run were used in the computer analysis. The demagnetization flow process occuring before the three cycles was also simulated, and the regenerator was given an initial temperature of 5.6 K at the start of the process. Prior testing of the computer program showed that the system achieves a cyclic steady-state after one flow process, and the demagnetization flow process was used for this purpose.

In the initial design of the experiment, the reservoir temperatures and mass flow rate were to be held constant, and the field was to be ramped between 1 T and 4 T at $0.5\,\mathrm{Ts}^{-1}$. In the actual experiment, the reservoirs varied in temperature, the mass flow timing was in error, and the field was ramped between 1.25 T and 4 T at $0.6\,\mathrm{Ts}^{-1}$. To make the computer program simulate the experimental conditions as closely as possible, cubic spline interpolation functions were created from the experimental data to evaluate the reservoir temperatures, field, field rate of change, and mass flow rate a functions of time. The three cycles are shown in Figs. 6.1a–6.1f. Figure 6.1a shows the mass of helium in the displacer cylinder as a function of time, Fig. 6.1b shows the helium mass flow rate (time derivative of helium mass in Fig. 6.1a), Fig. 6.1c shows $\mu_0 H$ as a function of time, Fig. 6.1d shows $\mu_0\, dH/dt$ (as a function of time), Fig. 6.1e shows the helium temperature outside the hot end of the regenerator as a function of time, and Fig. 6.1f shows the helium temperature outside the cold end of the regenerator as a function of time. The cycle is divided into its four processes based on the measured mass flow. The time for a process in one cycle is not necessarily the same as the time of the corresponding process of the next or previous cycle. This is due to timing errors in the experiment.

The solid curves in Figs. 6.1e and 6.1f represent the experimental temperatures measured outside the hot and cold ends of the regenerator. During the magnetization flow processes, the experimental helium temperatures outside the cold end of the regenerator were used as the cold reservoir boundary temperatures in the numerical analysis. The dashed curves represent the temperature of the helium leaving the regenerator and entering the hot reservoir, as predicted by the computer model. Likewise during demagnetization flow processes, experimental helium temperatures outside the hot end of the regenerator were used as the hot reservoir boundary temperatures in the numerical analysis. The dashed curves in these process represent the temperatures of the helium leaving the regenerator and entering the cold reservoir, as predicted by the computer model.

Figures 6.1e and 6.1f show a very large disagreement between the experimental and numerical results. The greatest discrepancy in the results is in the shape

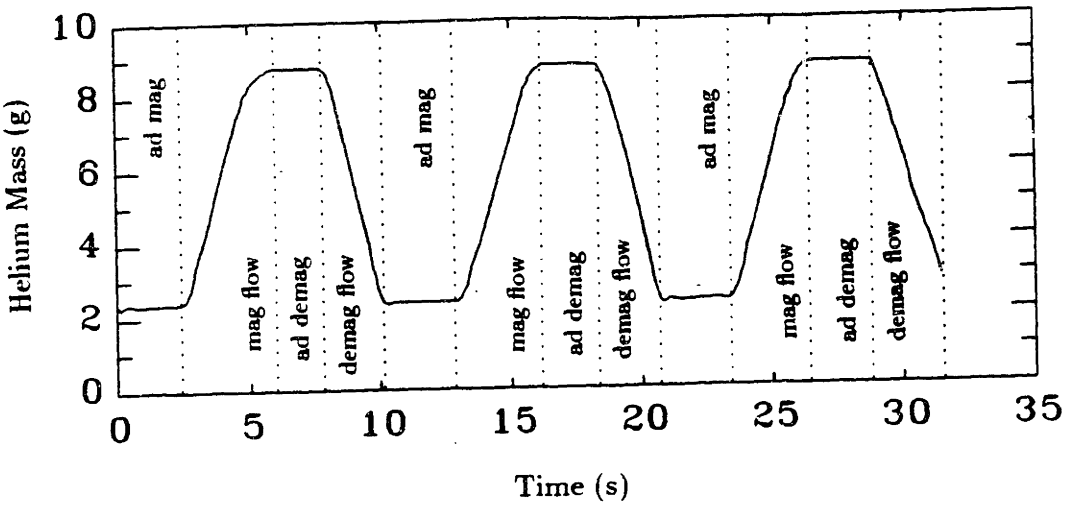

Fig. 6.1a Helium mass in displacer cylinder vs. time.

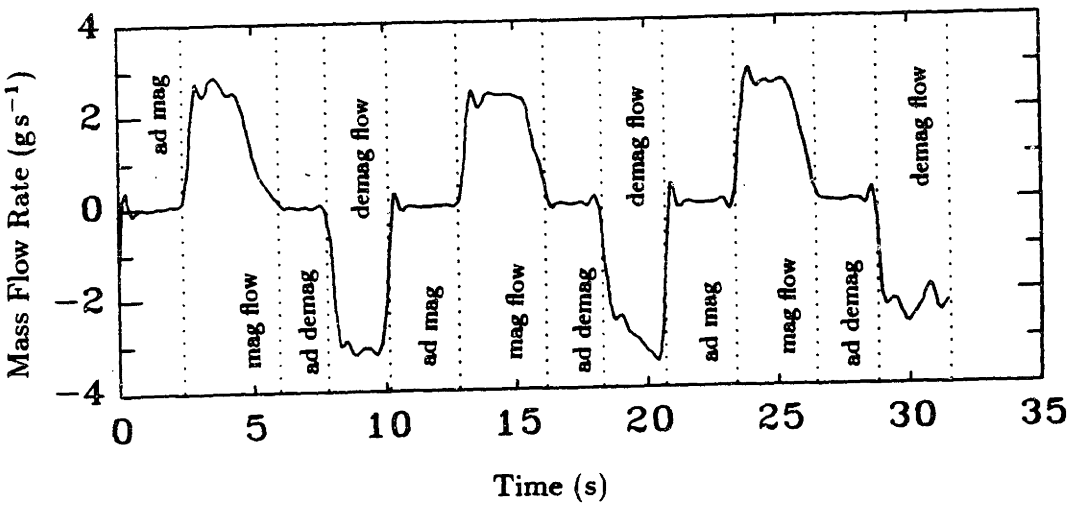

Fig. 6.1b Helium mass flow rate vs. time.

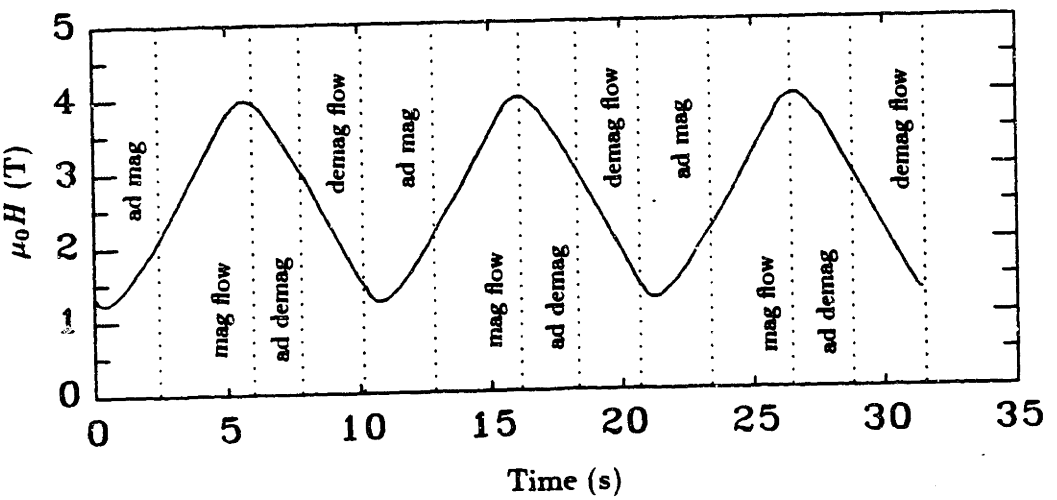

Fig. 6.1c $\mu_0 H$ vs. time.

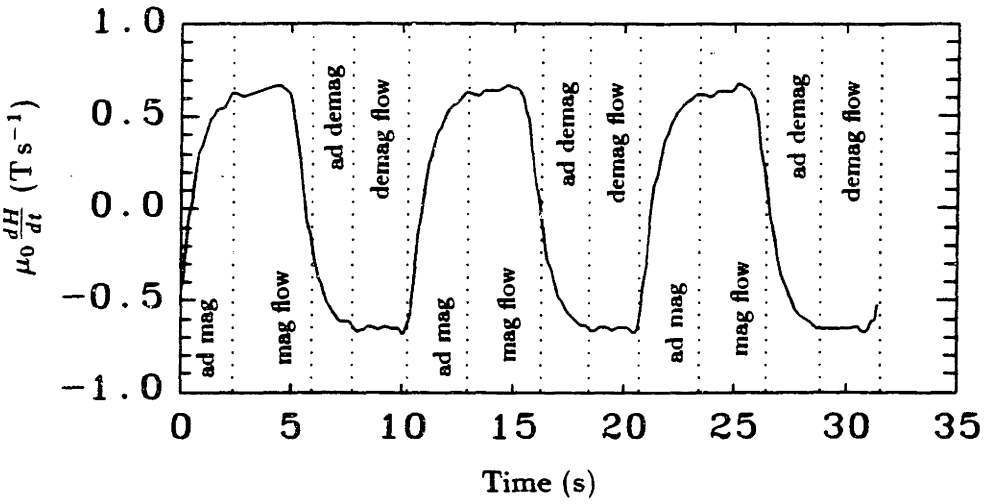

Fig. 6.1d $\mu_0 \, dH/dt$ vs. time.

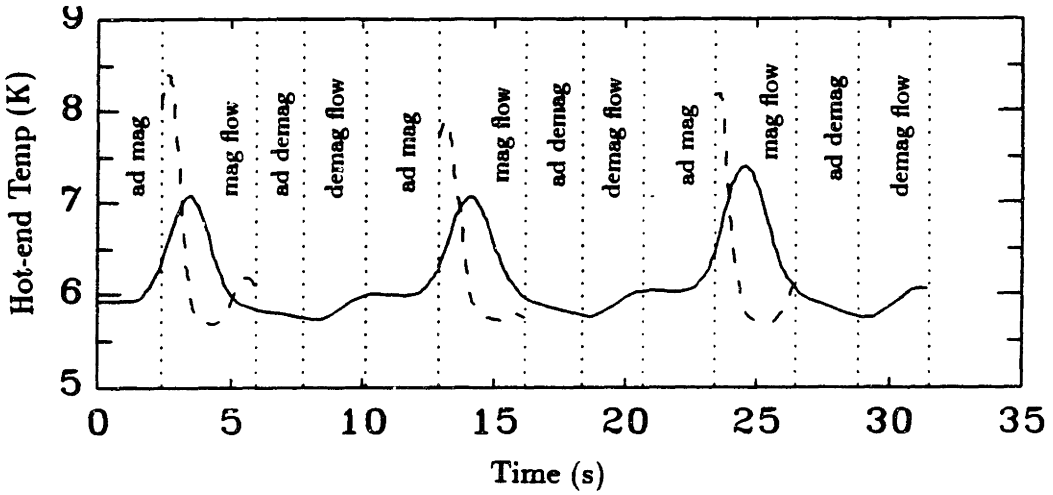

Fig. 6.1e Temperature outside the hot end of the regenerator vs. time.

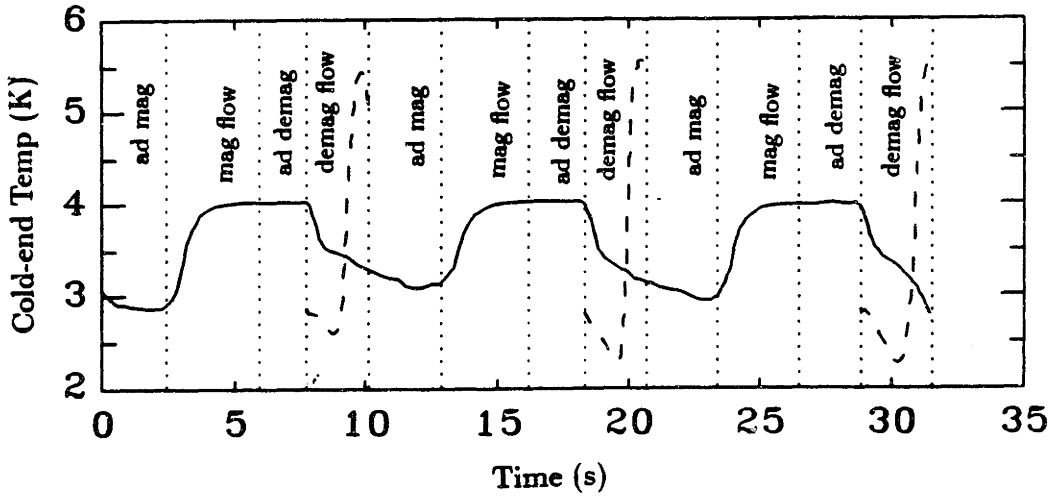

Fig. 6.1f Temperature outside the cold end of the regenerator vs. time.

of the curves of Fig. 6.1f toward the end of the demagnetization flow processes. The numerical results predict that the rate of magnetic work removed from the regenerator decreases as the field decreases, resulting in the propagation of a thermal wave from the hot end of the regenerator to the cold end. As the rate of magnetic work decreases, the regenerator loses the ability to cool the helium that is flowing from the hot reservoir. The temperature of the helium that emerges from the bottom of the regenerator and into the cold reservoir increases as the demagnetization flow process continues. The increase in temperature is actually very sharp, since the specific heat capacity of the GGG also decreases with field.

The experimental results for the demagnetization flow process show that the temperature of the helium emerging from the bottom of the regenerator continues to decrease throughout the process. The effects of a decrease in the magnetic work rate as the field decreases are not apparent.

The magnetization flow processes show a similar characteristic. The numerical results predict that the magnetic work rate is smaller at low fields, and the effect is seen at the beginning of the process. The experimental results reveal no effect of this kind.

The experimental results also differ from the numerical results in that the experimental adiabatic temperature swings are not as large as those of the numerical analysis. There is uncertainty to this observation, however, because the location of the temperature sensors is outside of the regenerator. An adiabatic temperature swing is not detected by the temperature sensor until the following flow process begins. If the regenerator temperature gradient at the start of the flow process is very large, the temperature sensor will not measure the adiabatic temperature accurately. The computer model also does not take into account natural convection effects, which may play a significant role in the nonflow processes.

Natural convection effects are noticeable during each of the adiabatic magnetization proceses in Fig. 6.1f. The experimental data at the cold end of the regenerator show that the helium temperature continues to decrease during adiabatic magnetization processes. This result occurs because gravitational effects cause the cold,

denser helium to fall out of the bottom of the regenerator.

6.4 Investigation of the Discrepancy Between the Results

There are many possible causes for the differences between the experimental and numerical results. An investigation was performed in order to determine the source of the discrepancy. The areas studied generally involved the effect of measurement errors on the results and the effect of variables which were not included in the computer model. When possible, the effects of a suspected error have been quantified. When it has been impossible to quantify the effects of an error, suggestions of how to measure the effect or avoid the error in future experiments have been made. The areas that will be discussed include the effects of errors in the heat transfer model, errors in the magnitude of the regenerator porosity, errors in temperature measurements, errors due to pressure variations, and errors in the thermodynamic properties.

6.5 Effects of a Heat Transfer Coefficient Error

The sensitivity of the flow processes to errors in the heat transfer coefficient was investigated by altering the heat transfer coefficient in the computer model and then solving the regenerator flow processes again. The heat transfer coefficient was evaluated as $\hbar = 1.75 k_{He}/d$, which is a 50% reduction in the value of the original model. The outflow helium temperatures at the hot and cold ends of the regenerator, which are calculated using the altered heat transfer coefficient, are shown as dashed curves in Figs. 6.2a and 6.2b. The experimental values of helium temperature are also shown in the figures as solid curves.

The reduced heat transfer coefficient has little effect on the shape and magnitude of the helium temperature profiles. The most noticeable change is found in the demagnetization flow processes, where the sharp increase in the helium temperature occurs at an earlier time in the process. It appears that the system would be very insensitive to any small errors in the heat transfer coefficient.

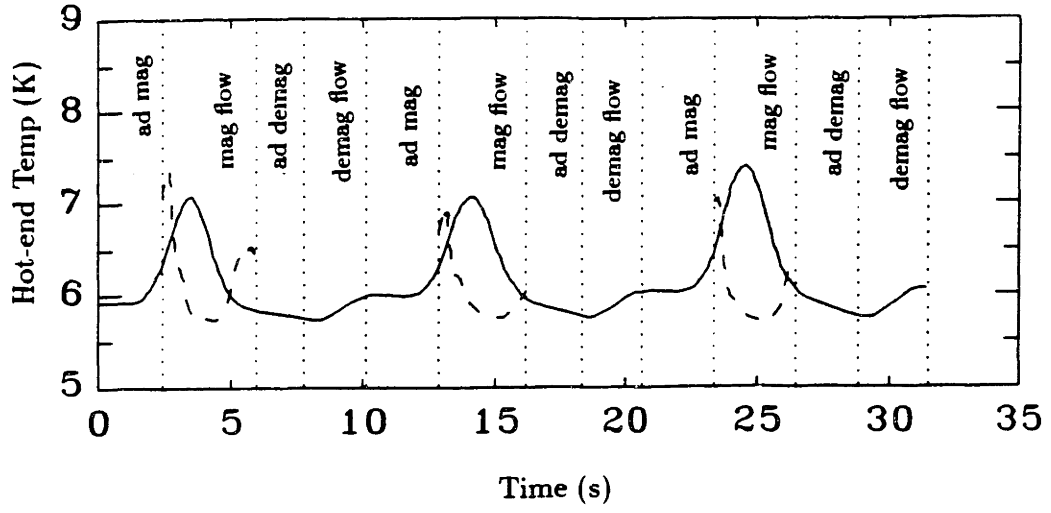

Fig. 6.2a Temperature outside the hot end of the regenerator vs. time.

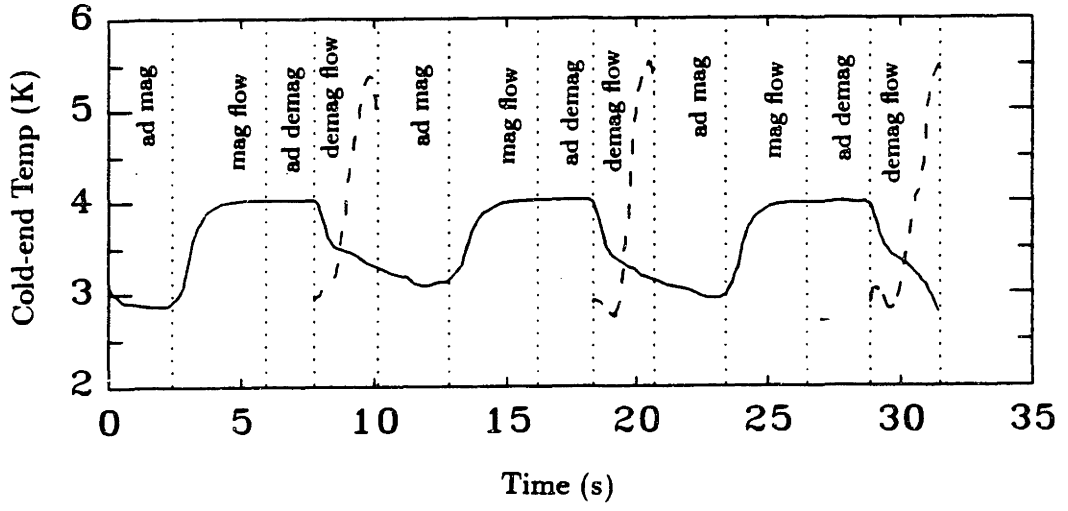

Fig. 6.2b Temperature outside the cold end of the regenerator vs. time.

6.6 Effects of Miscalculated Porosity

The sensitivity of the flow processes to errors in the porosity was also investigated numerically. The porosity used in the original calculations is 4.4%. Altered porosities of 6% and 10% were used in the error investigation, and resulting helium temperatures are shown with the experimentally measured temperatures in Figs. 6.3a and 6.3b.

The increase in porosity caused the adiabatic temperature sweeps to be smaller, as expected, and this is shown in the figures, but the flow processes were generally unchanged by the increase in porosity. The heat capacity of the additional entrained helium did not change the shape of the temperature profiles significantly.

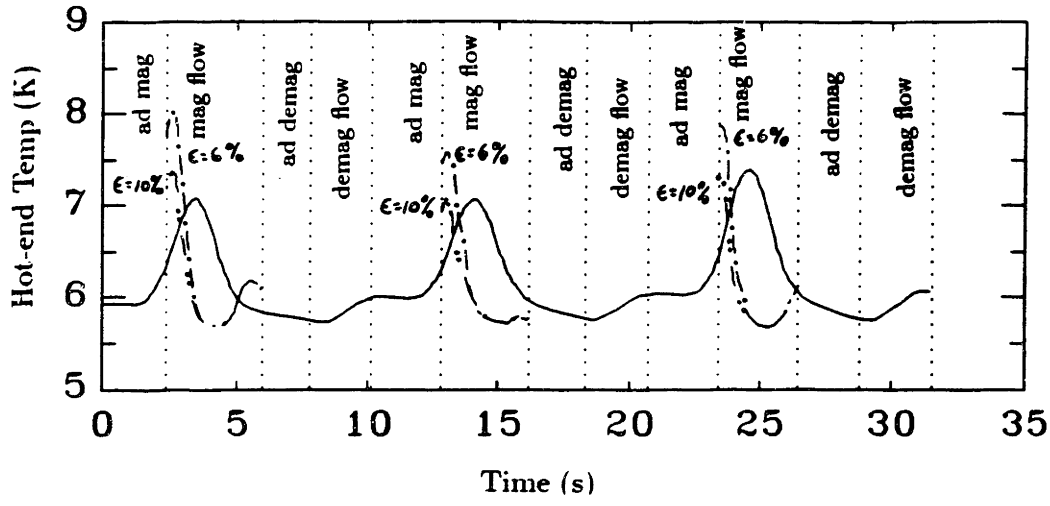

Fig. 6.3a Temperature outside the hot end of the regenerator vs. time.

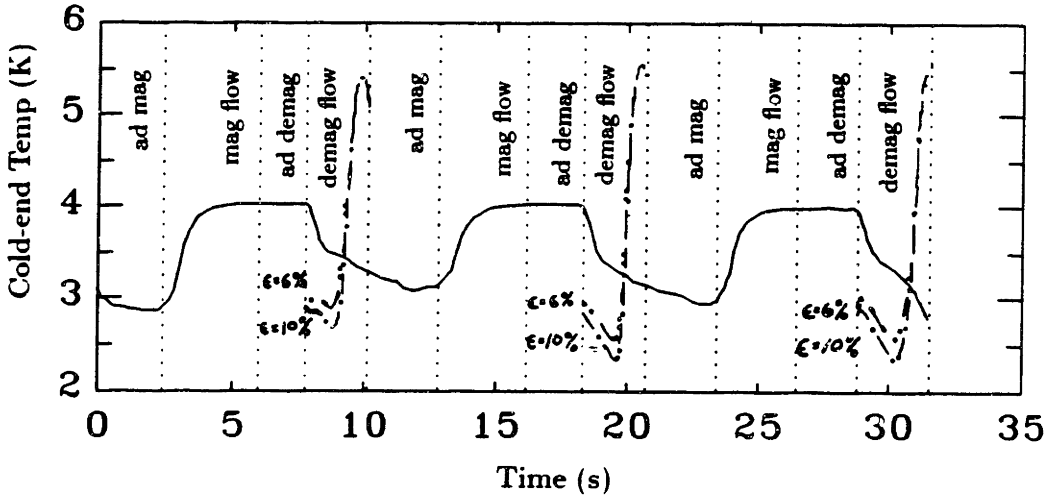

Fig. 6.3b Temperature outside the cold end of the regenerator vs. time.

6.7 Effects of Temperature Measurement Errors

One possible source of a large error is inaccuracy of the hot-end helium temperature. Although the carbon glass resistor used to measure the hot-end temperature was calibrated well for the temperature range of the experiment, the leads to the resistor were not in very good thermal contact with the helium stream. The sensor readings may have been influenced by heat transfer through the leads resulting in a measurement error of the helium temperature.

Since there is not enough data to adequately quantify the heat transfer processes of the sensor, helium stream, and sensor leads, it is difficult to predict the

error in the temperature measurement. It is possible, however, to investigate the sensitivity of the helium enthalpy to a temperature measurement error. Since the regenerator flow processes depend strongly on the helium enthalpy (Eq. 3.20), errors in the enthalpy cause errors in evaluating the path that the GGG temperature takes through the process.

Another factor suggesting that temperature measurement errors are responsible for some of the discrepancy between results is that the hot-end helium temperature throughout most of the experiment remained at 5.6 K, the temperature of the specific heat anomaly. The change in c_p near 5.6 K is dramatic. For a pressure of 3 atm the value of c_p at 5.6 K is ten times the value of c_p at 4 K, and it is four times the value of c_p at 7 K.

Because of the enormous variation in c_p with temperature near 5.6 K, small temperature errors produce large enthalpy errors. For example, an error of $\pm 5\%$ in temperature (± 0.3 K) produces an enthalpy error of $\pm 30\%$. Since c_p varies dramatically only in a small region of temperature, the effects of temperature measurement errors are nonlinear with temperature. It is possible that a moderate hot-end temperature error may be responsible for the discrepancy in the results.

In future experiments, two steps should be taken to ensure that the temperature measurement errors and the effects of temperature measurement errors on the system performance are small. First, the leads to the sensor must be placed in good thermal contact with the helium stream to ensure that the sensor actually measures the helium stream temperature, and second, the hot-end and cold-end temperature controllers should be improved so that the regenerator operates betweem 4 K and 10 K as originaly intended. Maintaining the hot reservoir at 10 K, where c_p does not vary much with temperature, will ensure that small temperature measurement errors do not produce large enthalpy errors.

6.8 Variations in System Pressure

It was found that during the experiments, control errors existed in the operation of the pressure compensator. This may have caused significant pressure variations in

the system. Since the enthalpy of helium at the temperature range and pressure of the experiment is a strong function of pressure, it is possible that pressure variations affected the performance of the system significantly. The computer model assumes a constant pressure of 3 atm, so a variation in pressure in the actual system would create a discrepancy between the experimental and numerical results.

The system pressure was monitored and controlled by a pressure regulator set at 3 atm, and it is possible that small pressure fluctuations were not detected by the regulator. Since the experiment was not equipped internally with pressure transducers, the system pressure was not measured accurately. At 5.6 K, a pressure change of ± 0.2 atm changes the helium enthalpy $\pm 15\%$, and the effect is nonlinear with temperature, because the specific volume is strong function of temperature. Between 3 K and 6 K, the specific volume varies be a factor of three. Pressure transducers should be installed in future experiments to measure the pressure more precisely. Improvements in the pressure compensator should also be implemented to minimize pressure variations.

6.9 Errors in the Thermodynamic Properties of GGG

Another possible cause for the discrepancy in the results is the inaccuracy of the thermodynamic properties of GGG. Although the properties are thermodynamically consistent, they may be in error, because the properties were based on a very small amount of data. Any errors in the magnetization or specific heat data used to generate the thermodynamic properties would be passed into the properties themselves.

Impurities in the GGG may have caused the thermodynamic properties of the actual material to be different from the derived properties. Some of the leftover paramagnetic salt should be used to test the magnetization as a function of applied field and temperature to determine whether or not the empirical magnetization function of Chapter 4 describes the actual material used in the MIT device.

6.10 Single-shot Flow Processes

It would be useful to experimentally perform some single-shot flow processes and compare the experimental results to results from the computer model. Performing single-shot flow processes has the advantage that the computer model and thermodynamic properties of GGG are tested without the effects of the nonflow processes. If the regenerator core temperature is initially set to 4.2 K (by flowing cold helium through it), three processes can be easily performed.

The first is to keep the field at 0 T and to flow helium from the hot reservoir maintained at 10 K. The temperature of the helium entering the cold reservoir can be monitored as the thermal wave propagates through the passive regenerator. Figure 6.4 shows the temperature profile of the helium entering the cold reservoir as predicted by the computer model for mass flow rates of $0.5\,g\,s^{-1}$, $1.0\,g\,s^{-1}$, $1.5\,g\,s^{-1}$, and $2.0\,g\,s^{-1}$. The pressure always remains at 3 atm. Since the field is zero throughout the process, the magnetization properties of GGG are not used in the numerical evaluation of the process. Therefore, the only GGG thermodynamic property tested in the process is the zero-field specific heat.

The second experiment involves setting the initial temperature of the regenerator to 4.2 K, and the initial field to zero. Heliurn flows from the cold reservoir at 4.2 K through the regenerator while the field is ramped from 0 T to 4 T at $0.5\,T\,s^{-1}$. The predicted outflow helium temperature is shown in Fig. 6.5 for helium mass flow rates of $0.5\,g\,s^{-1}$, $1.0\,g\,s^{-1}$, $1.5\,g\,s^{-1}$, and $2.0\,g\,s^{-1}$.

The third experiment involves setting the initial temperature of the regenerator to 4.2 K and the initial field to 4 T. Helium flows from the hot reservoir, which is maintained at 10 K, to the cold resevoir while the field is ramped down to 0 T at a rate of $0.5\,T\,s^{-1}$. The predicted outflow helium temperature is shown in Fig. 6.6 for helium mass flow rates of $0.5\,g\,s^{-1}$, $1.0\,g\,s^{-1}$, $1.5\,g\,s^{-1}$, and $2.0\,g\,s^{-1}$.

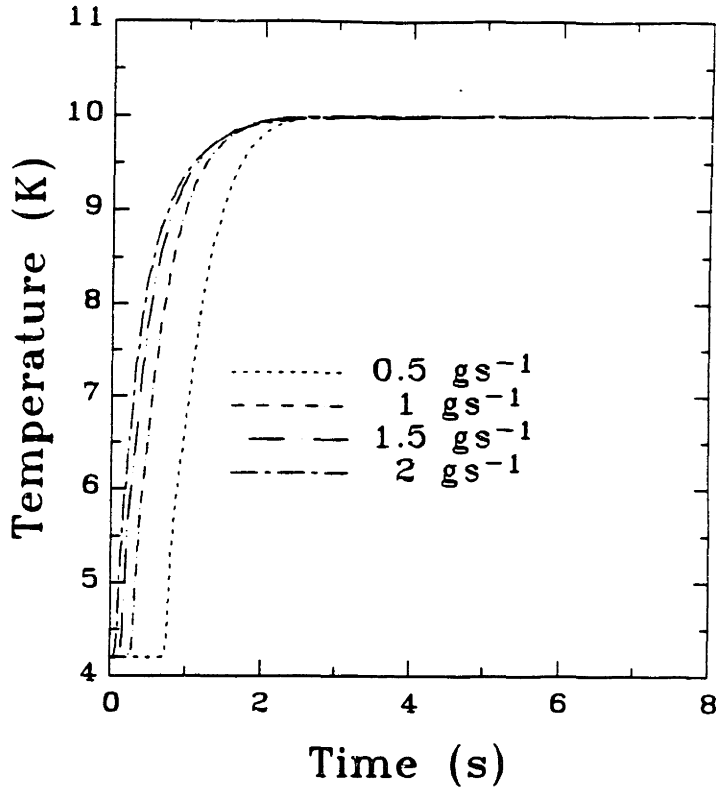

Fig. 6.4 Exiting helium temperature during a zero-field cold blow.

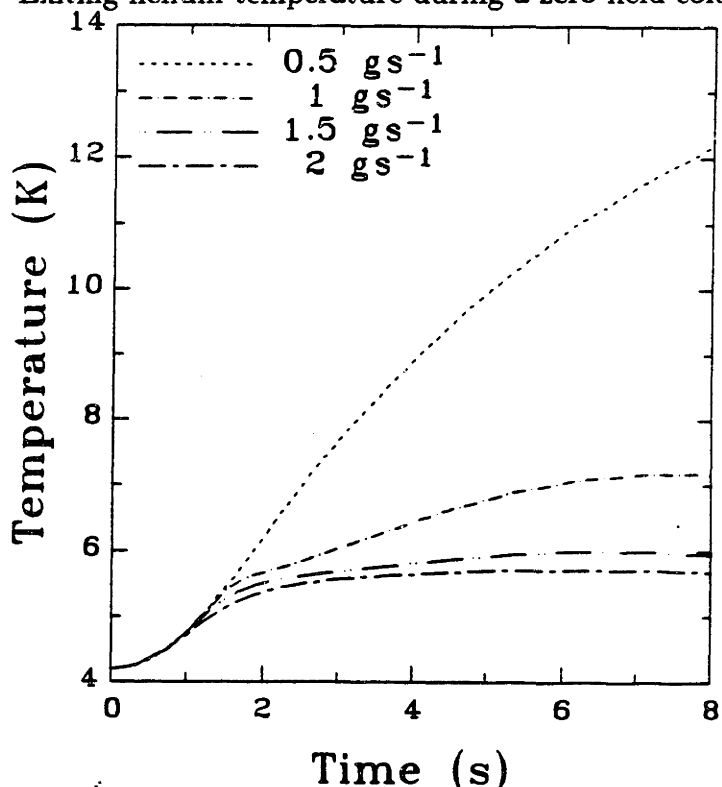

Fig. 6.5 Exiting helium temperature during a magnetization hot blow.

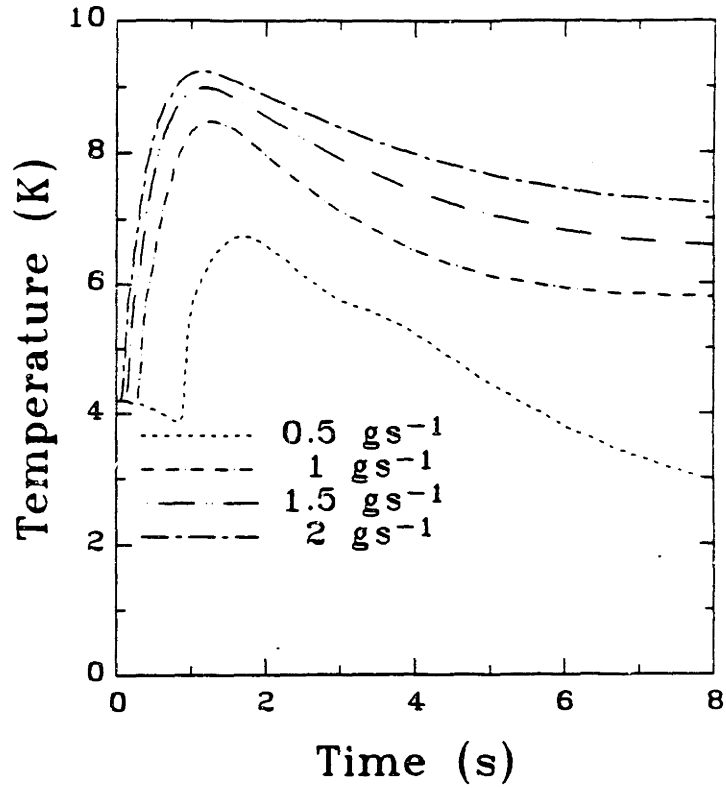

Fig. 6.6 Exiting helium temperature during a demagnetization cold blow.

Chapter 7 Conclusion

A simple model of the magnetically active regenerator was created and a computer algorithm was designed to evaluate the regenerator processes. As part of the analysis, an entropy function of applied field and temperature was derived for GGG, based on experimental magnetization data and zero-field specific heat data. The computer model was evaluated with field, helium mass flow, and reservoir conditions identical to an experimental evaluation of the regenerator. The results of the computer model were compared to the experimental results, and a large discrepancy was found. Several suspected sources of the discrepancy were investigated and it was found that hot-end helium temperature measurements and system pressure fluctuations were the most likely sources. Suggestions for improvements on the experiment have been made throughout Chapter 6, and suggestions for experimentally measuring several single-shot flow processes in the regenerator have been made in Section 6.10. For the three types of flow processes mentioned, results predicted by the computer model are shown.

Unfortunately, the small amount of existing experimental data does not adequately test the computer model. Improvements on temperature measurement and pressure compensation should be implemented so that future data will be more reliable. Considerably more experimental data is necessary in order to test the computer model more thoroughly. With adequate data, it should be possible to improve the model so that it predicts the performance of the regenerator with greater accuracy.

Appendix A Maxwell Relations For a Magnetic Material

The derivation of the Maxwell relations for a magnetic material undergoing a magnetic work process is analogous to that for a material undergoing a $p\,dv$ work process. The applied field H is analogous to the pressure p, and the quantity $-\mu_0 v\mathcal{M}$ is analogous to v. The differential magnetic work is

$$dw_{mag} = -\mu_0 v H\, d\mathcal{M} \tag{a1}$$

where μ_0 is the permeability of free space, v is specific volume, and $d\mathcal{M}$ is the differential change in magnetization.

The differential combined first and second law for a magnetic material undergoing a reversible heat and magnetic work process, derived in Chapter 2, is

$$\begin{aligned} du_{mag} &= T\,ds - dw_{mag} \\ &= T\,ds + \mu_0 v H\, d\mathcal{M} \end{aligned} \tag{a2}$$

where u_{mag} is the specific internal energy, T is the temperature, and s is the specific entropy. The magnetic enthalpy is defined as

$$h_{mag} = u_{mag} - \mu_0 v\mathcal{M}H \tag{a3}$$

The differential magnetic enthalpy, dh_{mag}, is then

$$\begin{aligned} dh_{mag} &= du_{mag} - \mu_0 v H\, d\mathcal{M} - \mu_0 v\mathcal{M}\, dH \\ &= T\,ds + \mu_0 v H\, d\mathcal{M} - \mu_0 v H\, d\mathcal{M} - \mu_0 v\mathcal{M}\, dH \\ &= T\,ds - \mu_0 v\mathcal{M}\, dH \end{aligned} \tag{a4}$$

The Helmholtz free energy for a magnetic system is defined as

$$f_{mag} = u_{mag} - Ts \tag{a5}$$

The differential Helmholtz free energy, df, is then

$$\begin{aligned} df_{mag} &= du_{mag} - T\,ds - s\,dT \\ &= T\,ds + \mu_0 v H\, d\mathcal{M} - T\,ds - s\,dT \\ &= -s\,dT + \mu_0 v H\, d\mathcal{M} \end{aligned} \tag{a6}$$

The Gibbs free energy for a magnetic system is defined as

$$g_{mag} = h_{mag} - Ts \tag{a7}$$

The differential Gibbs free energy, dg_{mag}, is then

$$\begin{aligned} dg_{mag} &= dh_{mag} - T\,ds - s\,dT \\ &= T\,ds - \mu_0 v\mathcal{M}\,dH - T\,ds - s\,dT \\ &= -s\,dT - \mu_0 v\mathcal{M}\,dH \end{aligned} \tag{a8}$$

The differential internal energy, enthalpy, Helmholtz free energy, and Gibbs free energy may also be expressed as the exact differentials

$$du_{mag} = \left(\frac{\partial u_{mag}}{\partial s}\right)_{\mathcal{M}} ds + \left(\frac{\partial u_{mag}}{\partial \mathcal{M}}\right)_{s} d\mathcal{M} \tag{a9}$$

$$dh_{mag} = \left(\frac{\partial h_{mag}}{\partial s}\right)_{H} ds + \left(\frac{\partial h_{mag}}{\partial H}\right)_{s} dH \tag{a10}$$

$$df_{mag} = \left(\frac{\partial f_{mag}}{\partial T}\right)_{\mathcal{M}} dT + \left(\frac{\partial f_{mag}}{\partial \mathcal{M}}\right)_{T} d\mathcal{M} \tag{a11}$$

$$dg_{mag} = \left(\frac{\partial g_{mag}}{\partial T}\right)_{H} dT + \left(\frac{\partial g_{mag}}{\partial H}\right)_{T} dH \tag{a12}$$

By comparing Eq. (a2) to Eq. (a9), Eq. (a4) to Eq. (a10), Eq. (a6) to Eq. (a11), and Eq. (a8) to Eq. (a12), the following relationships can be determined:

$$T = \left(\frac{\partial u_{mag}}{\partial s}\right)_{\mathcal{M}} = \left(\frac{\partial h_{mag}}{\partial s}\right)_{H} \tag{a13}$$

$$H = \left(\frac{\partial u_{mag}}{\partial \mathcal{M}}\right)_{s} = \left(\frac{\partial f_{mag}}{\partial \mathcal{M}}\right)_{T} \tag{a14}$$

$$-s = \left(\frac{\partial f_{mag}}{\partial T}\right)_{\mathcal{M}} = \left(\frac{\partial g_{mag}}{\partial T}\right)_{H} \tag{a15}$$

$$-\mu_0 v\mathcal{M} = \left(\frac{\partial h_{mag}}{\partial H}\right)_{s} = \left(\frac{\partial g_{mag}}{\partial H}\right)_{T} \tag{a16}$$

Equations (a13)–(a16) are sometimes called the "thermodynamic definitions" of T, H, $-s$, and $-\mu_0 v\mathcal{M}$.

Because du_{mag}, dh_{mag}, df_{mag}, and dg_{mag} are exact differentials, their mixed second order partial derivatives are equal. That is, given a property $z = z(x, y)$,

$$\frac{\partial^2 z}{\partial x \, \partial y} = \frac{\partial^2 z}{\partial y \, \partial x} \tag{a17}$$

Equating the mixed second order partial derivatives of u_{mag}, h_{mag}, f_{mag}, and g_{mag}, we get

$$\frac{\partial^2 u_{mag}}{\partial s \, \partial \mathcal{M}} = \left(\frac{\partial T}{\partial \mathcal{M}}\right)_s = \left(\frac{\partial H}{\partial s}\right)_{\mathcal{M}} \tag{a18}$$

$$\frac{\partial^2 h_{mag}}{\partial s \, \partial H} = \left(\frac{\partial T}{\partial H}\right)_s = -\mu_0 v \left(\frac{\partial \mathcal{M}}{\partial s}\right)_H \tag{a19}$$

$$\frac{\partial^2 f_{mag}}{\partial T \, \partial \mathcal{M}} = -\left(\frac{\partial s}{\partial \mathcal{M}}\right)_T = \left(\frac{\partial H}{\partial T}\right)_{\mathcal{M}} \tag{a20}$$

$$\frac{\partial^2 g_{mag}}{\partial T \, \partial H} = -\left(\frac{\partial s}{\partial H}\right)_T = -\mu_0 v \left(\frac{\partial \mathcal{M}}{\partial T}\right)_H \tag{a21}$$

Equations (a18)–(a21) are the Maxwell relations.

Appendix B Regenerator Core Dimensions

This appendix contains the calculations of the regenerator core dimensions. Calculations of heat transfer surface area per unit length, regenerator mass, and porosity are also included. The calculated quantities are used in the numerical analyis and are also used for the "order of magnitude" calculations performed in Appendix C.

The regenerator core is constructed from 120 GGG wafers, each having a diameter of 38.1 mm, and a thickness of 2.54 mm. The wafers are epoxied together to form four stacks, each cut longitudinally into 2.54–mm strips. The strips are reassembled with 100–μm spacers to create the flow passages, and the four sections assembled. A significant amount of GGG mass is lost during the fabrication process, so when the core is assembled, the regenerator sections have elliptical cross-sections. Figure B1 shows a top view of the GGG strips placed at their original positions in the circular cross-section. About 12 strips are fabricated from each regenerator section, and each strip is approximately 2.4 mm thick. A coordinate system is drawn on Fig. B1, and important points are mapped using simple trigonometry.

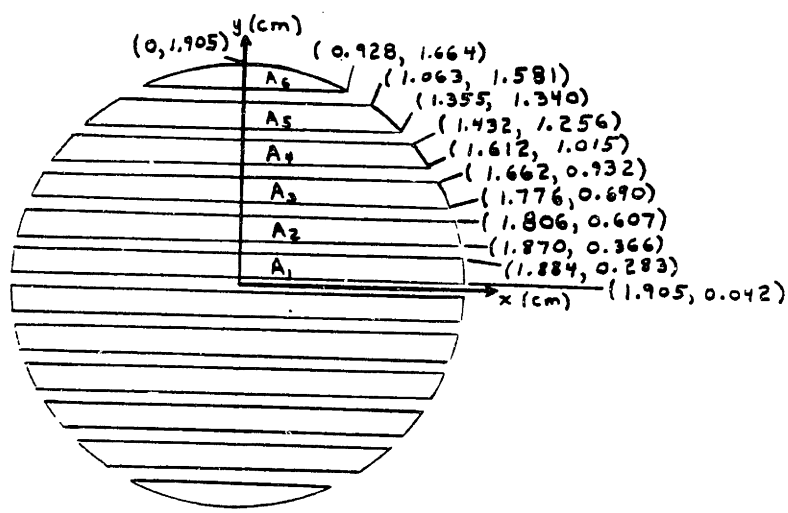

Fig. B1. Top view — circular cross-section of GGG strips (not to scale).

The surface area per unit length P is

$$\begin{aligned} P &= 4(0.9280 + 1.0634 + 1.3547 + 1.4322 + 1.6122 + 1.6166 \\ &\quad + 1.7755 + 1.8056 + 1.8695 + 1.8839 + 1.905)\,\text{cm} \\ &= 69.17\,\text{cm} \end{aligned}$$

The areas A_1, A_2, A_3, A_4, A_5, and A_6 are

$$\begin{aligned} A_1 &= \left(\frac{1.9045 + 1.8839}{2}\right)(0.241)\,\text{cm}^2 \\ &= 0.457\,\text{cm}^2 \end{aligned}$$

$$\begin{aligned} A_2 &= \left(\frac{1.8056 + 1.8695}{2}\right)(0.241)\,\text{cm}^2 \\ &= 0.443\,\text{cm}^2 \end{aligned}$$

$$\begin{aligned} A_3 &= \left(\frac{1.6616 + 1.7755}{2}\right)(0.241)\,\text{cm}^2 \\ &= 0.409\,\text{cm}^2 \end{aligned}$$

$$\begin{aligned} A_4 &= (1.4322)(1.2561)\,\text{cm}^2 - (1.6122)(1.0148)\,\text{cm}^2 \\ &\quad + \int_{1.4322\,\text{cm}}^{1.6122\,\text{cm}} \sqrt{(1.905)^2 - x^2}\,dx \\ &= 0.368\,\text{cm}^2 \end{aligned}$$

$$\begin{aligned} A_5 &= (1.0634)(1.5806)\text{cm}^2 - (1.3547)(1.3393)\,\text{cm}^2 \\ &\quad + \int_{1.0634\,\text{cm}}^{1.3547\,\text{cm}} \sqrt{(1.905)^2 - x^2}\,dx \\ &= 0.295\,\text{cm}^2 \end{aligned}$$

$$\begin{aligned} A_6 &= \int_{0}^{0.09280\,\text{cm}} \sqrt{(1.905)^2 - x^2}\,dx \\ &= 0.151\,\text{cm}^2 \end{aligned}$$

The cross-sectional area of each GGG segment (disk) is

$$\begin{aligned} A_{seg} &= 4(A_1 + A_2 + A_3 + A_4 + A_5 + A_6) \\ &= 4(0.457 + 0.443 + 0.409 + 0.368 + 0.294 + 0.151)\,\mathrm{cm}^2 \\ &= 8.488\,\mathrm{cm}^2 \end{aligned}$$

The volume of each GGG segment is

$$\begin{aligned} V_{seg} &= A_{seg} L_{seg} = (8.488\,\mathrm{cm}^2)(0.254\,\mathrm{cm} \\ &= 2.156 \end{aligned}$$

The mass of each GGG segment is

$$\begin{aligned} M_{seg} &= \rho_{GGG} V_{seg} \\ &= (7.14\,\mathrm{g\,cm}^{-3})(2.156\,\mathrm{cm}^3) \\ &= 15.39\,\mathrm{g} \end{aligned}$$

The helium volume of the regenerator consists of the flow channel spaces and the three remixing sections. The helium volume is

$$\begin{aligned} V_{He} &= (0.010\,\mathrm{cm})\left(\frac{69.17\,\mathrm{cm}}{2}\right)(30.48\,\mathrm{cm}) \\ &\quad + 3(0.038\,\mathrm{cm})\left(\frac{\pi}{4}\right)(3.81\,\mathrm{cm})^2 \\ &= 12.01\,\mathrm{cm}^3 \end{aligned}$$

The helium volume per segment is

$$\begin{aligned} V_{He,seg} &= \frac{V_{He}}{120} = \frac{12.01}{120}\,\mathrm{cm}^3 \\ &= 0.100\,\mathrm{cm}^3 \end{aligned}$$

The porosity is

$$\begin{aligned} \epsilon &= \frac{V_{He}}{120 V_{seg} + V_{He}} \\ &= \frac{12.01}{(120)(2.156) + 12.01} \\ &= 0.044 \end{aligned}$$

Appendix C Assumptions Regarding Regenerator Segments

In Chapter 3, several assumptions were stated concerning the behavior of the regenerator during flow and nonflow processes. During the processes, each of the 120 GGG segments was assumed to have one temperature as a function of time. It was assumed that there was infinite conduction through the GGG in each segment and no conduction between segments. This appendix contains calculations to justify these assumptions.

The assumption of isothermal segments is valid if the conduction resistance of each GGG segment is much smaller than both the conduction resistance of the epoxy joints connecting adjacent segments and the helium convection resistance of the segment.

The GGG conduction resistance is

$$R_{seg} = \frac{L_{seg}}{k_{GGG} A_{seg}} \tag{c1}$$

where L_{seg} is the length of a segment (0.254 cm), A_{seg} is the cross-sectional area of the regenerator (8.488 cm^2), and k_{GGG} is the conductivity of GGG. Conductivity values for GGG were obtained by curvefitting data in the temperature range of 4–10 K obtained by Daudin *et al.*[30] The resulting conductivity equation is

$$k_{GGG} = 0.2423\, T^{1.2381}\ \mathrm{W\,cm^{-1}K^{-1}} \tag{c2}$$

where T is in Kelvin. In the temperature range of 4–10 K, the GGG conductivity resistance calculated from Eqs. (c1) and (c2) is

$$7.13 \times 10^{-3}\ \mathrm{K^{-1}} \leq R_{seg} \leq 2.22 \times 10^{-2}\ \mathrm{K^{-1}} \tag{c3}$$

The conduction resistance of an epoxy joint is

$$R_{joint} = \frac{L_{joint}}{k_{joint} A_{seg}} \tag{c4}$$

where L_{joint} is the thickness of an epoxy joint (100 μm), and k_{joint} is the conductivity of the epoxy. The conductivities for several polymers in the temperature

range of 4–10 K were found in the literature[31] and a conservative value of 0.7 $\times 10^{-3}$ W cm^{-1} K^{-1} was selected for the calculation. Evaluating Eq. (c2), the value obtained for the conduction resistance of the joint is

$$R_{joint} = 1.683\,\mathrm{K}^{-1} \tag{c3}$$

and the ratio of R_{seg} to R_{joint} is

$$\frac{R_{seg}}{R_{joint}} \leq 0.013 \tag{c4}$$

The helium-GGG convection resistance for a single segment is

$$R_{conv} = \frac{1}{\hbar A_{conv}} \tag{c5}$$

where $\hbar$ is the heat transfer coefficient and A_{conv} is the heat transfer area. The heat transfer coefficient was modeled in Chapter 3 by Eq. (3.7),

$$\hbar = \frac{7.6\,k_{hel}}{d} \tag{3.7}$$

where k_{hel} is the helium conductivity and d is the flow channel width (100 μm). Appendix B contains a calculation of the heat transfer area per unit length of regenerator, which was found to be $P = 69.17$ cm^2. The heat transfer area in a single segment is

$$A_{conv} = PL_{seg} \tag{c6}$$

Combining Eqs. (c5), (3.7), and (c6) gives

$$R_{conv} = \frac{d}{7.6\,k_{hel} PL_{seg}} \tag{c7}$$

Because the helium conductivity varies significantly between 4 K and 10 K, it is necessary to compare values of R_{seg} and R_{conv} at various temperatures. Equations (c1) and (c7) have been evaluated and the results are shown in Table C1.

The GGG conduction resistance appears to be much smaller than both the conduction resistance of the epoxy joints and the helium-GGG convection resistance. The assumption of isothermal GGG segments appears to be a reasonable one.

Table C1 GGG Conduction and Convection Resistances†					
T	k_{GGG}	k_{he}	R_{seg}	R_{conv}	$\frac{R_{seg}}{R_{conv}}$
4	1.35	0.209×10^{-3}	2.22×10^{-2}	0.358	0.062
5	1.78	0.231×10^{-3}	1.68×10^{-2}	0.324	0.052
6	2.23	0.168×10^{-3}	1.34×10^{-2}	0.446	0.030
7	2.70	0.157×10^{-3}	1.11×10^{-2}	0.477	0.023
8	3.18	0.164×10^{-3}	9.41×10^{-3}	0.457	0.021
9	3.68	0.174×10^{-3}	2.13×10^{-3}	0.430	0.019
10	4.19	0.184×10^{-3}	7.14×10^{-3}	0.407	0.018

†T is in units of K; k_{GGG} and k_{he} are in units of (W cm^{-1} K^{-1}); and R_{seg} and R_{conv} are in units of K^{-1}.

The steady-state conduction loss through the regenerator between 10 K and 4.2 K was calculated by solving the conduction equation for the composite of 120 GGG segments and 119 epoxy joints. The following system of differential equations was solved:

$$q = -k_{GGG} A_{seg} \frac{dT}{dx} \qquad (0 \le x \le L_{seg})$$

$$q = -k_{GGG} A_{seg} \frac{dT}{dx} \qquad (L_{seg} \le x \le L_{seg} + L_{joint})$$

$$q = -k_{GGG} A_{seg} \frac{dT}{dx} \qquad (L_{seg} + L_{joint} \le x \le 2\,L_{seg} + L_{joint})$$

$$\vdots$$

$$q = -k_{GGG} A_{seg} \frac{dT}{dx} \qquad (119\,L_{seg} + 119\,L_{joint} \le x \le 120\,L_{seg} + 119\,L_{joint}) \quad (c8)$$

The boundary conditions are:

$$T = 4.2\,\mathrm{K} \qquad \text{at } x = 0 \quad (c9)$$

$$T = 10\,\mathrm{K} \qquad \text{at } x = 120\,L_{seg} + 119\,L_{joint} \quad (c10)$$

The conduction q is constant throughout the regenerator. The steady-state conduction resulting from the solutions of Eqs. (c8)–(c10) is 0.039 W, which is small

compared to the 1 W of refrigeration expected out of the device. The temperature profile for the steady-state conduction through the regenerator is shown in Fig. C1. The figure illustrates the isothermal behavior of the GGG segments.

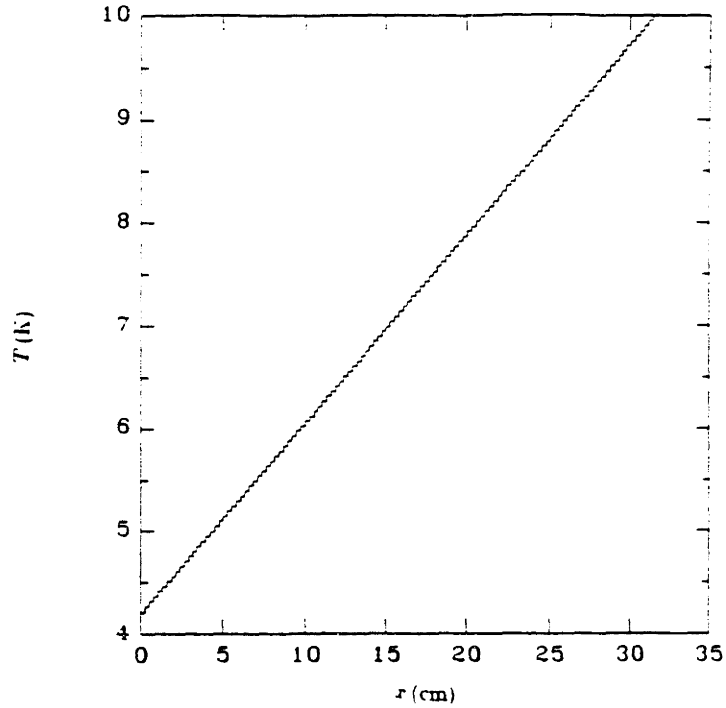

Fig. C1. Temperature Profile for Steady-state Conduction.

Appendix D Magnetization Curvefits

This appendix contains plots of all the curvefits of $\mu_0 H/v\mathcal{M}$ as a polynomial function of $\mu_0 H$. Figs. D–1 through D–43 show the curvefits for temperatures between 1 K and 25 K. On each plot are the values of coefficients c_0, c_1, c_2, c_3, and c_4 for the curvefit equation

$$\frac{\mu_0 H}{v\mathcal{M}} = c_0 = c_1\mu_0 H + c_2(\mu_0 H)^2 + c_3(\mu_0 H)^3 + c_4(\mu_0 H)^4 \qquad (d1)$$

Also included are plots of the curvefits of the coefficients c_0, c_1, c_2, c_3, and c_4 as polynomial functions of T. The equations of the curvefit coefficients are found in Chapter 4.

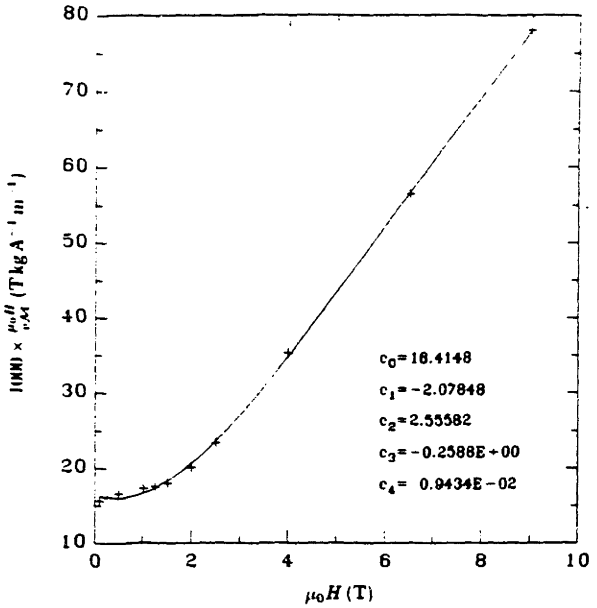

Fig. D-1 $\frac{\mu_0 H}{\nu \mathcal{M}}$ vs. T at 1 K

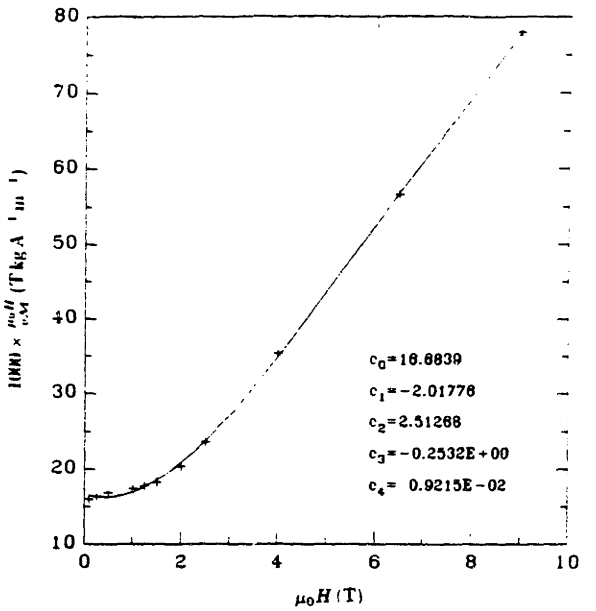

Fig. D-2 $\frac{\mu_0 H}{\nu \mathcal{M}}$ vs. T at 1.1 K

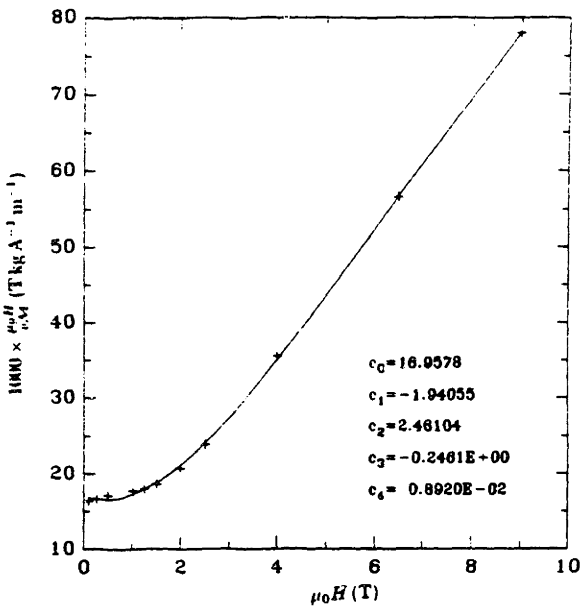

Fig. D-3 $\frac{\mu_0 H}{\nu \mathcal{M}}$ vs. T at 1.2 K

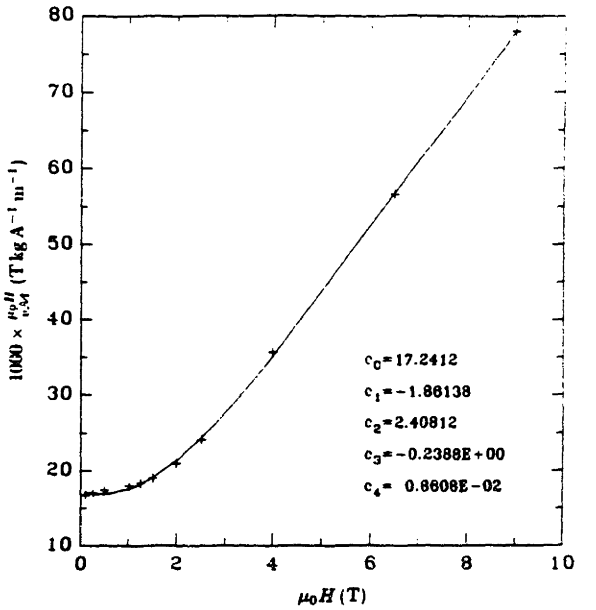

Fig. D-4 $\frac{\mu_0 H}{\nu \mathcal{M}}$ vs. T at 1.3 K

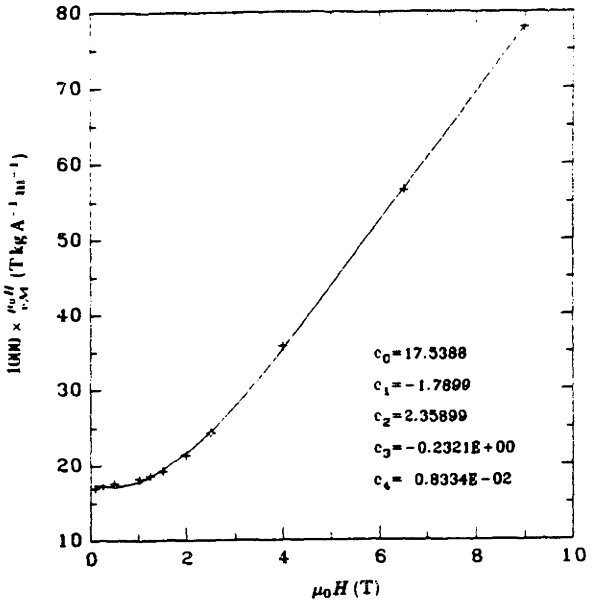

Fig. D-5 $\frac{\mu_0 H}{\upsilon \mathcal{M}}$ vs. T at 1.4 K

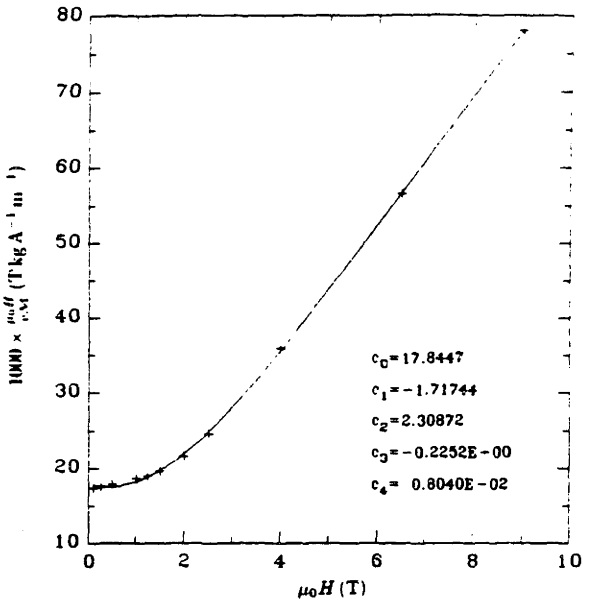

Fig. D-6 $\frac{\mu_0 H}{\upsilon \mathcal{M}}$ vs. T at 1.5 K

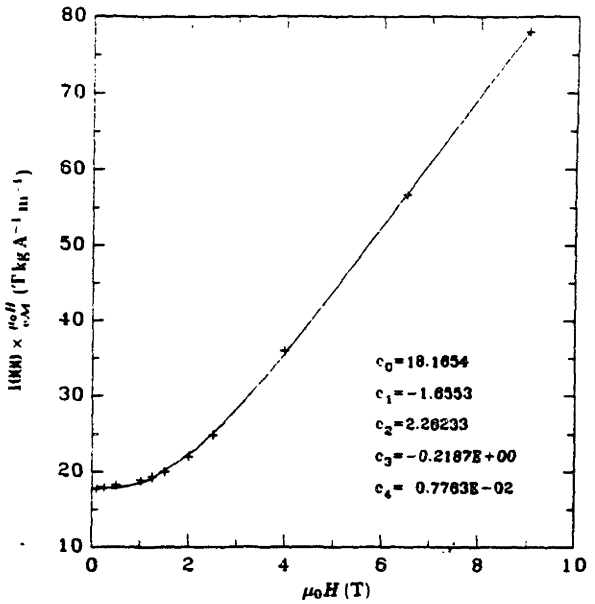

Fig. D-7 $\frac{\mu_0 H}{\upsilon \mathcal{M}}$ vs. T at 1.6 K

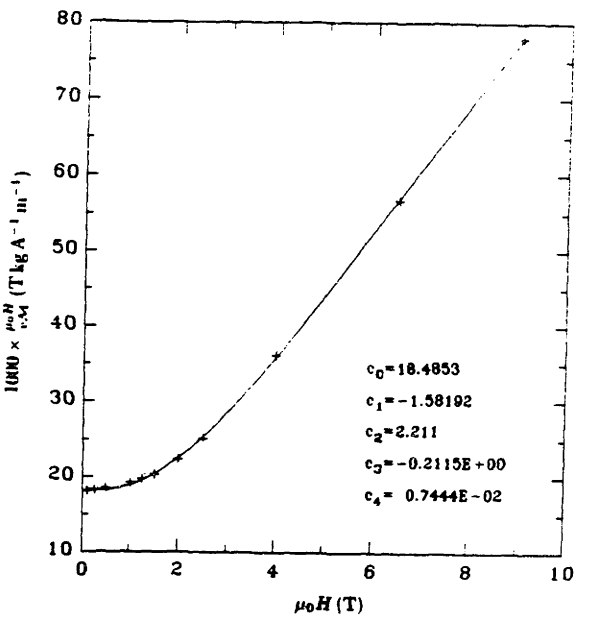

Fig. D-8 $\frac{\mu_0 H}{\upsilon \mathcal{M}}$ vs. T at 1.7 K

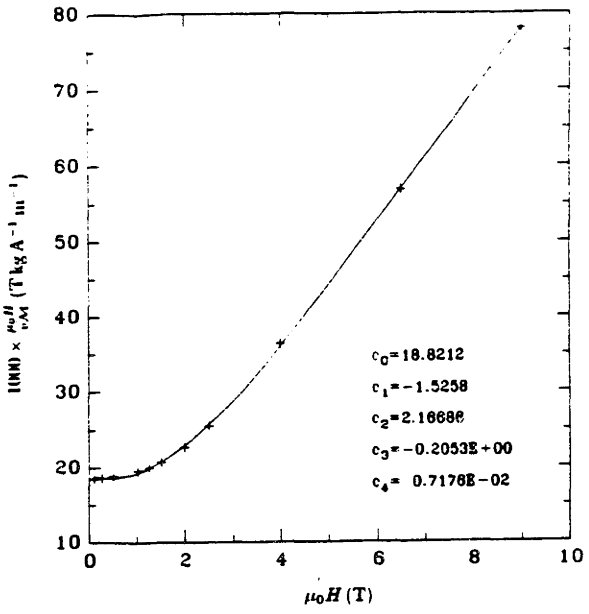

Fig. D-9 $\frac{\mu_0 H}{\nu \mathcal{M}}$ vs. T at 1.8 K

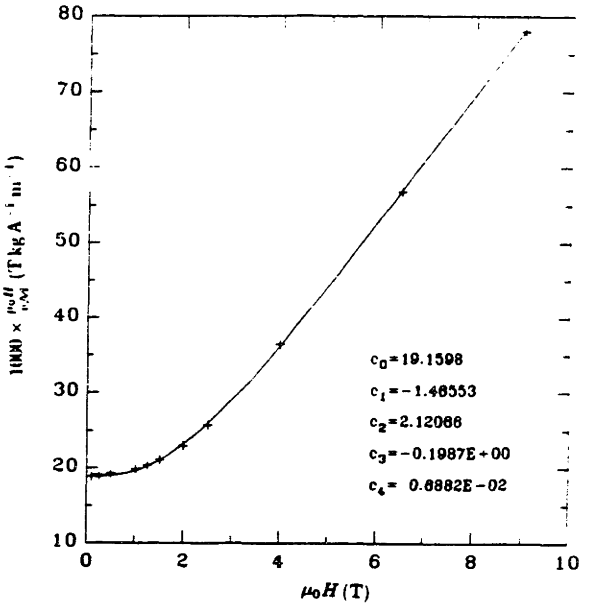

Fig. D-10 $\frac{\mu_0 H}{\nu \mathcal{M}}$ vs. T at 1.9 K

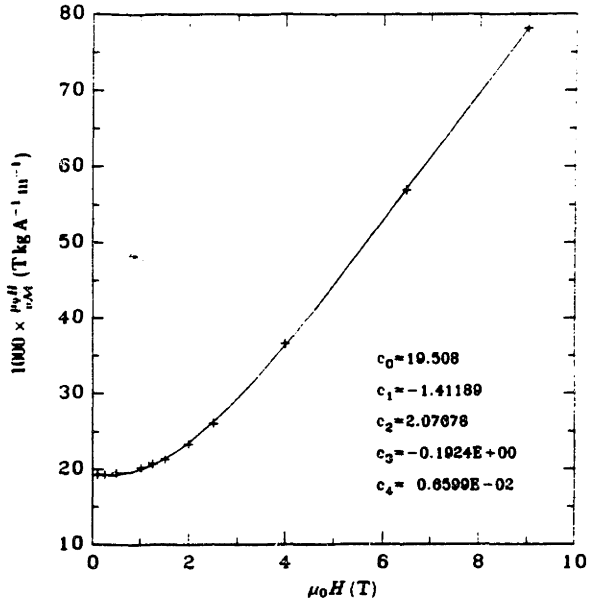

Fig. D-11 $\frac{\mu_0 H}{\nu \mathcal{M}}$ vs. T at 2 K

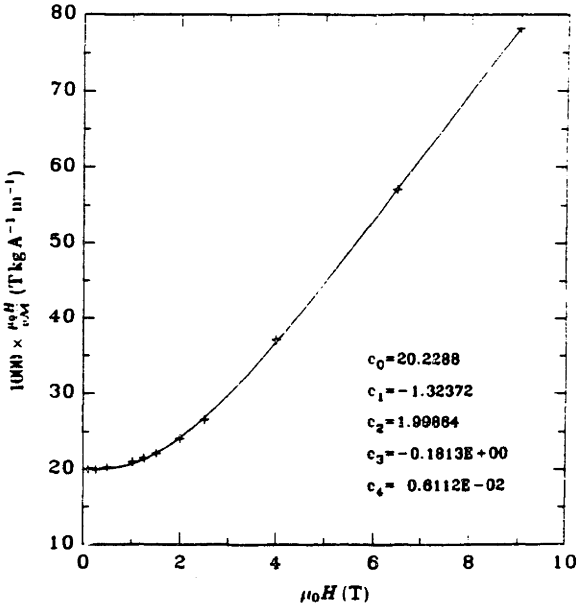

Fig. D-12 $\frac{\mu_0 H}{\nu \mathcal{M}}$ vs. T at 2.2 K

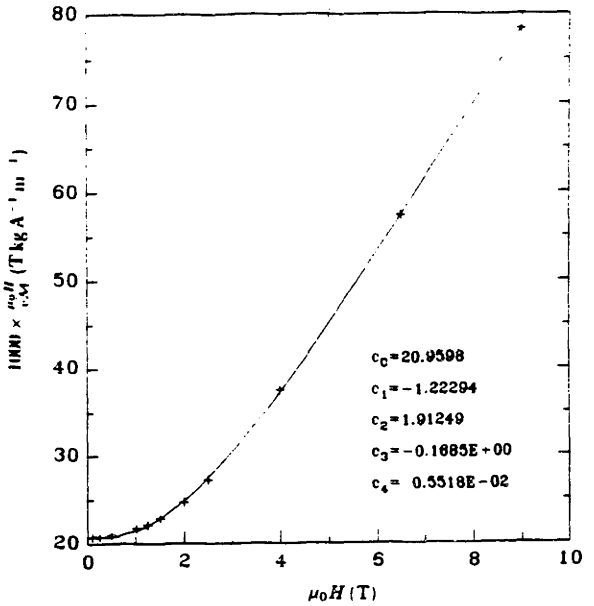

Fig. D-13 $\frac{\mu_0 H}{v\mathcal{M}}$ vs. T at 2.4 K

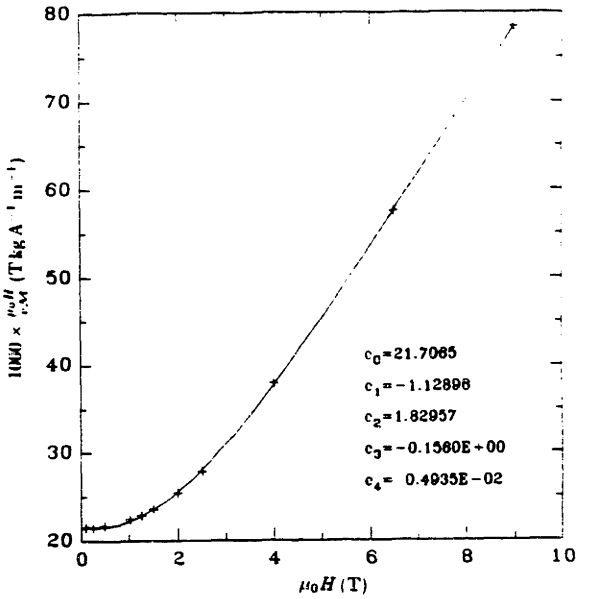

Fig. D-14 $\frac{\mu_0 H}{v\mathcal{M}}$ vs. T at 2.6 K

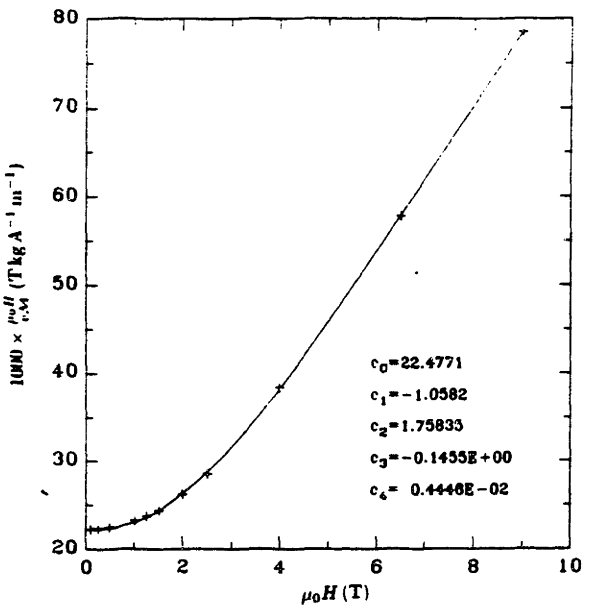

Fig. D-15 $\frac{\mu_0 H}{v\mathcal{M}}$ vs. T at 2.8 K

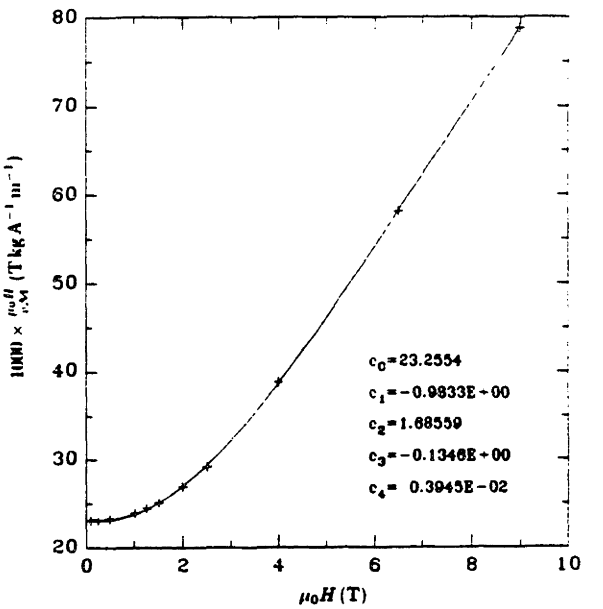

Fig. D-16 $\frac{\mu_0 H}{v\mathcal{M}}$ vs. T at 3 K

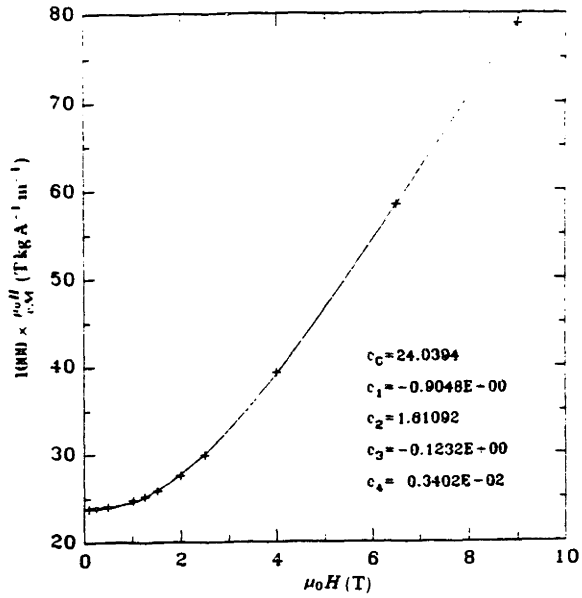

Fig. D-17 $\frac{\mu_0 H}{\nu \mathcal{M}}$ vs. T at 3.2 K

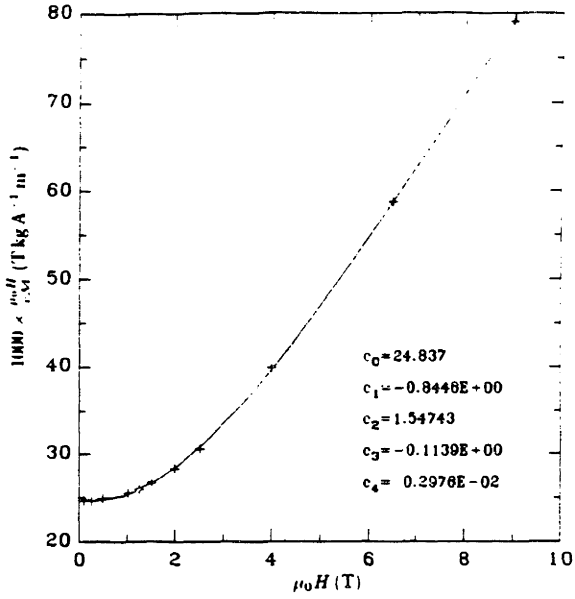

Fig. D-18 $\frac{\mu_0 H}{\nu \mathcal{M}}$ vs. T at 3.4 K

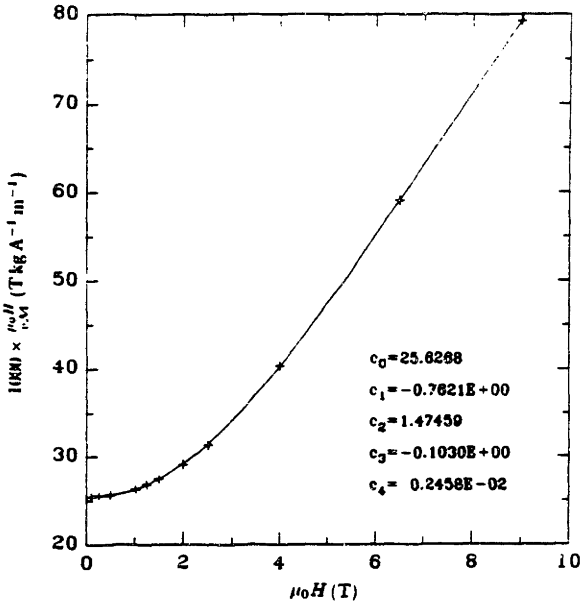

Fig. D-19 $\frac{\mu_0 H}{\nu \mathcal{M}}$ vs. T at 3.6 K

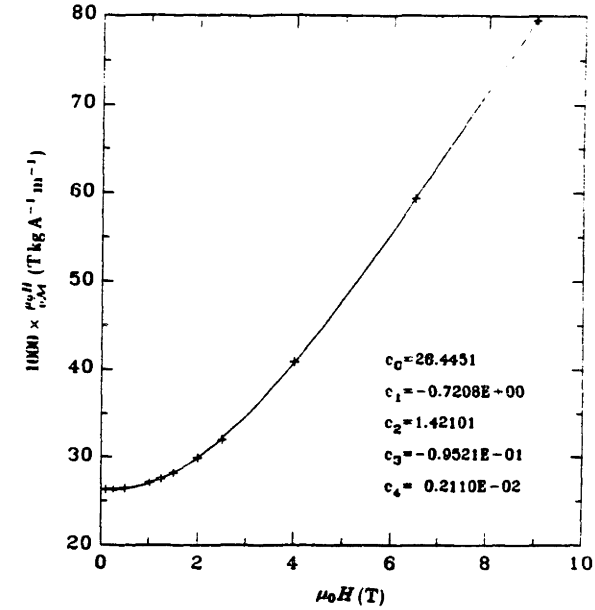

Fig. D-20 $\frac{\mu_0 H}{\nu \mathcal{M}}$ vs. T at 3.8 K

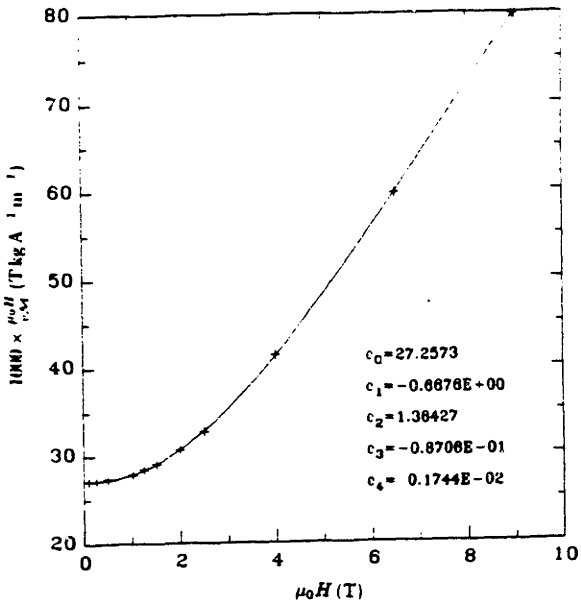

Fig. D-21 $\frac{\mu_0 H}{\nu \mathcal{M}}$ vs. T at 4 K

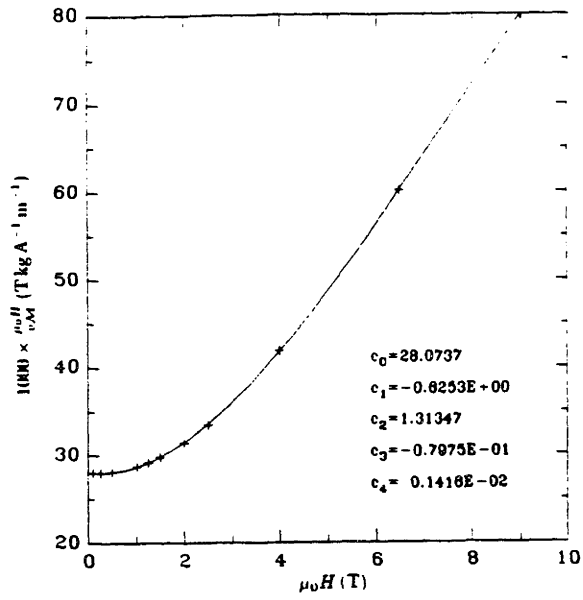

Fig. D-22 $\frac{\mu_0 H}{\nu \mathcal{M}}$ vs. T at 4.2 K

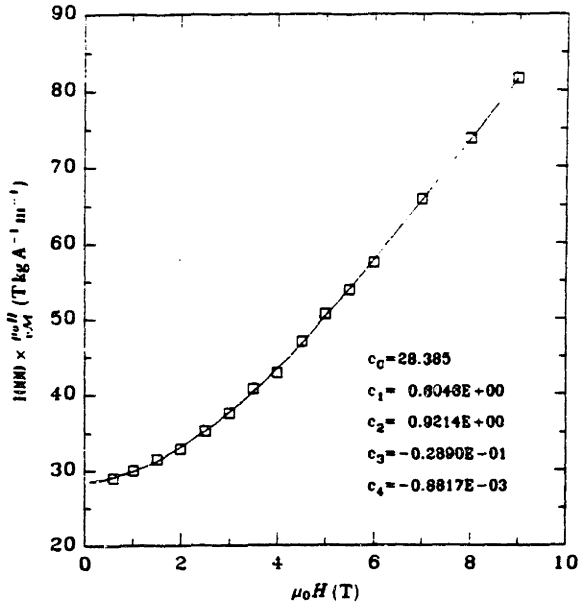

Fig. D-23 $\frac{\mu_0 H}{\nu \mathcal{M}}$ vs. T at 5 K

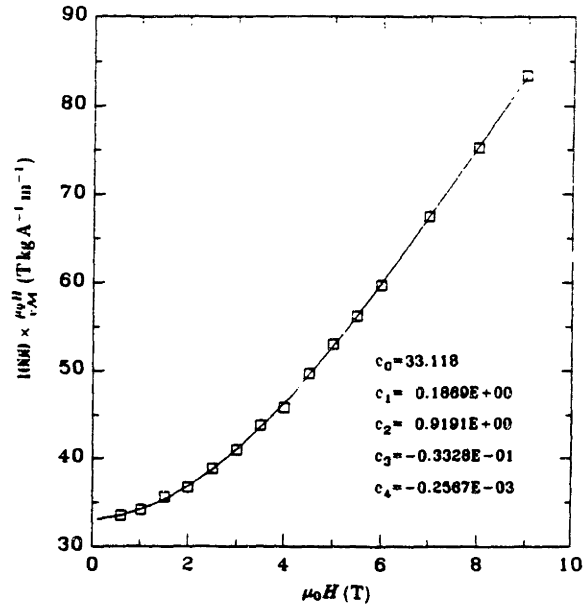

Fig. D-24 $\frac{\mu_0 H}{\nu \mathcal{M}}$ vs. T at 6 K

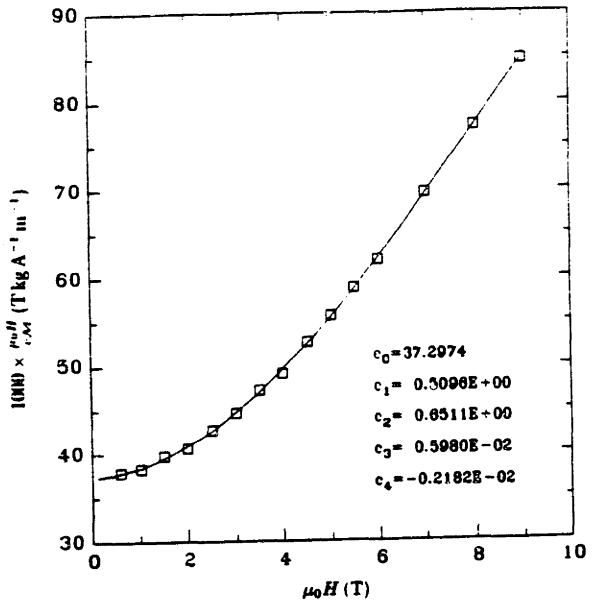

Fig. D-25 $\frac{\mu_0 H}{\nu \mathcal{M}}$ vs. T at 7 K

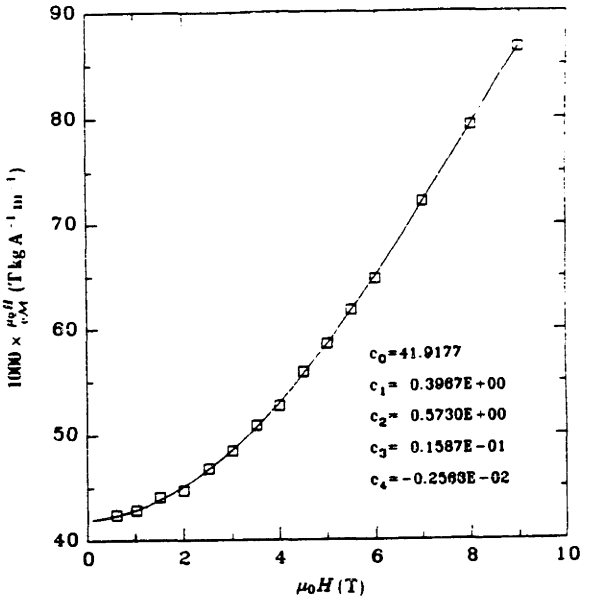

Fig. D-26 $\frac{\mu_0 H}{\nu \mathcal{M}}$ vs. T at 8 K

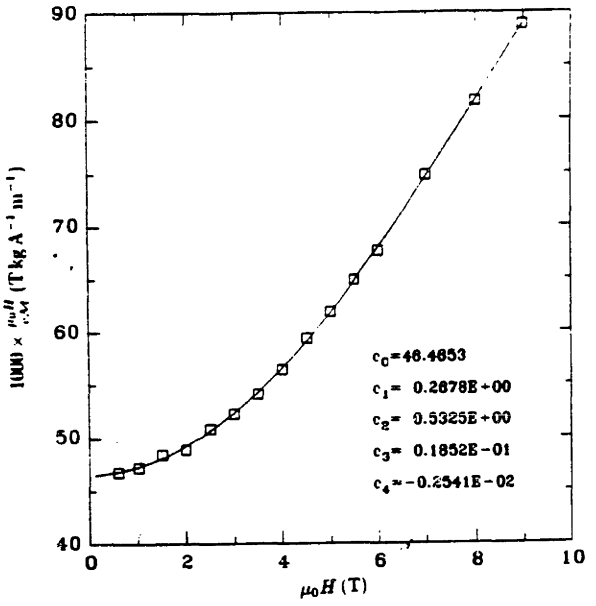

Fig. D-27 $\frac{\mu_0 H}{\nu \mathcal{M}}$ vs. T at 9 K

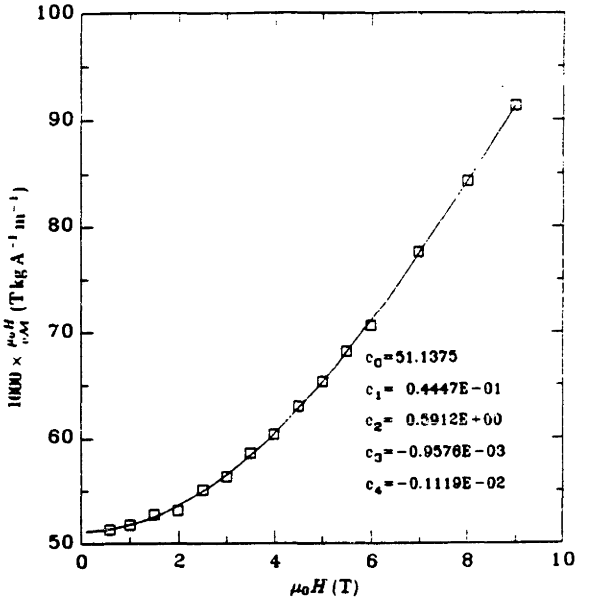

Fig. D-28 $\frac{\mu_0 H}{\nu \mathcal{M}}$ vs. T at 10 K

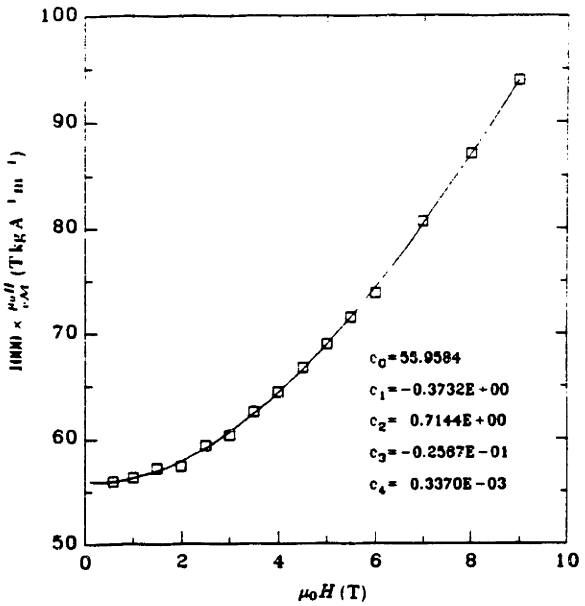

Fig. D-29 $\frac{\mu_0 H}{\upsilon \mathcal{M}}$ vs. T at 11 K

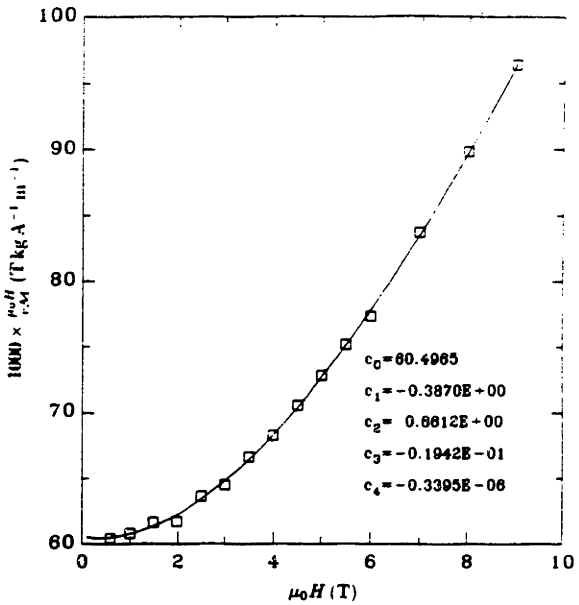

Fig. D-30 $\frac{\mu_0 H}{\upsilon \mathcal{M}}$ vs. T at 12 K

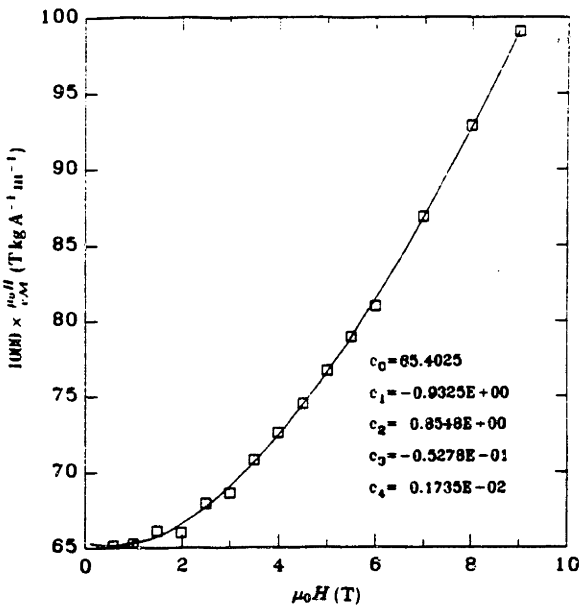

Fig. D-31 $\frac{\mu_0 H}{\upsilon \mathcal{M}}$ vs. T at 13 K

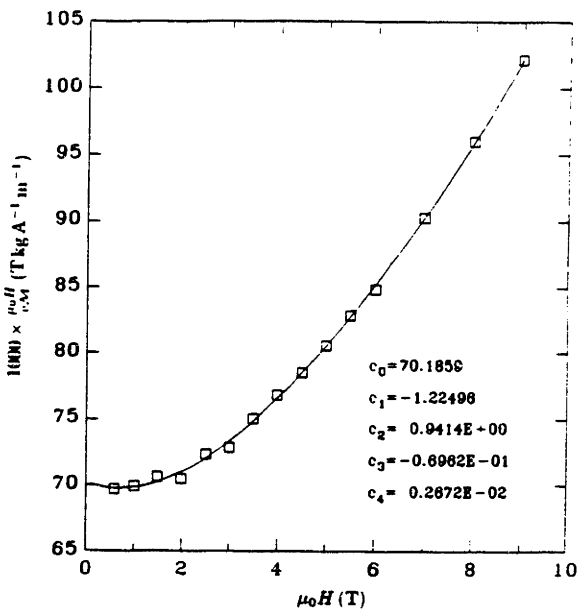

Fig. D-32 $\frac{\mu_0 H}{\upsilon \mathcal{M}}$ vs. T at 14 K

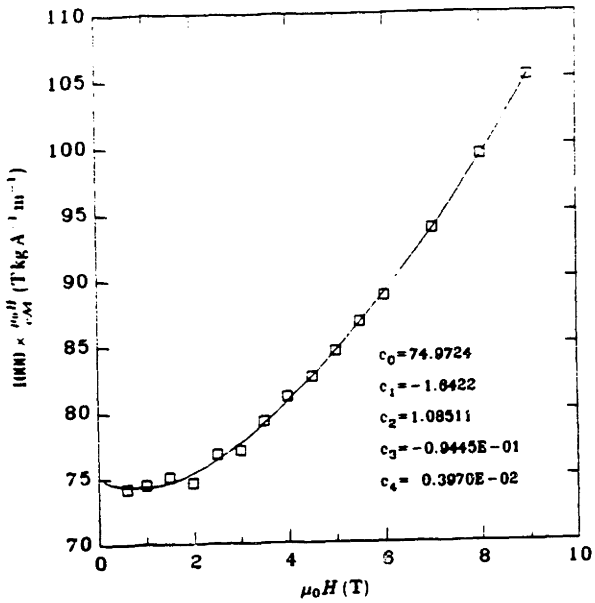

Fig. D-33 $\frac{\mu_0 H}{\nu \mathcal{M}}$ vs. T at 15 K

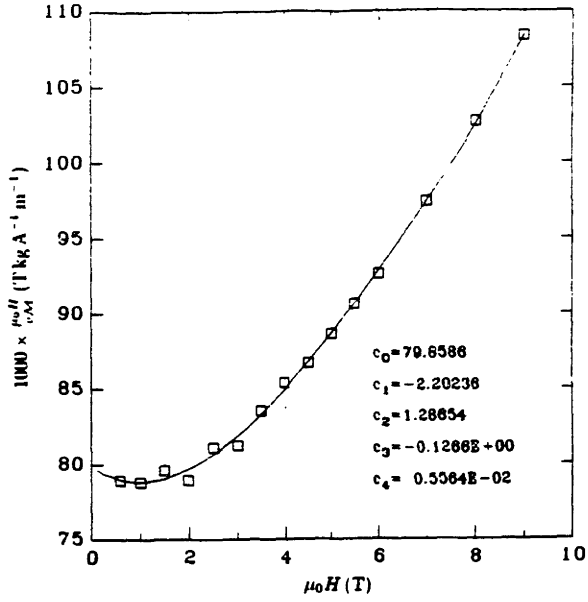

Fig. D-34 $\frac{\mu_0 H}{\nu \mathcal{M}}$ vs. T at 16 K

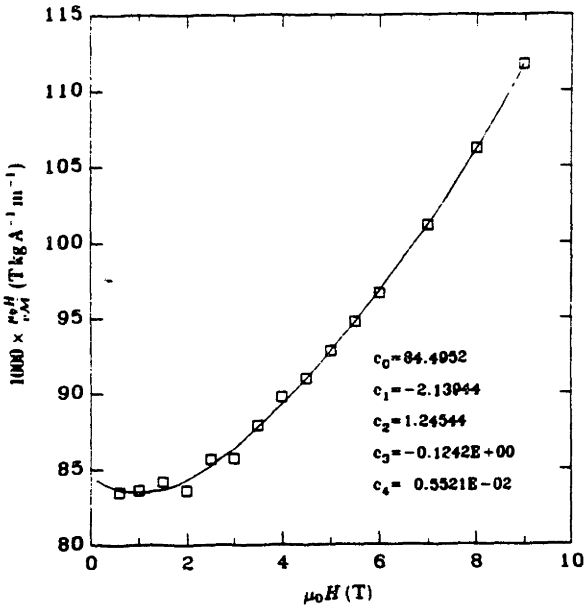

Fig. D-35 $\frac{\mu_0 H}{\nu \mathcal{M}}$ vs. T at 17 K

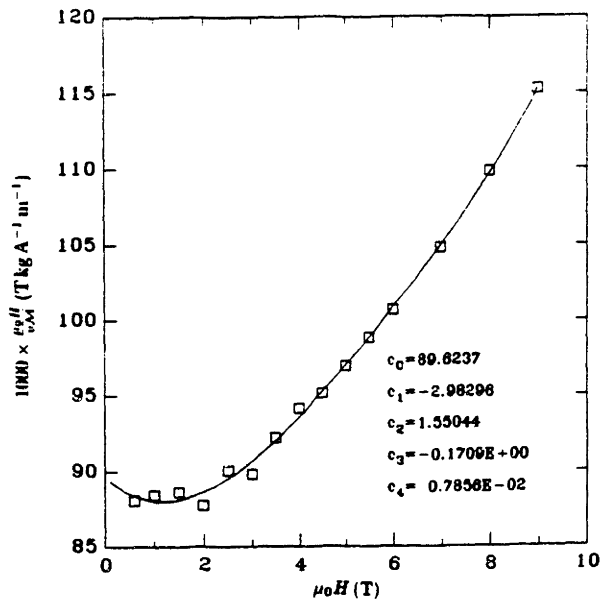

Fig. D-36 $\frac{\mu_0 H}{\nu \mathcal{M}}$ vs. T at 18 K

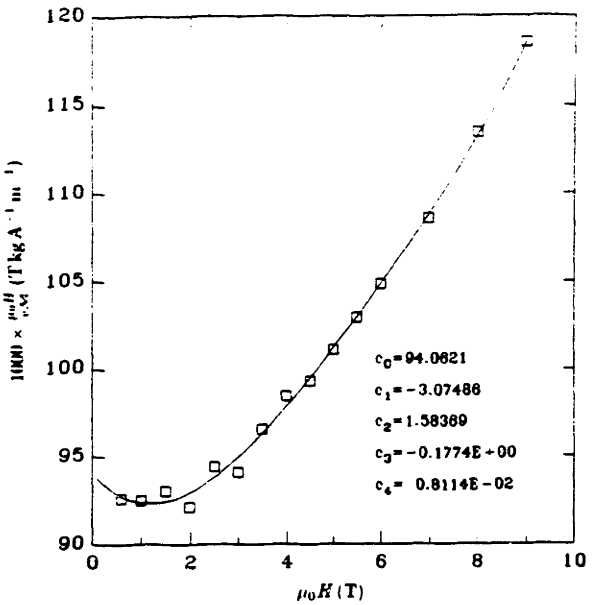

Fig. D-37 $\frac{\mu_0 H}{\upsilon \mathcal{M}}$ vs. T at 19 K

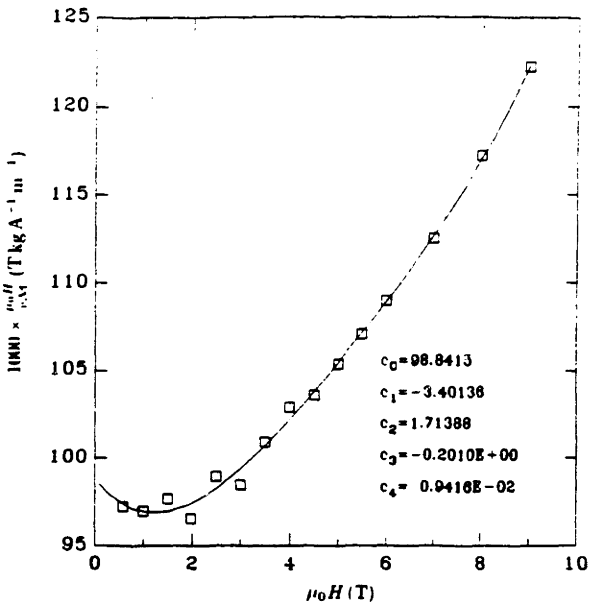

Fig. D-38 $\frac{\mu_0 H}{\upsilon \mathcal{M}}$ vs. T at 20 K

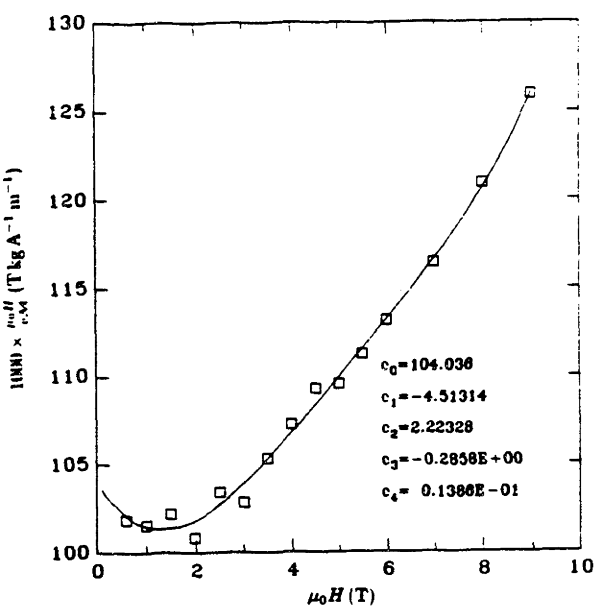

Fig. D-39 $\frac{\mu_0 H}{\upsilon \mathcal{M}}$ vs. T at 21 K

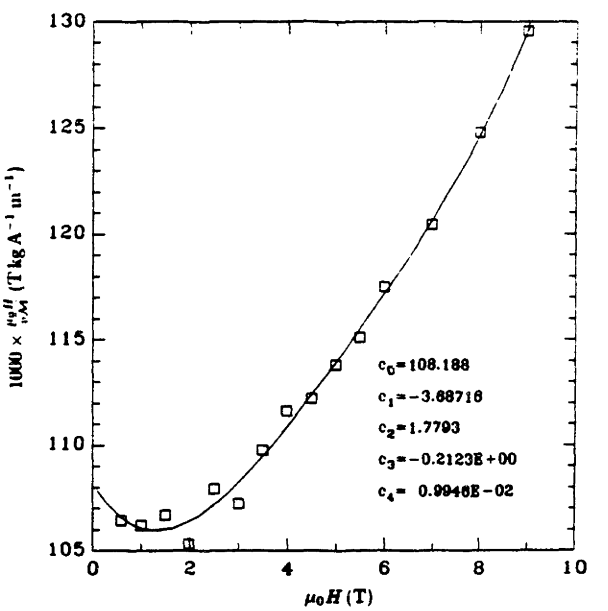

Fig. D-40 $\frac{\mu_0 H}{\upsilon \mathcal{M}}$ vs. T at 22 K

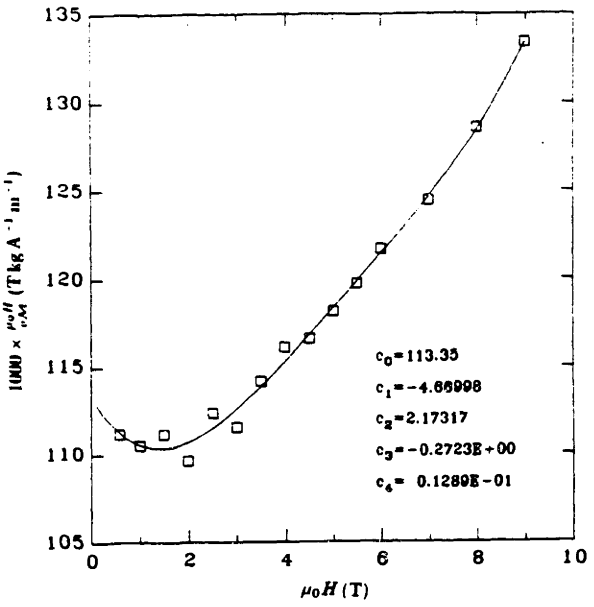

Fig. D-41 $\frac{\mu_0 H}{\upsilon \mathcal{M}}$ vs. T at 1 K

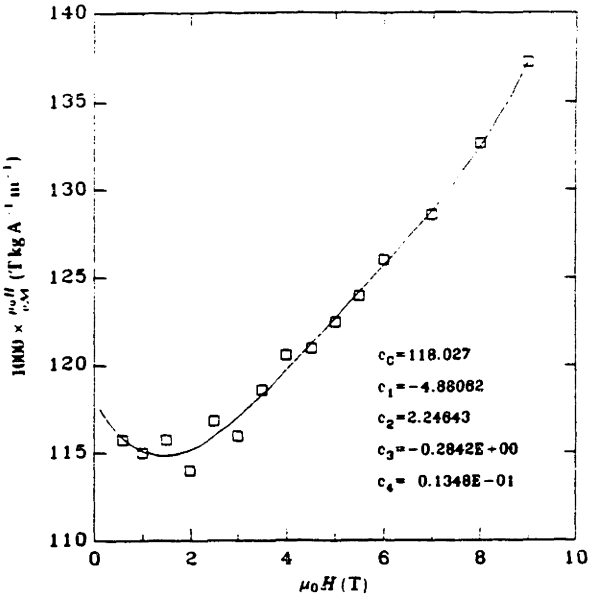

Fig. D-42 $\frac{\mu_0 H}{\upsilon \mathcal{M}}$ vs. T at 1.1 K

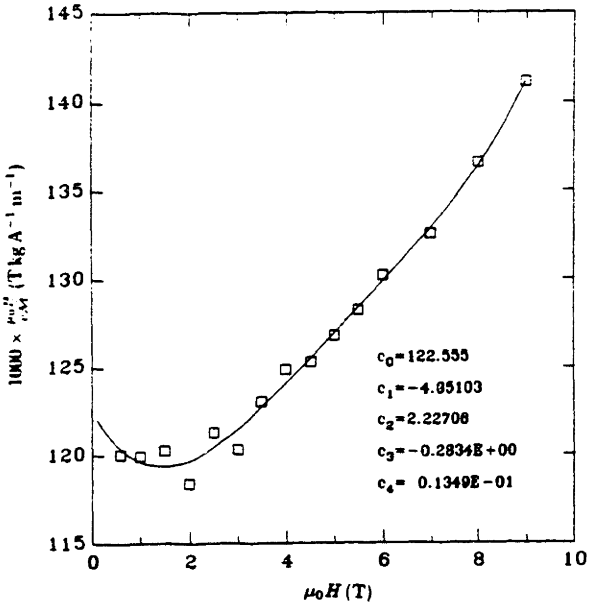

Fig. D-43 $\frac{\mu_0 H}{\upsilon \mathcal{M}}$ vs. T at 1.2 K

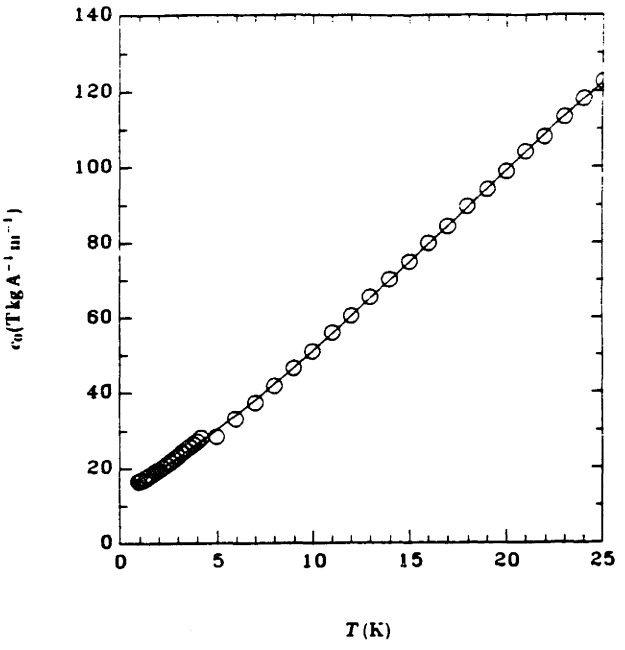

Fig. D-44 Curvefit of c_0 as a polynomial of T.

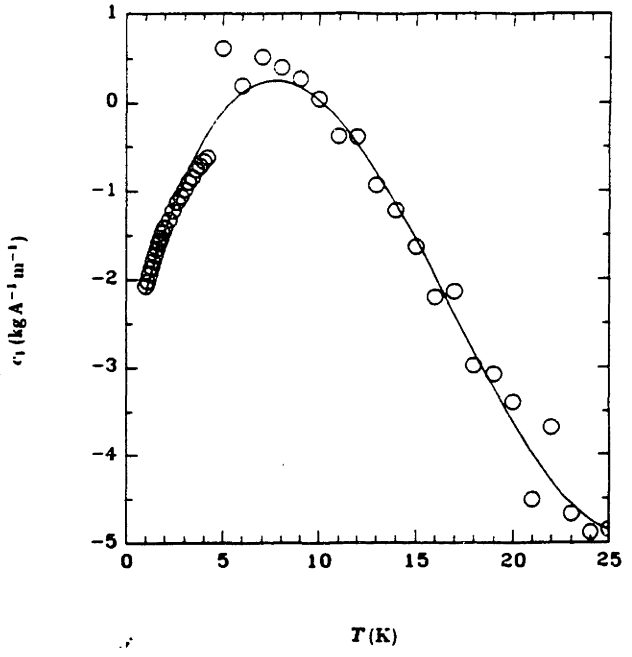

Fig. D-45 Curvefit of c_1 as a polynomial of T.

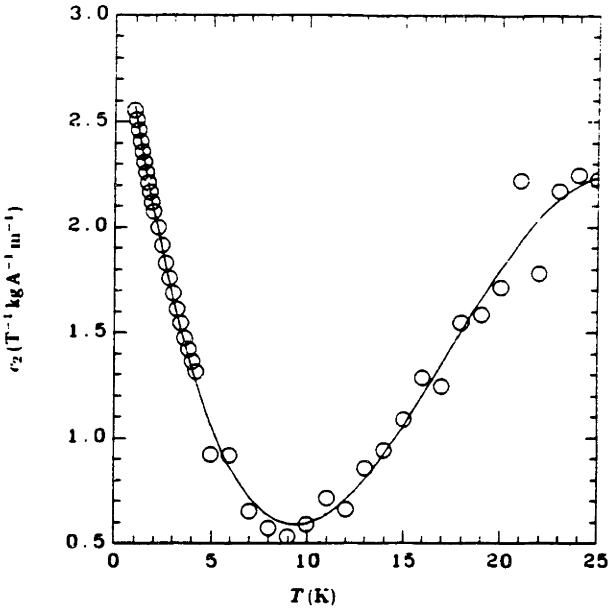

Fig. D-46 Curvefit of c_2 as a polynomial of T.

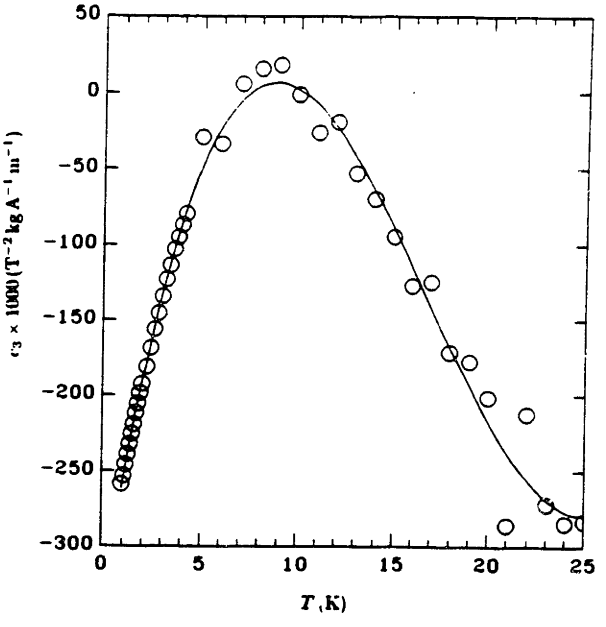

Fig. D-47 Curvefit of c_3 as a polynomial of T.

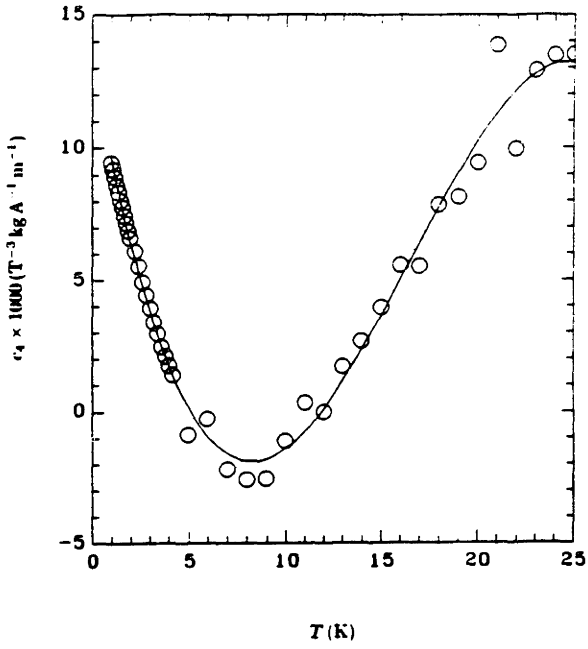

Fig. D-48 Curvefit of c_4 as a polynomial of T.

Appendix E Thermodynamic Properties of GGG

This appendix contains graphs and tables of the thermodynamic properties derived in Chapter 4. the properties are all expressed in SI units.

The contents of this appendix are 1) a $v\mathcal{M}$ vs. T plot 2) $\mu_0 H$ vs. $v\mathcal{M}$ plot 3) a T–s plot 4) an s–T plot and 5) tables of $v\mathcal{M}$, C_H, $v(\partial\mathcal{M}/\partial T)_H$, and s over the temperature range of 1.8 k to 25 K and over the field range of 0 T to 7 T.

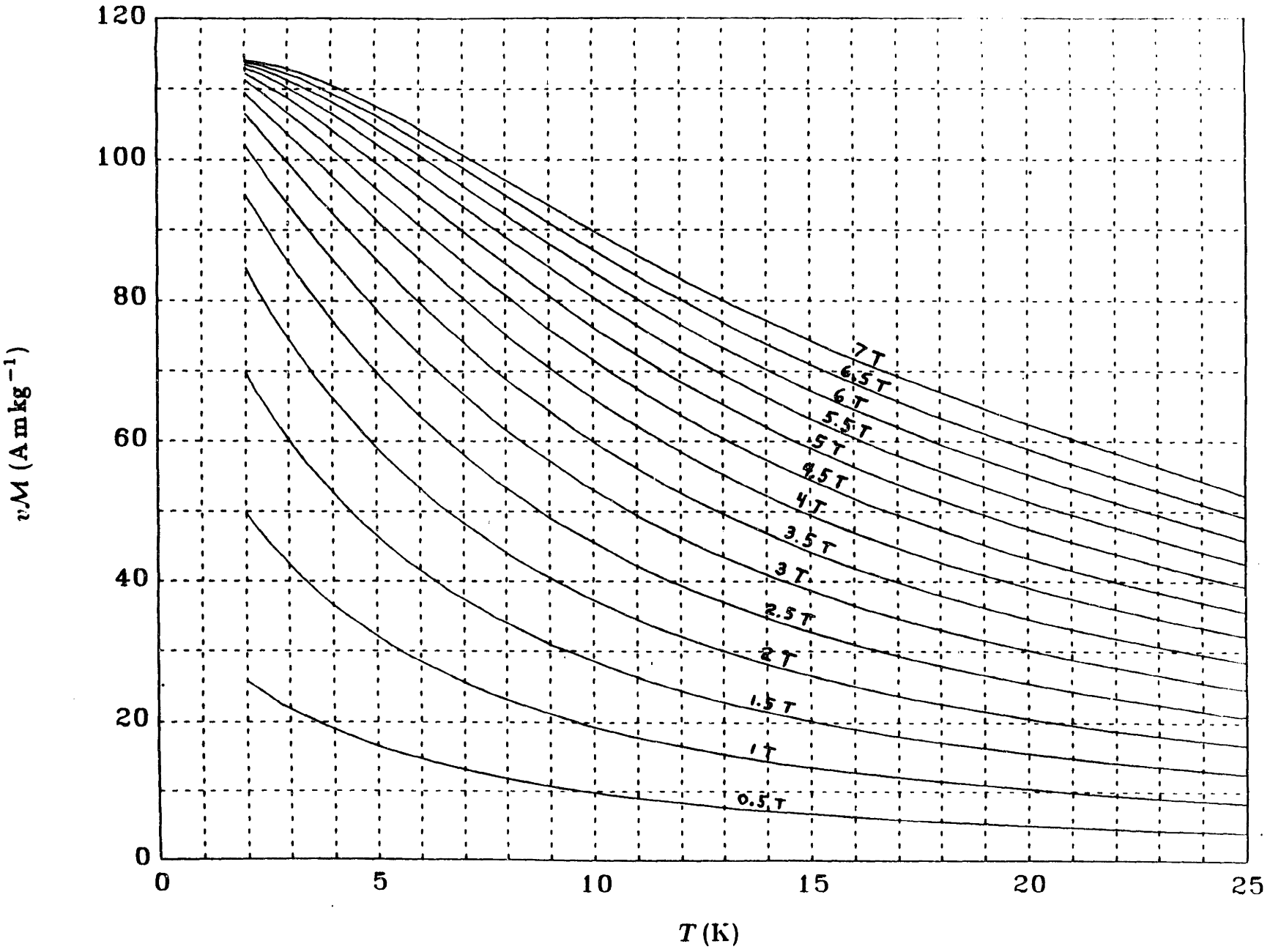

Fig. E-1. $v\mathcal{M}$ vs. T plot of GGG.

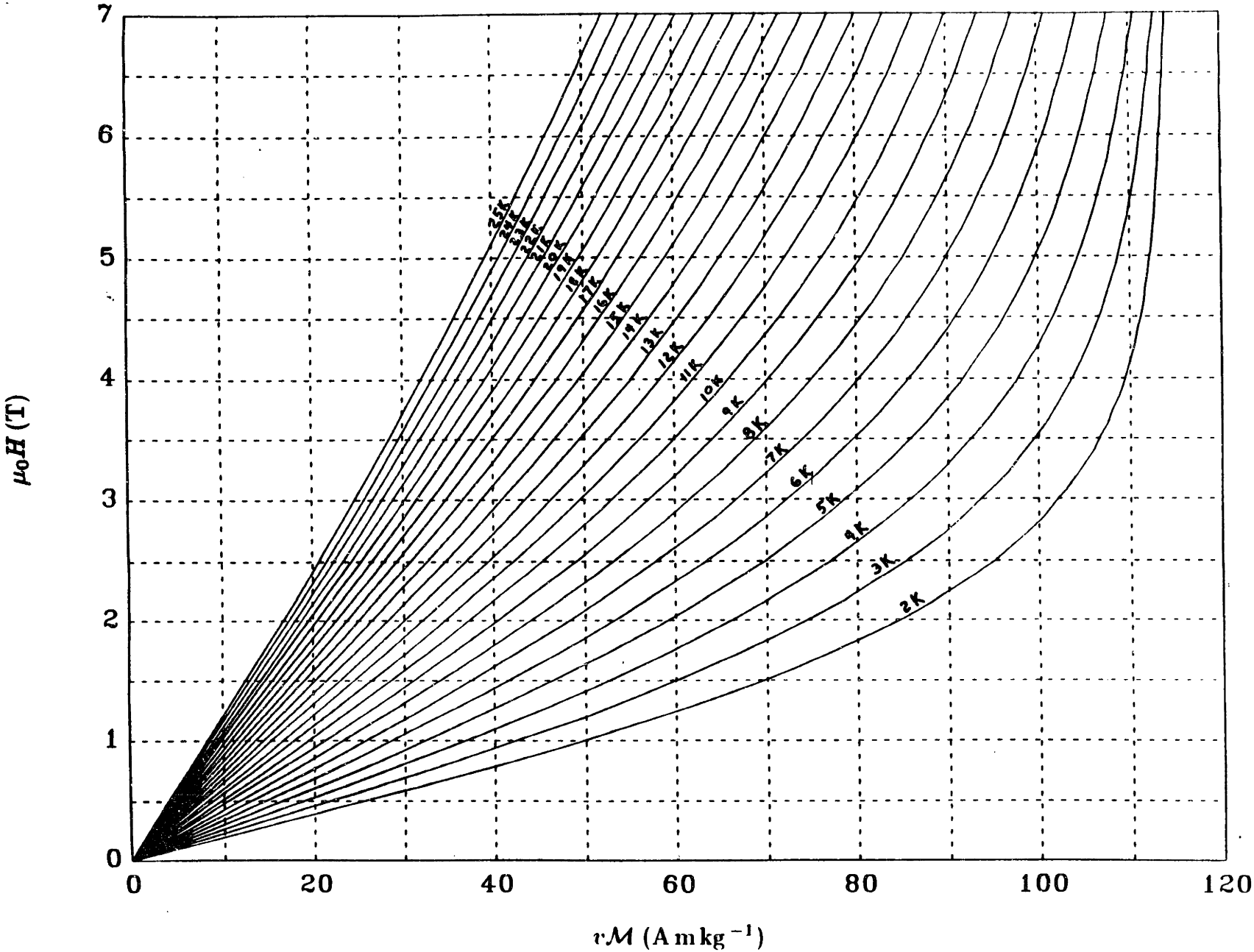

Fig. E-2. $\mu_0 H$ vs. $v\mathcal{M}$ plot of GGG.

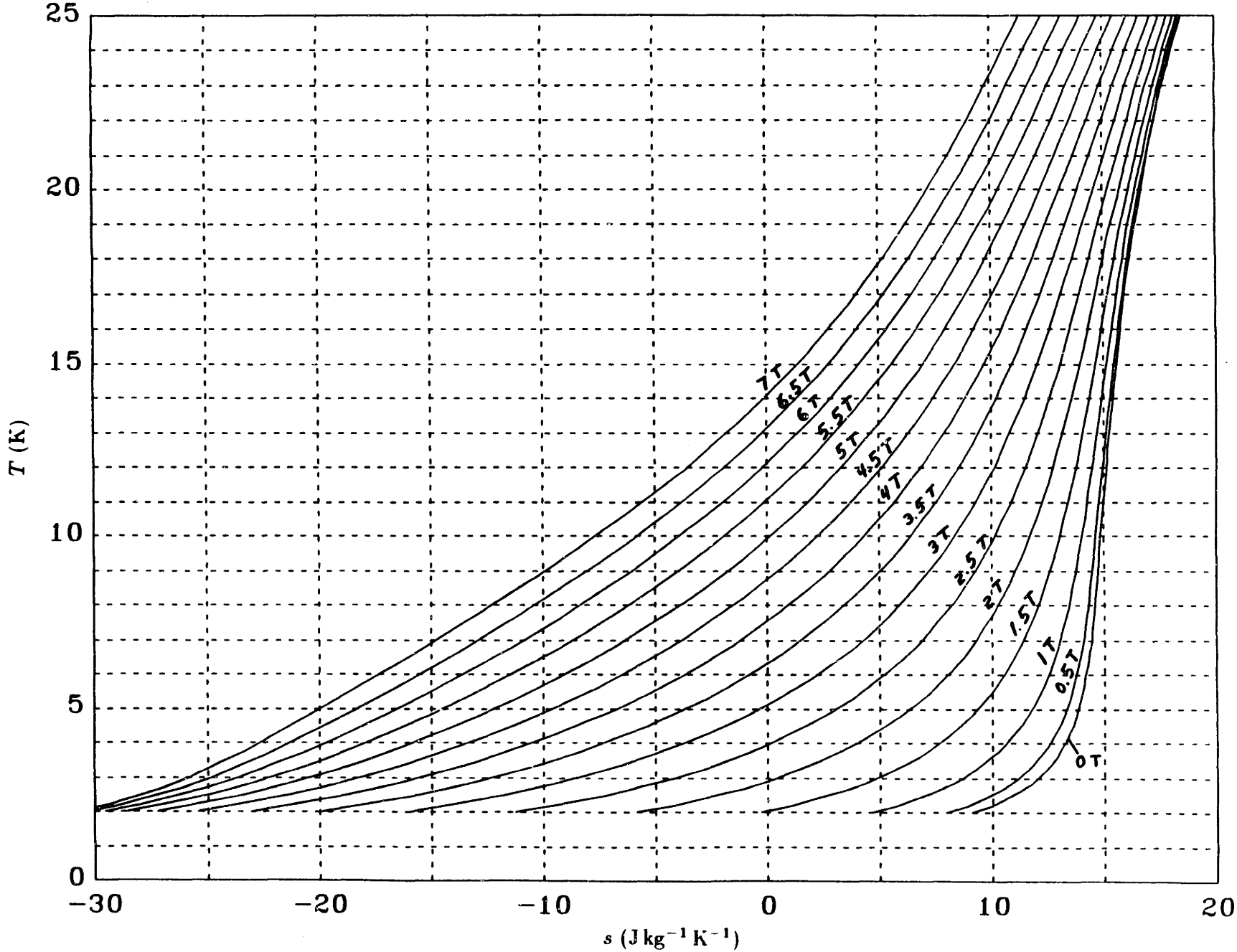

Fig. E-3. T vs. s plot of GGG.

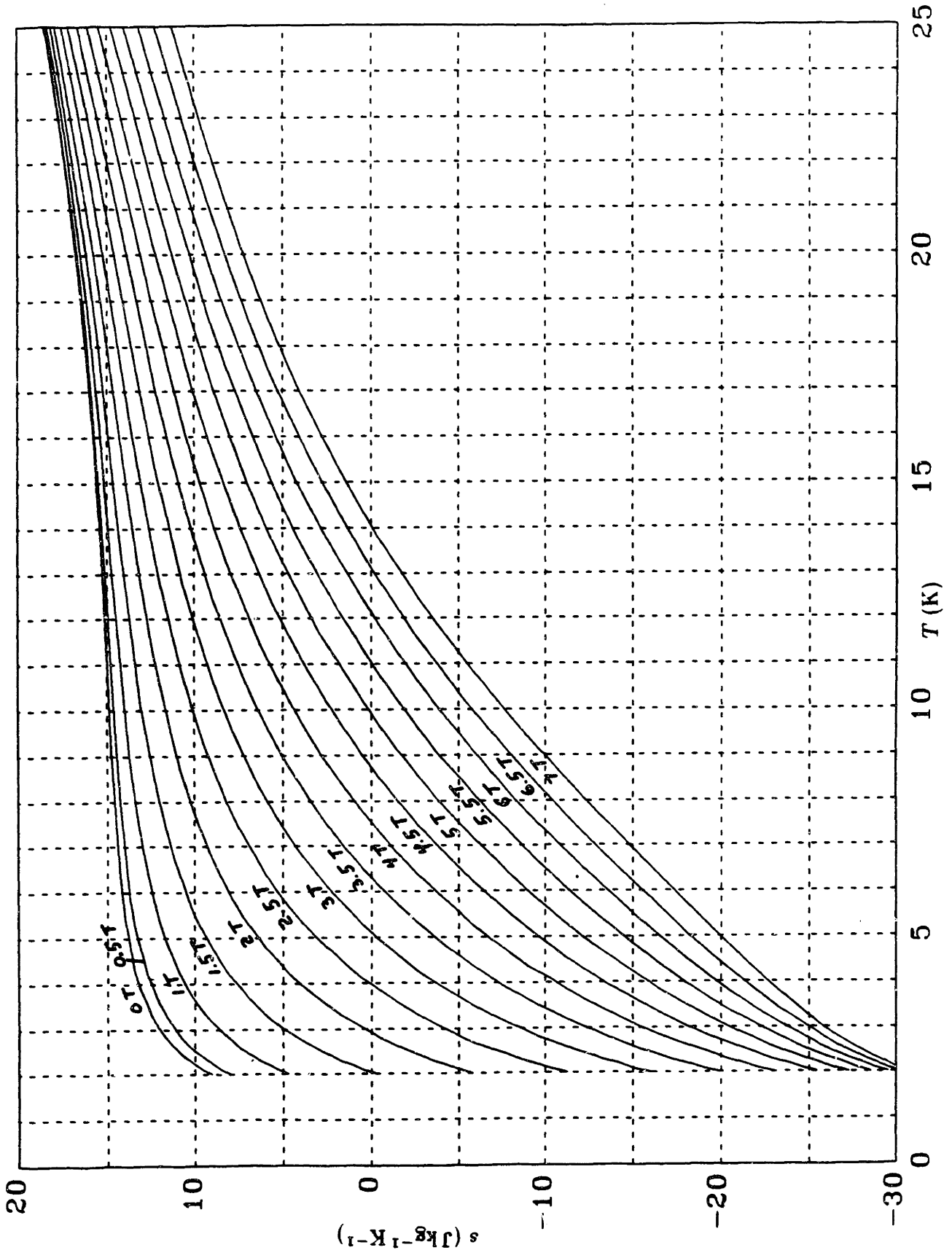

Fig. E-4. s vs. T plot of GGG.

$\mu_0 H = 0\,\mathrm{T}$

T (K)	$v\mathcal{M}$ ($\mathrm{Am\,kg^{-1}}$)	c_H ($\mathrm{J\,kg^{-1}\,K}$)	$v(\frac{\partial \mathcal{M}}{\partial T})_H$ ($\mathrm{Am\,kg^{-1}\,K^{-1}}$)	s ($\mathrm{J\,kg^{-1}\,K^{-1}}$)
1.8	0.000	10.973	0.000	7.999
2.0	0.000	9.598	0.000	9.082
2.2	0.000	8.414	0.000	9.940
2.4	0.000	7.408	0.000	10.628
2.6	0.000	6.558	0.000	11.186
2.8	0.000	5.838	0.000	11.645
3.0	0.000	5.226	0.000	12.026
3.5	0.000	4.053	0.000	12.738
4.0	0.000	3.239	0.000	13.223
4.5	0.000	2.657	0.000	13.569
5.0	0.000	2.233	0.000	13.826
5.5	0.000	1.919	0.000	14.023
6.0	0.000	1.687	0.000	14.180
6.5	0.000	1.515	0.000	14.308
7.0	0.000	1.391	0.000	14.415
7.5	0.000	1.305	0.000	14.508
8.0	0.000	1.251	0.000	14.590
9.0	0.000	1.221	0.000	14.735
10.0	0.000	1.278	0.000	14.866
11.0	0.000	1.408	0.000	14.993
12.0	0.000	1.606	0.000	15.124
13.0	0.000	1.871	0.000	15.262
14.0	0.000	2.201	0.000	15.413
15.0	0.000	2.597	0.000	15.578
16.0	0.000	3.063	0.000	15.760
17.0	0.000	3.601	0.000	15.961
18.0	0.000	4.212	0.000	16.184
19.0	0.000	4.902	0.000	16.430
20.0	0.000	5.673	0.000	16.701
21.0	0.000	6.529	0.000	16.998
22.0	0.000	7.474	0.000	17.323
23.0	0.000	8.512	0.000	17.678
24.0	0.000	9.646	0.000	18.064
25.0	0.000	10.880	0.000	18.482

$\mu_0 H = 0.5\,\mathrm{T}$

T (K)	$v\mathcal{M}$ ($\mathrm{Am\,kg^{-1}}$)	c_H ($\mathrm{J\,kg^{-1}\,K}$)	$v(\frac{\partial \mathcal{M}}{\partial T})_H$ ($\mathrm{Am\,kg^{-1}\,K^{-1}}$)	s ($\mathrm{J\,kg^{-1}\,K^{-1}}$)
1.8	26.736	11.606	-4.825	6.813
2.0	25.800	10.246	-4.541	7.964
2.2	24.918	9.072	-4.280	8.884
2.4	24.086	8.072	-4.039	9.629
2.6	23.301	7.224	-3.818	10.241
2.8	22.558	6.504	-3.613	10.749
3.0	21.855	5.889	-3.423	11.177
3.5	20.251	4.702	-3.005	11.990
4.0	18.838	3.866	-2.656	12.560
4.5	17.586	3.258	-2.361	12.978
5.0	16.470	2.806	-2.110	13.297
5.5	15.470	2.464	-1.894	13.548
6.0	14.571	2.203	-1.708	13.750
6.5	13.758	2.004	-1.547	13.918
7.0	13.021	1.853	-1.405	14.061
7.5	12.350	1.742	-1.281	14.185
8.0	11.737	1.664	-1.172	14.295
9.0	10.660	1.590	-0.989	14.486
10.0	9.746	1.607	-0.843	14.653
11.0	8.964	1.703	-0.725	14.810
12.0	8.289	1.872	-0.628	14.965
13.0	7.702	2.110	-0.549	15.124
14.0	7.188	2.417	-0.482	15.291
15.0	6.735	2.794	-0.426	15.470
16.0	6.334	3.242	-0.378	15.665
17.0	5.977	3.764	-0.337	15.877
18.0	5.658	4.362	-0.302	16.108
19.0	5.373	5.040	-0.271	16.362
20.0	5.115	5.800	-0.244	16.639
21.0	4.883	6.646	-0.221	16.942
22.0	4.673	7.583	-0.200	17.273
23.0	4.482	8.613	-0.182	17.632
24.0	4.308	9.740	-0.166	18.022
25.0	4.150	10.968	-0.151	18.445

$\mu_0 H = 1.0\,\mathrm{T}$

T (K)	$v\mathcal{M}$ ($\mathrm{Am\,kg^{-1}}$)	c_H ($\mathrm{J\,kg^{-1}\,K}$)	$v(\frac{\partial \mathcal{M}}{\partial T})_H$ ($\mathrm{Am\,kg^{-1}\,K^{-1}}$)	s ($\mathrm{J\,kg^{-1}\,K^{-1}}$)
1.8	51.613	13.570	-9.075	3.275
2.0	49.852	12.248	-8.549	4.635
2.2	48.191	11.096	-8.064	5.747
2.4	46.623	10.106	-7.618	6.669
2.6	45.142	9.258	-7.206	7.443
2.8	43.739	8.530	-6.825	8.102
3.0	42.410	7.900	-6.471	8.668
3.5	39.375	6.655	-5.693	9.788
4.0	36.696	5.742	-5.040	10.614
4.5	34.318	5.047	-4.488	11.248
5.0	32.195	4.505	-4.016	11.751
5.5	30.291	4.072	-3.612	12.159
6.0	28.574	3.722	-3.262	12.498
6.5	27.021	3.437	-2.957	12.784
7.0	25.611	3.205	-2.691	13.030
7.5	24.325	3.017	-2.457	13.244
8.0	23.149	2.866	-2.250	13.434
9.0	21.080	2.660	-1.903	13.759
10.0	19.320	2.563	-1.626	14.033
11.0	17.810	2.559	-1.402	14.276
12.0	16.503	2.640	-1.218	14.502
13.0	15.363	2.803	-1.066	14.719
14.0	14.363	3.043	-0.938	14.935
15.0	13.480	3.362	-0.831	15.156
16.0	12.696	3.759	-0.739	15.385
17.0	11.997	4.236	-0.661	15.627
18.0	11.371	4.794	-0.593	15.884
19.0	10.807	5.436	-0.535	16.160
20.0	10.299	6.165	-0.484	16.457
21.0	9.838	6.984	-0.439	16.777
22.0	9.419	7.895	-0.400	17.123
23.0	9.037	8.902	-0.365	17.496
24.0	8.688	10.009	-0.334	17.898
25.0	8.368	11.219	-0.306	18.330

$\mu_0 H = 1.5\,\mathrm{T}$

T (K)	$v\mathcal{M}$ ($\mathrm{Am\,kg^{-1}}$)	c_H ($\mathrm{J\,kg^{-1}\,K}$)	$v(\frac{\partial \mathcal{M}}{\partial T})_H$ ($\mathrm{Am\,kg^{-1}\,K^{-1}}$)	s ($\mathrm{J\,kg^{-1}\,K^{-1}}$)
1.8	71.945	16.225	-11.363	-1.927
2.0	69.730	14.975	-10.789	-0.283
2.2	67.626	13.875	-10.255	1.091
2.4	65.626	12.919	-9.755	2.257
2.6	63.722	12.090	-9.289	3.257
2.8	61.909	11.368	-8.852	4.126
3.0	60.180	10.734	-8.442	4.888
3.5	56.193	9.446	-7.526	6.442
4.0	52.632	8.454	-6.740	7.636
4.5	49.436	7.662	-6.062	8.584
5.0	46.555	7.010	-5.473	9.356
5.5	43.950	6.463	-4.960	9.998
6.0	41.585	5.998	-4.510	10.540
6.5	39.431	5.599	-4.114	11.004
7.0	37.464	5.256	-3.764	11.406
7.5	35.661	4.961	-3.453	11.758
8.0	34.006	4.709	-3.176	12.070
9.0	31.073	4.316	-2.707	12.601
10.0	28.563	4.051	-2.327	13.041
11.0	26.396	3.899	-2.016	13.419
12.0	24.513	3.850	-1.759	13.755
13.0	22.864	3.897	-1.545	14.065
14.0	21.411	4.036	-1.365	14.358
15.0	20.125	4.265	-1.212	14.644
16.0	18.980	4.582	-1.082	14.929
17.0	17.955	4.988	-0.970	15.218
18.0	17.035	5.484	-0.873	15.517
19.0	16.205	6.070	-0.789	15.829
20.0	15.454	6.748	-0.716	16.157
21.0	14.771	7.522	-0.651	16.504
22.0	14.149	8.392	-0.595	16.874
23.0	13.580	9.363	-0.545	17.268
24.0	13.058	10.437	-0.500	17.689
25.0	12.578	11.616	-0.461	18.139

$\mu_0 H = 2.0\,\mathrm{T}$

T (K)	$v\mathcal{M}$ ($\mathrm{Am\,kg^{-1}}$)	c_H ($\mathrm{J\,kg^{-1}\,K}$)	$v(\frac{\partial \mathcal{M}}{\partial T})_H$ ($\mathrm{Am\,kg^{-1}\,K^{-1}}$)	s ($\mathrm{J\,kg^{-1}\,K^{-1}}$)
1.8	86.963	18.648	-11.619	-7.745
2.0	84.684	17.512	-11.168	-5.841
2.2	82.494	16.505	-10.736	-4.220
2.4	80.389	15.625	-10.324	-2.822
2.6	78.363	14.858	-9.931	-1.603
2.8	76.415	14.184	-9.555	-0.527
3.0	74.540	13.586	-9.197	0.431
3.5	70.153	12.345	-8.369	2.428
4.0	66.156	11.354	-7.631	4.010
4.5	62.509	10.527	-6.972	5.298
5.0	59.173	9.816	-6.383	6.370
5.5	56.116	9.194	-5.855	7.275
6.0	53.309	8.642	-5.381	8.051
6.5	50.726	8.150	-4.955	8.723
7.0	48.346	7.710	-4.572	9.311
7.5	46.148	7.317	-4.226	9.829
8.0	44.115	6.966	-3.913	10.290
9.0	40.481	6.381	-3.373	11.075
10.0	37.338	5.936	-2.926	11.723
11.0	34.604	5.618	-2.554	12.273
12.0	32.210	5.417	-2.242	12.752
13.0	30.103	5.327	-1.979	13.182
14.0	28.239	5.342	-1.756	13.576
15.0	26.581	5.459	-1.565	13.948
16.0	25.100	5.676	-1.401	14.307
17.0	23.772	5.992	-1.259	14.660
18.0	22.575	6.406	-1.137	15.014
19.0	21.493	6.918	-1.030	15.373
20.0	20.511	7.530	-0.936	15.743
21.0	19.617	8.243	-0.855	16.128
22.0	18.799	9.059	-0.782	16.529
23.0	18.049	9.980	-0.719	16.952
24.0	17.359	11.008	-0.662	17.398
25.0	16.722	12.146	-0.612	17.870

$\mu_0 H = 2.5\,\mathrm{T}$

T (K)	$v\mathcal{M}$ ($\mathrm{Am\,kg^{-1}}$)	c_H ($\mathrm{J\,kg^{-1}\,K}$)	$v(\frac{\partial \mathcal{M}}{\partial T})_H$ ($\mathrm{Am\,kg^{-1}\,K^{-1}}$)	s ($\mathrm{J\,kg^{-1}\,K^{-1}}$)
1.8	97.254	20.289	-10.521	-13.320
2.0	95.176	19.281	-10.257	-11.236
2.2	93.151	18.393	-9.995	-9.441
2.4	91.178	17.621	-9.736	-7.874
2.6	89.257	16.951	-9.480	-6.491
2.8	87.386	16.364	-9.227	-5.257
3.0	85.565	15.845	-8.979	-4.146
3.5	81.228	14.761	-8.378	-1.788
4.0	77.182	13.879	-7.809	0.124
4.5	73.413	13.120	-7.274	1.714
5.0	69.902	12.444	-6.774	3.061
5.5	66.633	11.829	-6.308	4.217
6.0	63.589	11.262	-5.876	5.222
6.5	60.752	10.738	-5.475	6.102
7.0	58.108	10.252	-5.105	6.880
7.5	55.642	9.802	-4.763	7.572
8.0	53.340	9.387	-4.448	8.191
9.0	49.180	8.660	-3.888	9.253
10.0	45.537	8.064	-3.411	10.134
11.0	42.335	7.594	-3.005	10.879
12.0	39.508	7.246	-2.657	11.524
13.0	37.004	7.016	-2.360	12.095
14.0	34.775	6.900	-2.104	12.610
15.0	32.784	6.895	-1.883	13.085
16.0	30.999	7.000	-1.692	13.533
17.0	29.392	7.212	-1.526	13.963
18.0	27.941	7.530	-1.381	14.383
19.0	26.624	7.956	-1.255	14.801
20.0	25.426	8.488	-1.144	15.223
21.0	24.332	9.127	-1.047	15.652
22.0	23.329	9.876	-0.961	16.093
23.0	22.407	10.734	-0.885	16.551
24.0	21.556	11.705	-0.818	17.028
25.0	20.768	12.790	-0.759	17.527

$\mu_0 H = 3.0\,\mathrm{T}$

T (K)	$v\mathcal{M}$ ($\mathrm{Am\,kg^{-1}}$)	c_H ($\mathrm{J\,kg^{-1}\,K}$)	$v(\frac{\partial \mathcal{M}}{\partial T})_H$ ($\mathrm{Am\,kg^{-1}\,K^{-1}}$)	s ($\mathrm{J\,kg^{-1}\,K^{-1}}$)
1.8	103.928	21.050	-8.807	-18.165
2.0	102.175	20.154	-8.721	-15.995
2.2	100.440	19.377	-8.625	-14.111
2.4	98.726	18.715	-8.519	-12.454
2.6	97.033	18.151	-8.406	-10.979
2.8	95.364	17.668	-8.286	-9.652
3.0	93.719	17.248	-8.160	-8.448
3.5	89.722	16.392	-7.826	-5.856
4.0	85.896	15.706	-7.473	-3.713
4.5	82.250	15.111	-7.112	-1.899
5.0	78.785	14.565	-6.750	-0.335
5.5	75.500	14.050	-6.392	1.029
6.0	72.391	13.554	-6.043	2.230
6.5	69.454	13.076	-5.707	3.296
7.0	66.682	12.615	-5.384	4.248
7.5	64.068	12.172	-5.076	5.103
8.0	61.603	11.749	-4.785	5.875
9.0	57.091	10.967	-4.249	7.213
10.0	53.083	10.283	-3.776	8.332
11.0	49.519	9.704	-3.361	9.284
12.0	46.344	9.236	-2.997	10.108
13.0	43.509	8.881	-2.680	10.832
14.0	40.971	8.642	-2.403	11.481
15.0	38.692	8.517	-2.161	12.072
16.0	36.639	8.506	-1.950	12.621
17.0	34.783	8.608	-1.765	13.139
18.0	33.101	8.824	-1.603	13.636
19.0	31.571	9.153	-1.460	14.122
20.0	30.175	9.595	-1.335	14.602
21.0	28.895	10.150	-1.226	15.083
22.0	27.719	10.820	-1.129	15.570
23.0	26.634	11.606	-1.043	16.068
24.0	25.629	12.508	-0.968	16.581
25.0	24.695	13.530	-0.902	17.112

$\mu_0 H = 3.5\,\mathrm{T}$

T (K)	$v\mathcal{M}$ ($\mathrm{Am\,kg^{-1}}$)	c_H ($\mathrm{J\,kg^{-1}\,K}$)	$v(\frac{\partial \mathcal{M}}{\partial T})_H$ ($\mathrm{Am\,kg^{-1}\,K^{-1}}$)	s ($\mathrm{J\,kg^{-1}\,K^{-1}}$)
1.8	108.077	21.087	-6.991	-22.112
2.0	106.674	20.264	-7.039	-19.934
2.2	105.263	19.567	-7.072	-18.036
2.4	103.847	18.992	-7.090	-16.359
2.6	102.428	18.520	-7.095	-14.858
2.8	101.010	18.131	-7.087	-13.500
3.0	99.594	17.808	-7.068	-12.261
3.5	96.080	17.196	-6.977	-9.565
4.0	92.626	16.748	-6.833	-7.299
4.5	89.254	16.374	-6.650	-5.348
5.0	85.981	16.028	-6.437	-3.641
5.5	82.820	15.687	-6.204	-2.129
6.0	79.779	15.340	-5.958	-0.779
6.5	76.863	14.984	-5.705	0.435
7.0	74.074	14.620	-5.449	1.532
7.5	71.413	14.251	-5.195	2.528
8.0	68.878	13.880	-4.945	3.436
9.0	64.175	13.149	-4.467	5.028
10.0	59.933	12.458	-4.023	6.377
11.0	56.114	11.832	-3.621	7.535
12.0	52.678	11.288	-3.258	8.540
13.0	49.585	10.841	-2.935	9.425
14.0	46.796	10.497	-2.648	10.216
15.0	44.278	10.263	-2.394	10.931
16.0	41.998	10.142	-2.170	11.589
17.0	39.929	10.136	-1.972	12.203
18.0	38.045	10.246	-1.798	12.785
19.0	36.326	10.473	-1.644	13.345
20.0	34.750	10.818	-1.509	13.890
21.0	33.302	11.281	-1.390	14.429
22.0	31.966	11.864	-1.285	14.966
23.0	30.728	12.566	-1.193	15.509
24.0	29.576	13.390	-1.112	16.061
25.0	28.501	14.338	-1.041	16.626

$\mu_0 H = 4.0\,\mathrm{T}$

T (K)	$v\mathcal{M}$ ($\mathrm{Am\,kg^{-1}}$)	c_H ($\mathrm{J\,kg^{-1}\,K}$)	$v(\frac{\partial \mathcal{M}}{\partial T})_H$ ($\mathrm{Am\,kg^{-1}\,K^{-1}}$)	s ($\mathrm{J\,kg^{-1}\,K^{-1}}$)
1.8	110.571	20.616	-5.338	-25.184
2.0	109.489	19.824	-5.476	-23.054
2.2	108.382	19.170	-5.597	-21.196
2.4	107.252	18.648	-5.702	-19.552
2.6	106.102	18.239	-5.792	-18.076
2.8	104.936	17.921	-5.868	-16.736
3.0	103.756	17.675	-5.930	-15.509
3.5	100.763	17.280	-6.030	-12.817
4.0	97.738	17.067	-6.060	-10.525
4.5	94.712	16.934	-6.033	-8.523
5.0	91.713	16.822	-5.957	-6.744
5.5	88.761	16.702	-5.843	-5.147
6.0	85.875	16.558	-5.699	-3.699
6.5	83.066	16.382	-5.533	-2.381
7.0	80.344	16.174	-5.351	-1.174
7.5	77.716	15.937	-5.158	-0.066
8.0	75.187	15.675	-4.959	0.954
9.0	70.429	15.098	-4.556	2.768
10.0	66.073	14.488	-4.160	4.327
11.0	62.102	13.883	-3.786	5.679
12.0	58.492	13.318	-3.439	6.863
13.0	55.213	12.816	-3.122	7.908
14.0	52.237	12.397	-2.836	8.842
15.0	49.532	12.073	-2.579	9.686
16.0	47.070	11.854	-2.349	10.457
17.0	44.825	11.746	-2.145	11.172
18.0	42.772	11.752	-1.964	11.843
19.0	40.889	11.875	-1.804	12.481
20.0	39.157	12.119	-1.663	13.096
21.0	37.557	12.483	-1.539	13.696
22.0	36.074	12.970	-1.430	14.287
23.0	34.694	13.581	-1.334	14.877
24.0	33.403	14.318	-1.250	15.470
25.0	32.190	15.182	-1.177	16.072

$\mu_0 H = 4.5\,\mathrm{T}$

T (K)	$v\mathcal{M}$ ($\mathrm{Am\,kg^{-1}}$)	c_H ($\mathrm{J\,kg^{-1}\,K}$)	$v(\frac{\partial \mathcal{M}}{\partial T})_H$ ($\mathrm{Am\,kg^{-1}\,K^{-1}}$)	s ($\mathrm{J\,kg^{-1}\,K^{-1}}$)
1.8	112.032	19.831	-3.955	-27.496
2.0	111.222	19.032	-4.146	-25.449
2.2	110.375	18.385	-4.321	-23.666
2.4	109.494	17.883	-4.481	-22.089
2.6	108.583	17.505	-4.627	-20.674
2.8	107.644	17.230	-4.759	-19.387
3.0	106.681	17.038	-4.876	-18.205
3.5	104.180	16.810	-5.112	-15.600
4.0	101.581	16.803	-5.273	-13.357
4.5	98.918	16.899	-5.367	-11.373
5.0	96.223	17.027	-5.404	-9.586
5.5	93.523	17.146	-5.391	-7.957
6.0	90.839	17.231	-5.338	-6.462
6.5	88.190	17.271	-5.252	-5.080
7.0	85.591	17.261	-5.140	-3.801
7.5	83.054	17.200	-5.007	-2.611
8.0	80.587	17.092	-4.860	-1.505
9.0	75.886	16.756	-4.538	0.490
10.0	71.516	16.303	-4.200	2.233
11.0	67.485	15.787	-3.865	3.763
12.0	63.783	15.254	-3.543	5.114
13.0	60.392	14.741	-3.242	6.314
14.0	57.290	14.278	-2.965	7.390
15.0	54.453	13.888	-2.713	8.361
16.0	51.856	13.586	-2.485	9.247
17.0	49.475	13.384	-2.281	10.064
18.0	47.286	13.291	-2.100	10.826
19.0	45.269	13.312	-1.939	11.545
20.0	43.403	13.452	-1.796	12.230
21.0	41.671	13.713	-1.671	12.893
22.0	40.055	14.098	-1.562	13.539
23.0	38.542	14.610	-1.466	14.176
24.0	37.118	15.251	-1.384	14.811
25.0	35.771	16.022	-1.313	15.449

$\mu_0 H = 5.0\,\mathrm{T}$

T (K)	$v\mathcal{M}$ ($\mathrm{Am\,kg^{-1}}$)	c_H ($\mathrm{J\,kg^{-1}\,K}$)	$v(\frac{\partial \mathcal{M}}{\partial T})_H$ ($\mathrm{Am\,kg^{-1}\,K^{-1}}$)	s ($\mathrm{J\,kg^{-1}\,K^{-1}}$)
1.8	112.880	18.870	-2.856	-29.187
2.0	112.286	18.037	-3.075	-27.243
2.2	111.651	17.369	-3.280	-25.557
2.4	110.975	16.859	-3.472	-24.069
2.6	110.263	16.487	-3.650	-22.735
2.8	109.516	16.229	-3.815	-21.523
3.0	108.738	16.065	-3.967	-20.409
3.5	106.670	15.952	-4.292	-17.946
4.0	104.458	16.110	-4.542	-15.808
4.5	102.139	16.407	-4.724	-13.894
5.0	99.744	16.760	-4.844	-12.147
5.5	97.304	17.115	-4.910	-10.533
6.0	94.842	17.438	-4.930	-9.030
6.5	92.380	17.710	-4.911	-7.623
7.0	89.936	17.918	-4.859	-6.302
7.5	87.526	18.059	-4.780	-5.061
8.0	85.160	18.135	-4.680	-3.892
9.0	80.597	18.103	-4.437	-1.756
10.0	76.298	17.872	-4.158	0.141
11.0	72.286	17.501	-3.866	1.828
12.0	68.565	17.048	-3.576	3.331
13.0	65.129	16.563	-3.298	4.677
14.0	61.963	16.088	-3.037	5.887
15.0	59.048	15.654	-2.796	6.981
16.0	56.363	15.286	-2.577	7.980
17.0	53.887	15.002	-2.379	8.897
18.0	51.597	14.815	-2.203	9.749
19.0	49.475	14.735	-2.046	10.547
20.0	47.500	14.769	-1.908	11.304
21.0	45.654	14.923	-1.787	12.027
22.0	43.921	15.201	-1.682	12.728
23.0	42.285	15.606	-1.591	13.412
24.0	40.734	16.143	-1.514	14.087
25.0	39.254	16.815	-1.448	14.759

$\mu_0 H = 5.5\,\mathrm{T}$

T (K)	$v\mathcal{M}$ ($\mathrm{Am\,kg^{-1}}$)	c_H ($\mathrm{J\,kg^{-1}\,K}$)	$v(\frac{\partial \mathcal{M}}{\partial T})_H$ ($\mathrm{Am\,kg^{-1}\,K^{-1}}$)	s ($\mathrm{J\,kg^{-1}\,K^{-1}}$)
1.8	113.386	17.827	-2.013	-30.394
2.0	112.960	16.940	-2.244	-28.564
2.2	112.490	16.231	-2.463	-26.984
2.4	111.976	15.694	-2.670	-25.596
2.6	111.422	15.306	-2.865	-24.356
2.8	110.831	15.046	-3.049	-23.232
3.0	110.204	14.890	-3.220	-22.199
3.5	108.496	14.845	-3.597	-19.913
4.0	106.618	15.128	-3.903	-17.915
4.5	104.604	15.594	-4.142	-16.107
5.0	102.486	16.148	-4.320	-14.436
5.5	100.293	16.724	-4.443	-12.870
6.0	98.051	17.277	-4.517	-11.391
6.5	95.783	17.780	-4.549	-9.988
7.0	93.509	18.215	-4.544	-8.654
7.5	91.244	18.570	-4.510	-7.384
8.0	89.003	18.845	-4.450	-6.177
9.0	84.635	19.156	-4.276	-3.936
10.0	80.468	19.188	-4.052	-1.914
11.0	76.539	19.005	-3.804	-0.092
12.0	72.863	18.670	-3.548	1.548
13.0	69.441	18.246	-3.296	3.026
14.0	66.266	17.785	-3.056	4.361
15.0	63.324	17.327	-2.831	5.573
16.0	60.597	16.907	-2.626	6.677
17.0	58.066	16.550	-2.439	7.691
18.0	55.712	16.274	-2.273	8.629
19.0	53.514	16.094	-2.126	9.503
20.0	51.455	16.020	-1.997	10.327
21.0	49.515	16.062	-1.885	11.109
22.0	47.679	16.226	-1.789	11.859
23.0	45.932	16.518	-1.708	12.586
24.0	44.258	16.943	-1.641	13.298
25.0	42.646	17.508	-1.585	14.001

$\mu_0 H = 6.0\,\mathrm{T}$

T (K)	$v\mathcal{M}$ ($\mathrm{Am\,kg^{-1}}$)	c_H ($\mathrm{J\,kg^{-1}\,K}$)	$v(\frac{\partial \mathcal{M}}{\partial T})_H$ ($\mathrm{Am\,kg^{-1}\,K^{-1}}$)	s ($\mathrm{J\,kg^{-1}\,K^{-1}}$)
1.8	113.722	16.757	-1.385	-31.236
2.0	113.421	15.805	-1.618	-29.521
2.2	113.075	15.043	-1.841	-28.052
2.4	112.686	14.465	-2.053	-26.770
2.6	112.255	14.049	-2.255	-25.629
2.8	111.785	13.771	-2.446	-24.599
3.0	111.277	13.609	-2.626	-23.655
3.5	109.861	13.596	-3.029	-21.564
4.0	108.259	13.969	-3.366	-19.728
4.5	106.505	14.573	-3.640	-18.049
5.0	104.629	15.302	-3.854	-16.477
5.5	102.660	16.078	-4.014	-14.982
6.0	100.624	16.849	-4.125	-13.550
6.5	98.543	17.574	-4.193	-12.172
7.0	96.437	18.231	-4.224	-10.846
7.5	94.324	18.802	-4.222	-9.568
8.0	92.219	19.280	-4.194	-8.339
9.0	88.078	19.952	-4.076	-6.025
10.0	84.086	20.273	-3.900	-3.904
11.0	80.288	20.302	-3.692	-1.968
12.0	76.707	20.112	-3.469	-0.208
13.0	73.351	19.772	-3.244	1.389
14.0	70.216	19.342	-3.027	2.839
15.0	67.293	18.876	-2.822	4.157
16.0	64.566	18.413	-2.634	5.361
17.0	62.019	17.987	-2.463	6.464
18.0	59.633	17.624	-2.311	7.481
19.0	57.390	17.341	-2.178	8.426
20.0	55.271	17.155	-2.063	9.311
21.0	53.258	17.078	-1.966	10.145
22.0	51.334	17.119	-1.884	10.940
23.0	49.484	17.289	-1.818	11.704
24.0	47.694	17.596	-1.765	12.446
25.0	45.950	18.049	-1.724	13.173

$\mu_0 H = 6.5\,\mathrm{T}$

T (K)	$v\mathcal{M}$ ($\mathrm{Am\,kg^{-1}}$)	c_H ($\mathrm{J\,kg^{-1}\,K}$)	$v(\frac{\partial \mathcal{M}}{\partial T})_H$ ($\mathrm{Am\,kg^{-1}\,K^{-1}}$)	s ($\mathrm{J\,kg^{-1}\,K^{-1}}$)
1.8	113.986	15.692	-0.923	-31.807
2.0	113.778	14.668	-1.153	-30.208
2.2	113.525	13.847	-1.374	-28.850
2.4	113.229	13.220	-1.586	-27.674
2.6	112.891	12.766	-1.788	-26.635
2.8	112.514	12.462	-1.981	-25.700
3.0	112.100	12.285	-2.163	-24.847
3.5	110.912	12.277	-2.576	-22.961
4.0	109.534	12.714	-2.927	-21.297
4.5	107.996	13.432	-3.218	-19.760
5.0	106.326	14.312	-3.452	-18.301
5.5	104.552	15.269	-3.634	-16.892
6.0	102.700	16.239	-3.769	-15.522
6.5	100.791	17.176	-3.861	-14.185
7.0	98.845	18.045	-3.915	-12.879
7.5	96.881	18.825	-3.938	-11.607
8.0	94.912	19.504	-3.932	-10.370
9.0	91.011	20.539	-3.857	-8.009
10.0	87.219	21.157	-3.720	-5.809
11.0	83.585	21.413	-3.545	-3.778
12.0	80.135	21.380	-3.352	-1.915
13.0	76.883	21.135	-3.153	-0.212
14.0	73.827	20.748	-2.959	1.341
15.0	70.962	20.279	-2.775	2.757
16.0	68.272	19.777	-2.606	4.049
17.0	65.744	19.283	-2.454	5.233
18.0	63.359	18.827	-2.320	6.322
19.0	61.098	18.435	-2.205	7.330
20.0	58.943	18.127	-2.108	8.267
21.0	56.876	17.920	-2.029	9.146
22.0	54.879	17.829	-1.967	9.977
23.0	52.937	17.867	-1.919	10.770
24.0	51.036	18.047	-1.886	11.533
25.0	49.162	18.384	-1.863	12.276

$\mu_0 H = 7.0\,\mathrm{T}$

T (K)	$v\mathcal{M}$ ($\mathrm{Am\,kg^{-1}}$)	c_H ($\mathrm{J\,kg^{-1}\,K}$)	$v(\frac{\partial \mathcal{M}}{\partial T})_H$ ($\mathrm{Am\,kg^{-1}\,K^{-1}}$)	s ($\mathrm{J\,kg^{-1}\,K^{-1}}$)
1.8	114.232	14.647	-0.582	-32.179
2.0	114.093	13.550	-0.807	-30.694
2.2	113.910	12.665	-1.025	-29.446
2.4	113.684	11.985	-1.233	-28.375
2.6	113.417	11.490	-1.433	-27.436
2.8	113.112	11.153	-1.623	-26.598
3.0	112.769	10.955	-1.805	-25.836
3.5	111.761	10.937	-2.217	-24.156
4.0	110.561	11.419	-2.572	-22.669
4.5	109.198	12.231	-2.870	-21.279
5.0	107.700	13.245	-3.113	-19.940
5.5	106.093	14.365	-3.307	-18.625
6.0	104.401	15.520	-3.455	-17.326
6.5	102.645	16.652	-3.561	-16.039
7.0	100.846	17.723	-3.631	-14.765
7.5	99.020	18.704	-3.669	-13.508
8.0	97.182	19.578	-3.679	-12.272
9.0	93.519	20.967	-3.634	-9.881
10.0	89.935	21.881	-3.526	-7.621
11.0	86.480	22.365	-3.378	-5.510
12.0	83.185	22.493	-3.210	-3.556
13.0	80.063	22.347	-3.034	-1.760
14.0	77.116	22.004	-2.861	-0.115
15.0	74.338	21.531	-2.698	1.387
16.0	71.716	20.986	-2.548	2.760
17.0	69.235	20.415	-2.416	4.015
18.0	66.878	19.857	-2.302	5.166
19.0	64.624	19.342	-2.208	6.225
20.0	62.456	18.897	-2.133	7.206
21.0	60.353	18.545	-2.076	8.119
22.0	58.298	18.305	-2.036	8.976
23.0	56.275	18.198	-2.012	9.786
24.0	54.269	18.243	-2.002	10.561
25.0	52.267	18.461	-2.003	11.310

Appendix F Helium Properties

The analysis of the magnetically active regenerator required some of the thermodynamic and transport properties of helium–4 at 3 atm of pressure. These properties included density, enthalpy, entropy, specific heat at constant pressure, and thermal conductivity. A table of the properties was generated from a helium properties program for temperatures from 2.14 K to 10 K at increments of 0.02 K and from 10 K to 20 K at increments of 0.05 K, and is shown at the end of this appendix (Table F1). A fortran subroutine that used cubic splines was created to interpolate the properties given temperature. Interpolation with cubic splines has advantages in that 1) the evaluation of cubic splines is efficient, 2) the interpolation functions reproduce the original tabulated data (curvefitting methods such as least squares methods do not necessarily reproduce the original data), and 3) the first derivatives of the curvefits are continuous over the entire interval 2.14 K $\leq$ T $\leq$ 20 K.

The method used to develop the cubic splines is described in detail in *Numerical Methods* by Robert W. Hornbeck (Prentice-Hall, Inc., New Jersey, 1975). The method simply uses a cubic equation (spline) to interpolate values of a property between two data points. Given n pieces of data, (x_1, y_1), (x_2, y_2), $\ldots$, (x_n, y_n), the method creates $n-1$ cubic splines, each of the form

$$F_i(x) = c_{i0} + c_{i1}x + c_{i2}x^2 + c_{i3}x^3 \qquad (x_i \leq x \leq x_{i+1}) \qquad (f2)$$

for $i = 1, 2, \ldots, n-1$.

We will let $f(x)$ denote the interpolation funtion over the entire interval $x_1 \leq x \leq x_n$. Because the second derivative of a cubic equation is linear, $f''(x)$ is linear in each interval $x_i \leq x \leq x_{i+1}$ and is given by

$$f''(x) = f''(x_i) + \frac{x - x_i}{x_{i+1} - x_i}\left[f''(x_{i+1}) - f''(x_i)\right] \qquad (f3)$$

Integrating Eq. (f3) twice, and applying the boundary conditions

$$f(x_i) = y_i \qquad (f4)$$

and

$$f(x_{i+1}) = y_{i+1} \tag{f5}$$

for the interval $x_i \leq x \leq x_{i+1}$, we get

$$\begin{aligned} f(x) = F_i(x) = & \frac{f''(x_i)}{6}\left[\frac{(x_{i+1}-x)^3}{\Delta x_i} - \Delta x_i(x_{i+1}-x)\right] \\ & + \frac{f''(x_{i+1})}{6}\left[\frac{(x-x_i)^3}{\Delta x_i} - \Delta x_i(x-x_i)\right] \\ & + y_i\left[\frac{x_{i+1}-x}{\Delta x_i}\right] + y_{i+1}\left[\frac{x-x_i}{\Delta x_i}\right] \end{aligned} \tag{f6}$$

where $\Delta x_i = x_{i+1} - x_i$. Equation (f6) is the cubic spline for interval i and is used to interpolate values of $y = f(x)$ between y_i and y_{i+1}. There are $n-1$ splines to describe y in the interval $x_i \leq x \leq x_n$.

Because $f''(x_i)$ and $f''(x_{i+1})$ are unknown in each of the $n-1$ splines of (f6), boundary conditions must be invoked so that the $2(n-1)$ unknowns can be determined. First, we will match the first and second derivatives of $f(x)$ at the common point of neighboring splines. That is equivalent to the setting

$$F_i'(x_{i+1}) = F_{i+1}'(x_{i+1}) \tag{f7}$$

and

$$F_i''(x_{i+1}) = F_{i+1}''(x_{i+1}) \tag{f8}$$

for $i = 1, 2, \ldots, n-2$. Equations(f7) and (f8) provide $2(n-2)$ boundary conditions for Eq. (f6).

Two more boundary conditions are needed. If we set

$$f''(x_1) = 0 \tag{f9}$$

and

$$f''(x_n) = 0 \tag{f10}$$

we can solve for all the unknowns in (f6). By invoking boundary conditions (f9) and (f10), we have produced what is known as a "natural cubic spline."

Substituting boundary conditions (f7) and (f8) into Eq. (f8) produces the following set of equations:

$$\left[\frac{\Delta x_{i-1}}{\Delta x_i}\right] f''(x_{i+1}) + \left[\frac{2(x_{i+1}-x_{i-1}}{\Delta x_i}\right] f''(x_{i+1}) = 6\left[\frac{y_{i+1}-y_i}{(\Delta x_i)^2} - \frac{y_i - y_{i-1}}{(\Delta x_i)(\Delta x_{i-1})}\right] \quad (i = 2,3,\ldots,n-1) \quad (f11)$$

Equations (f9), (f10), and (f11) can now be solved simultaneously to determine $f''(x_i)$ for $i = 1,2,\ldots,n$. Equation (f6) describes the interpolation for each interval.

A fortran program was constructed to solve Eqs. (f7)–(f11) for each of the helium properties. A subroutine was then written using Eq. (f6) to interpolate all of the helium properties. The subroutine uses data found in two computer files. HEPROP.DAT contains the original helium properties data, shown in Fig. D1, and HECURV.DAT contains the second derivatives f'' for each of the properties. (The name HECURV.DAT stands for "helium properties curvature data.") Figures F1–F5 are graphs of the helium properties that result from the cubic spline fits.

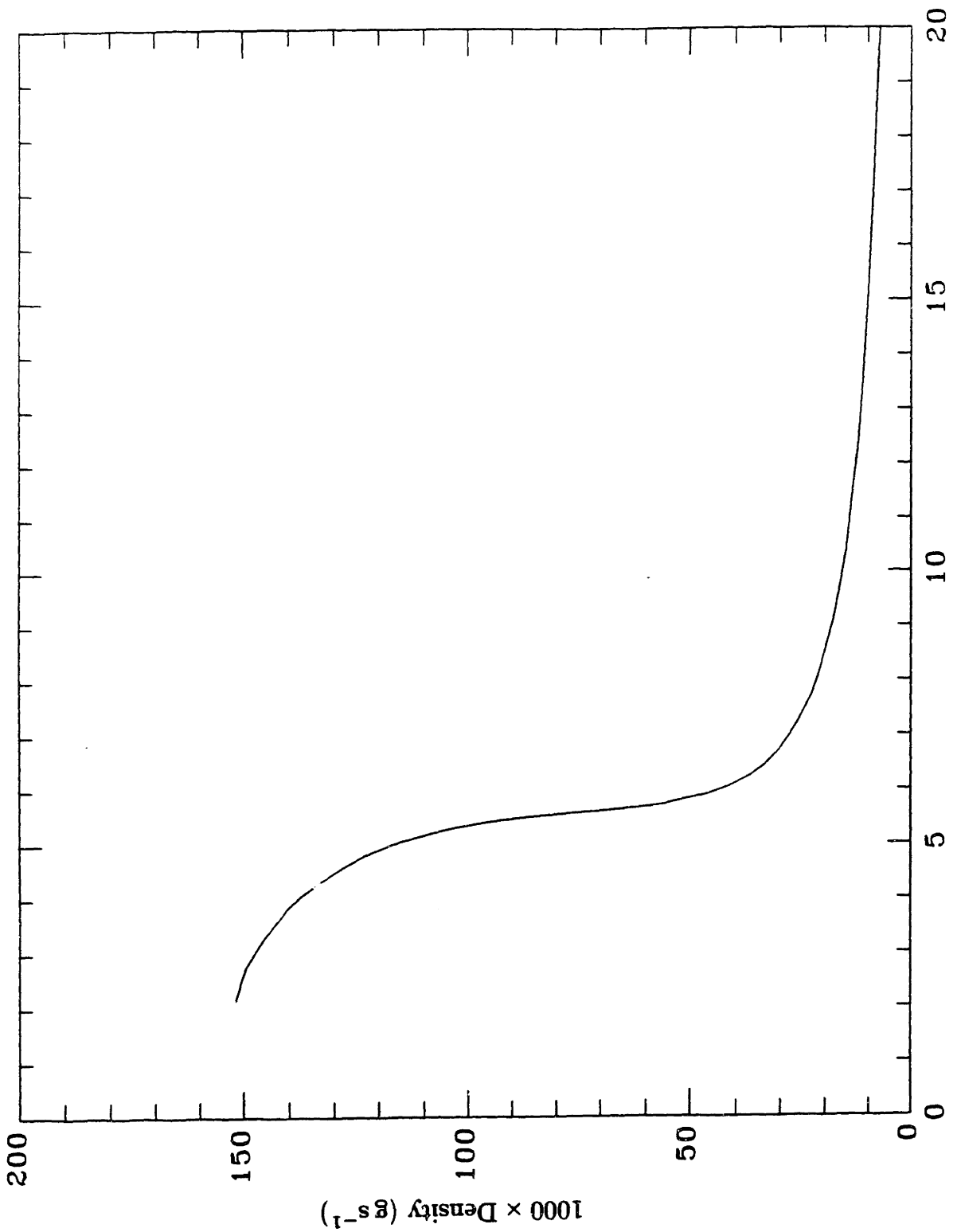

Fig. F1 Helium density vs. temperature.

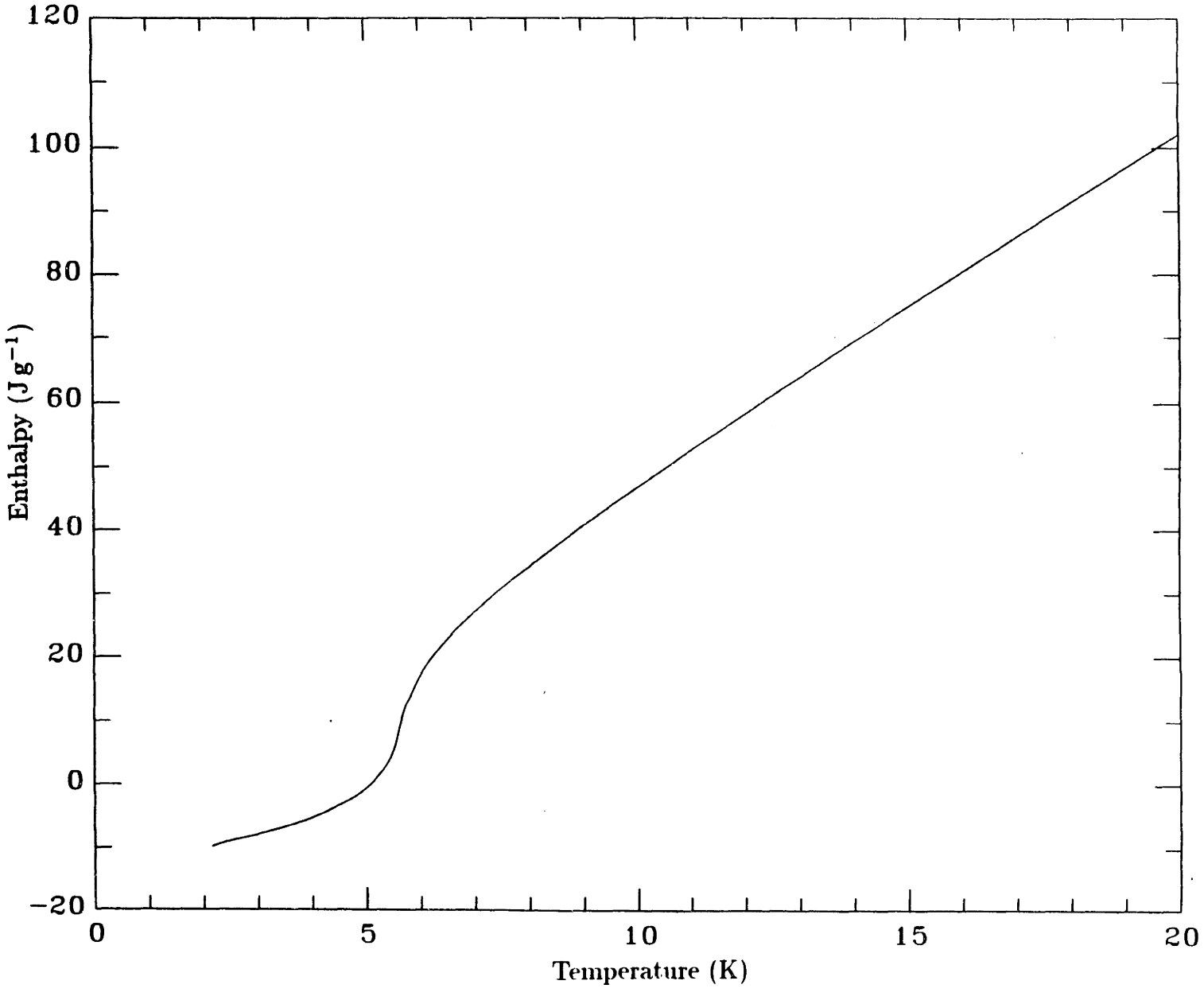

Fig. F2 Specific enthalpy of helium vs. temperature.

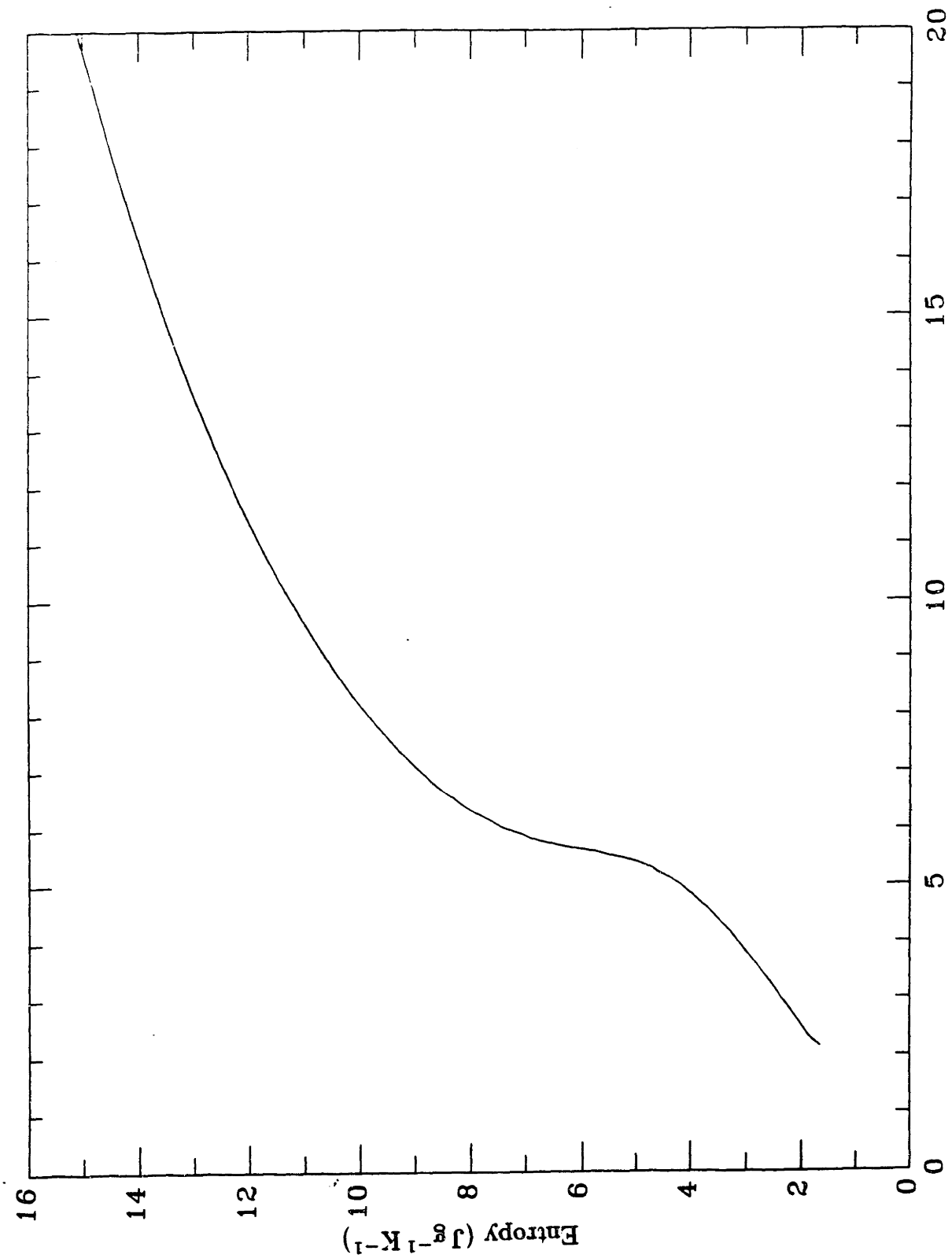

Fig. F3 Specific entropy of helium vs. temperature.

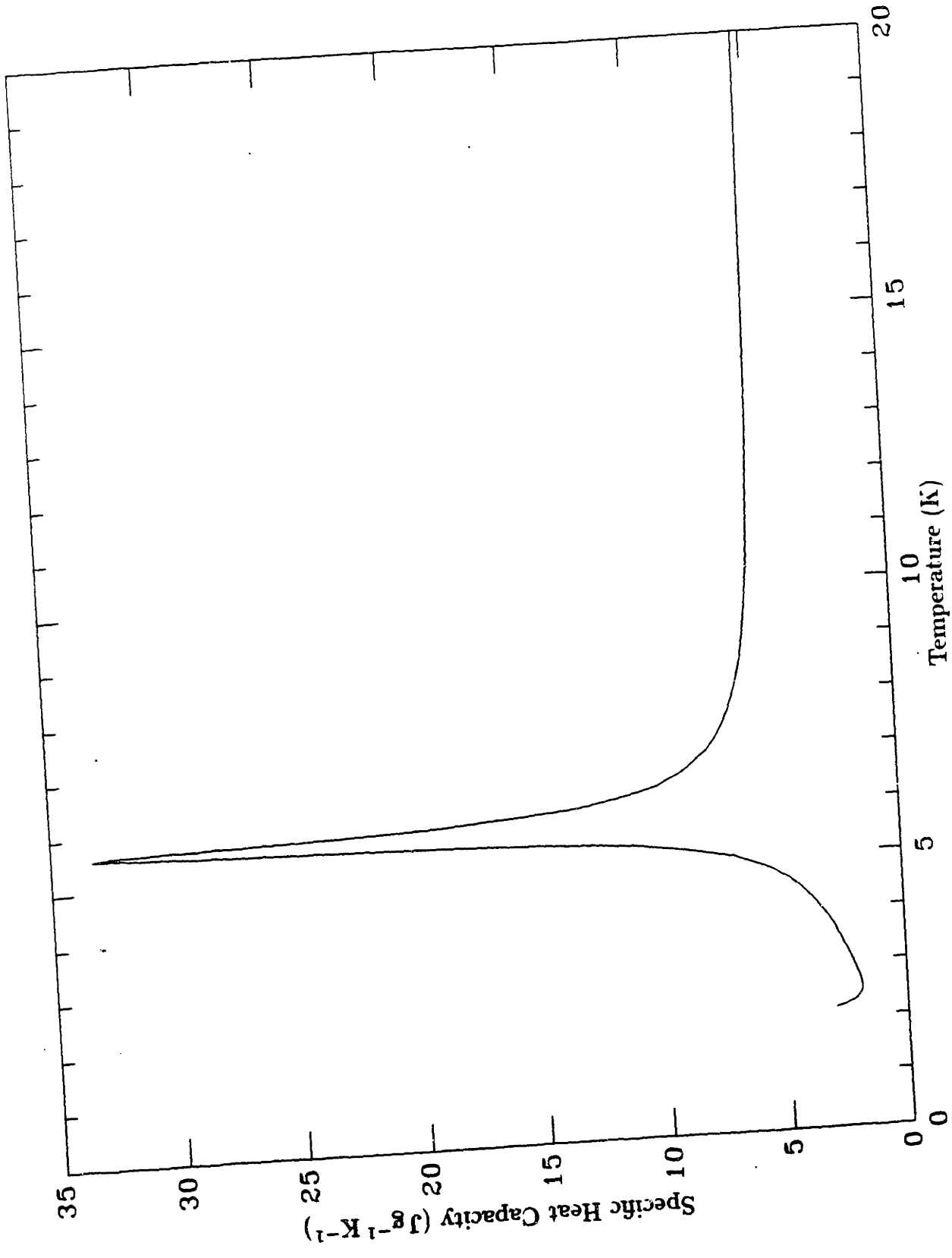

Fig. F4 Specific heat capacity of helium vs. temperature.

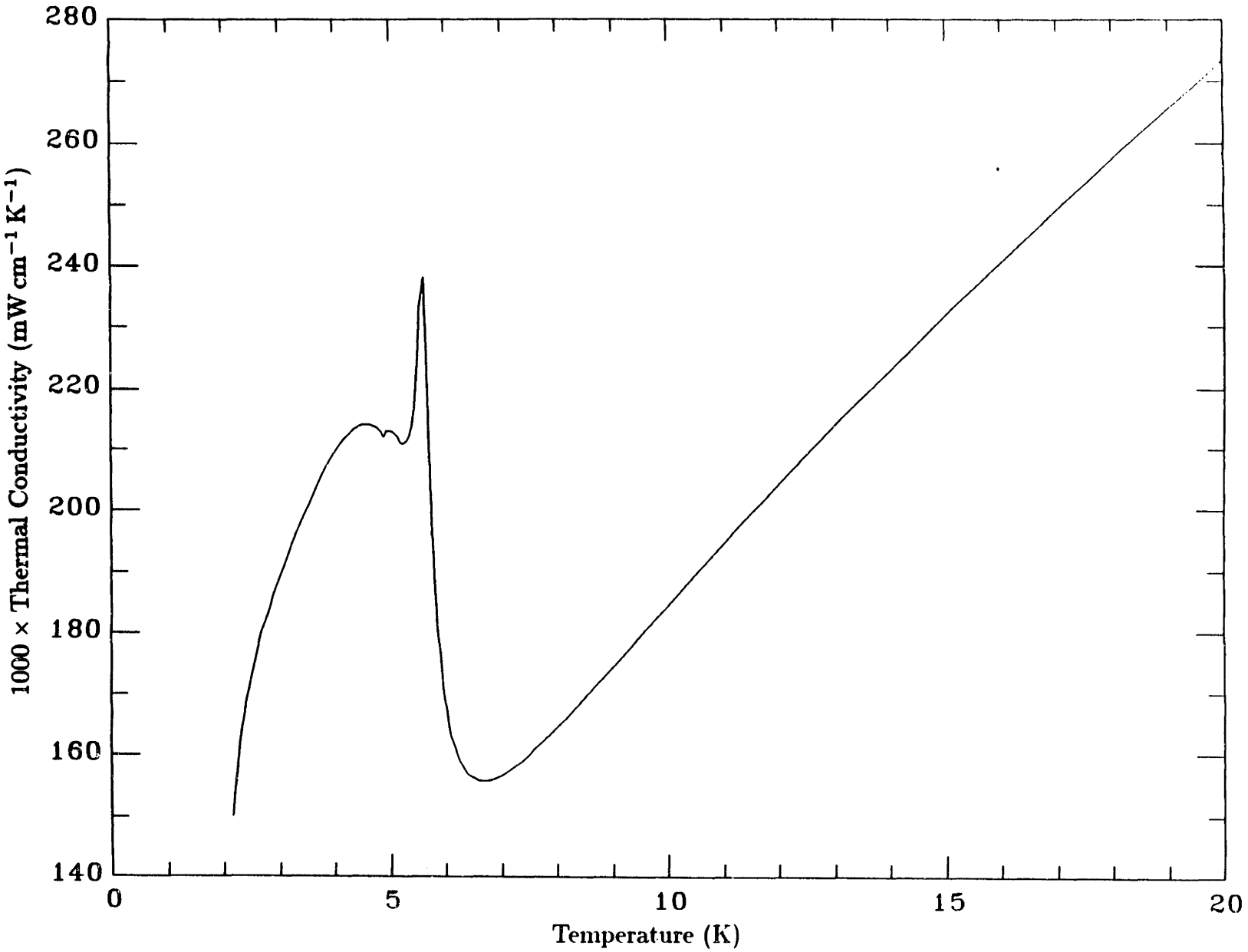

Fig. F5 Thermal conductivity of helium vs. temperature.

Appendix G Computer Program

Figure G1 of this appendix contains a flowchart of the computer algorithm discussed in Chapter 6. The appendix also contains three sets of fortran computer codes. The first program listed is SIM.FOR, which is the simulation of the experiment. The second program is MAGFLOW.FOR, which evaluates a magnetization flow process, and the third program is DEMFLOW.FOR, which evaluates a demagnetization flow process. These three programs and small variations of them have been used to generate all of the numerical results of this thesis.

The subroutines GGGPROP and HEPROP generate the GGG and helium properties respectively for the analysis. GGGPROP uses the equations that were formulated in Chapter 4, and HEPROP evaluates tabulated data using cubic splines as interpolation functions. The method of cubic splines is discussed in Appendix F.

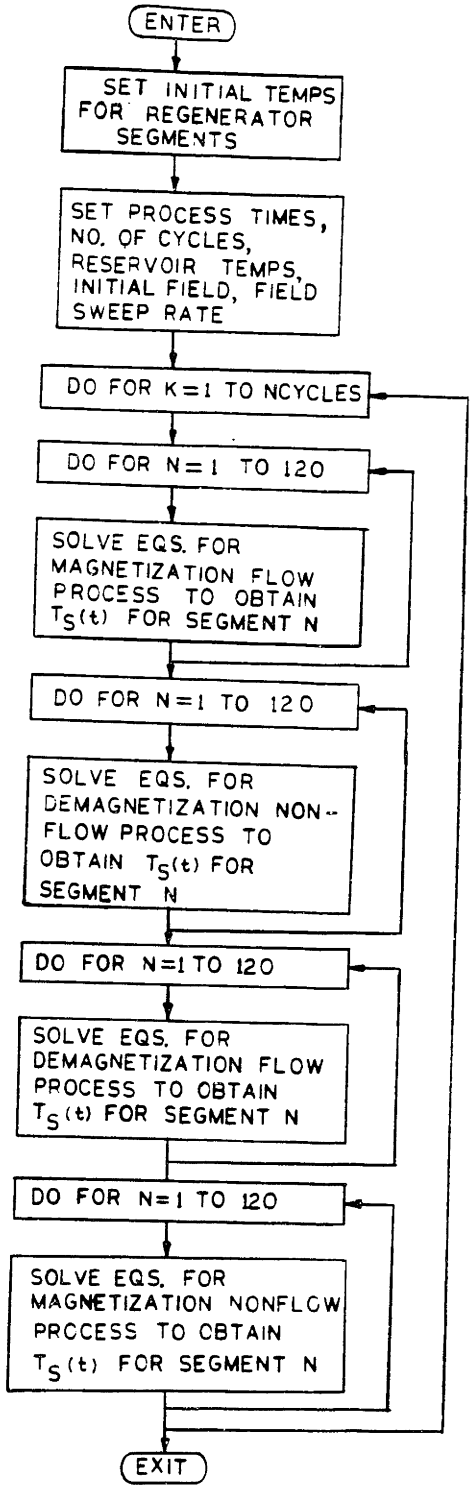

Fig. G1 Flowchart of computer algorithm.

```
C
C   Regenerator Simulation Program
C
C
C       This program is a numerical simulation of a magnetically active
C   regenerator, based on the differential equations derived in chapter
C   3 and the GGG thermodynamic properties derived in chapter 5.  It
C   uses the Second Order Runge Kutta method to solve the differential
C   equations.  Values of field, mass flow, and reservoir temps (source of
C   flow) that were recorded during experiments were used in the program.
C
C
      PROGRAM SIM
      DIMENSION TSALT(120),SSALT(120),dSdT(120),dSduoH(120),THEL(401,121),
     1 RHOHEL(401,121),HHEL(401,121),SHEL(401,121),CPHEL(401,121),
     2 CONDHEL(401,121),uoH(401),duoHdt(401),FLOW(401),TCOLD(401),
     3 THOT(401),TEXPCOLD(401),TEXPHOT(401),DMEXP(401)
      COMMON HETEMP(594),HEDENS(594),CURVDENS(594),HEENTH(594),
     1 CURVENTH(594),HEENTR(594),CURVENTR(594),HECP(594),CURVCP(594),
     2 HECOND(594),CURVCOND(594),uoHH(200),TH(200),TC(200),DM(200),
     3 CURVuoH(200),CURVTH(200),CURVTC(200),CURVM(200),T1(200),T2(200),
     4 T3(200),T4(200)
      DATA DL/0.254/,D/0.01016/,A/8.488/,RHO/7.14/,POR/0.044/,
     1 VSEG/2.156/,P/69.17/,DMSEG/15.39/
      OPEN(UNIT=2,FILE='HEPROP.DAT',TYPE='OLD')
      OPEN(UNIT=3,FILE='HECURV.DAT',TYPE='OLD')
      OPEN(UNIT=7,FILE='SIM.DAT',TYPE='OLD')
      OPEN(UNIT=4,FILE='SIM2.OUT',TYPE='NEW')
      OPEN(UNIT=1,FILE='SIMCOND.DAT',TYPE='OLD')
      OPEN(UNIT=8,FILE='COLDDIFF.DAT',TYPE='NEW')
C
C   READ SIMULATION CONDITIONS
C
      READ(1,*) NPTS
      DO 10 I=1,NPTS
      READ(1,*) uoHH(I),TH(I),TC(I),DM(I)
      T1(I)=(I-1.)*0.3
      T2(I)=T1(I)+0.05
      T3(I)=T1(I)+0.1
      T4(I)=T1(I)+0.25
10    CONTINUE
      DO 20 I=1,NPTS
      READ(1,*) CURVuoH(I),CURVTH(I),CURVTC(I),CURVM(I)
20    CONTINUE
C
C   READ INPUT DATA FROM 'MAGFRIG.DAT'.
C
      READ(7,*) NtSTPS,NSEG,NCYCLES
      READ(7,*) ITGRAD,TINITIAL,TLOW,THIGH
      READ(7,*) IENTRAIN,INFHTC
C
C   READ HELIUM PROPERTY DATA FROM 'HEPROP.DAT' AND 'HECURV.DAT'
C
      DO 30 I=1,394
      HETEMP(I)=2.12+I*0.02
      READ(2,*) HEDENS(I),HEENTH(I),HEENTR(I),HECP(I),HECOND(I)
      READ(3,*) CURVDENS(I),CURVENTH(I),CURVENTR(I),CURVCP(I),
     1 CURVCOND(I)
30    CONTINUE
      DO 40 I=395,594
      HETEMP(I)=10.+(I-394)*0.05
      READ(2,*) HEDENS(I),HEENTH(I),HEENTR(I),HECP(I),HECOND(I)
      READ(3,*) CURVDENS(I),CURVENTH(I),CURVENTR(I),CURVCP(I),
     1 CURVCOND(I)
40    CONTINUE
      WRITE(4,4000)
      IF (ITGRAD .EQ. 1) THEN
        WRITE(4,4020) TLOW,THIGH
      ELSE
        WRITE(4,4030) TINITIAL
      END IF
      WRITE(4,4060) NSEG
      WRITE(4,4070) DL
      WRITE(4,4120) NtSTPS
C
C   INITIALIZE GGG AND HELIUM TEMPS BY ESTABLISHING A TEMPERATURE GRADIENT
C
      t=5.65
      uoHINIT=FLD(t)
      FLOWINIT=-dmdt(t)
      THEL(1,NSEG+1)=TEMPH(t)
      CALL HEPROP(THEL(1,NSEG+1),RHOHEL(1,NSEG+1),HHEL(1,NSEG+1),
     1 SHEL(1,NSEG+1),CPHEL(1,NSEG+1),CONDHEL(1,NSEG+1),IERR)
```

```
      DO 50 N=NSEG,1,-1
      IF (ITGRAD .EQ. 1) THEN
        TSALT(N)=((NSEG*TLOW-THIGH)+(THIGH-TLOW)*N)/(NSEG-1.)
      ELSE
        TSALT(N)=TINITIAL
      END IF
      CALL TSDATA(0,TSALT(N),SSALT(N),uoHINIT,dSdT(N),dSduoH(N))
      IF (INFHTC .EQ. 1) THEN
        EXPON=0.
      ELSE
        HTC=3.8*CONDHEL(1,N+1)/D
        EXPON=EXP(-HTC*P*DL/(FLOWINIT*CPHEL(1,N+1)))
      END IF
      THEL(1,N)=TSALT(N)+(THEL(1,N+1)-TSALT(N))*EXPON
      CALL HEPROP(THEL(1,N),RHOHEL(1,N),HHEL(1,N),SHEL(1,N),
     1 CPHEL(1,N),CONDHEL(1,N),IERR)
   50 CONTINUE
C
C   START CYCLES
C
      DO 200 K=1,NCYCLES
C
C*********************************************************************
C
C   PROCESS 1:  DEMAGNETIZATION WITH FLOW FROM THE HOT TO COLD RESERVOIR.
C
C*********************************************************************
C
      WRITE(8,*) ' DEMAG FLOW'
      IF (K .EQ. 1) THEN
        t=5.65
        Dt=(8.65-5.65)/NTSTPS
      ELSE IF (K .EQ. 2) THEN
        t=15.85
        Dt=(18.25-15.85)/NTSTPS
      ELSE IF (K .EQ. 3) THEN
        t=26.35
        Dt=(28.75-26.35)/NTSTPS
      ELSE IF (K .EQ. 4) THEN
        t=36.85
        Dt=(39.55-36.85)/NTSTPS
      END IF
      DO 60 J=1,NTSTPS+1
      THEL(J,NSEG+1)=TEMPH(t)
      TEXPCOLD(J)=TEMPC(t)
      CALL HEPROP(THEL(J,NSEG+1),RHOHEL(J,NSEG+1),HHEL(J,NSEG+1),
     1 SHEL(J,NSEG+1),CPHEL(J,NSEG+1),CONDHEL(J,NSEG+1),IERR)
      uoH(J)=FLD(t)
      duoHdt(J)=FLDDERIV(t)
      FLOW(J)=-dmdt(t)
      t=t+Dt
   60 CONTINUE
      DO 80 N=NSEG,1,-1
      TYPE *, 'CYCLE',K,'  P1   N=',N
      DO 70 J=1,NTSTPS
      DERIV1=-(FLOW(J)*(HHEL(J,N)-HHEL(J,N+1))+DMSEG*TSALT(N)*
     1 dSduoH(N)*duoHdt(J))/(POR*VSEG*RHOHEL(J,N)*CV(THEL(J,N))+
     2 DMSEG*TSALT(N)*dSdT(N))
      TSALTINT=TSALT(N)+Dt/2.*DERIV1
      uoHINT=(uoH(J)+uoH(J+1))/2.
      duoHdtINT=(duoHdt(J)+duoHdt(J+1))/2.
      CALL TSDATA(0,TSALTINT,SSALTINT,uoHINT,dSdTINT,dSduoHINT)
      TININT=(THEL(J,N+1)+THEL(J+1,N+1))/2.
      CALL HEPROP(TININT,RHOININT,HININT,SININT,CPININT,CONININT,IERR)
      FLOWINT=(FLOW(J)+FLOW(J))/2.
      IF (INFHTC .EQ. 1) THEN
        EXPON=0.
      ELSE
        HTC=3.8*CONININT/D
        EXPON=EXP(-HTC*P*DL/(FLOWINT*CPININT))
      END IF
      TOUTINT=TSALTINT+(TININT-TSALTINT)*EXPON
      CALL HEPROP(TOUTINT,RHOOUTINT,HOUTINT,SOUTINT,CPOUTINT,CONOUTINT,
     1 IERR)
      DERIV2=-(FLOWINT*(HOUTINT-HININT)+DMSEG*TSALTINT*
     1 dSduoHINT*duoHdtINT)/(POR*VSEG*RHOOUTINT*CV(TOUTINT)+
     2 DMSEG*TSALTINT*dSdTINT)
      TSALT(N)=TSALT(N)+Dt*DERIV2
      IF (INFHTC .EQ. 1) THEN
        EXPON=0.
      ELSE
        HTC=3.8*CONDHEL(J+1,N+1)/D
        EXPON=EXP(-HTC*P*DL/(FLOW(J+1)*CPHEL(J+1,N+1)))
```

```
          END IF
          THEL(J+1,N)=TSALT(N)+(THEL(J+1,N+1)-TSALT(N))*EXPON
          CALL HEPROP(THEL(J+1,N),RHOHEL(J+1,N),HHEL(J+1,N),SHEL(J+1,N),
        1 CPHEL(J+1,N),CONDHEL(J+1,N),IERR)
          IF (IERR .EQ. 1) GOTO 210
          CALL TSDATA(0,TSALT(N),SSALT(N),uoH(J+1),dSdT(N),dSduoH(N))
          IF (N .EQ. 1) TYPE *, 'J=',J+1,'  THEL=',THEL(J+1,1)
          IF (N .EQ. 1) WRITE(8,*) TSALT(1),THEL(J,1)
   70     CONTINUE
   80     CONTINUE
          DO 90 J=1,NtSTPS+1
          WRITE (4,4140) J,THEL(J,1),TEXPCOLD(J),THEL(J,NSEG+1),
        1 FLOW(J),uoH(J)
   90     CONTINUE
C
C  CALCULATE HEAT AND ENTROPY FLUXES FROM COLD END AND TO HOT END
C
          QCOLD=0.
          ENTRCOLD=0.
          QHOT=0.
          ENTRHOT=0.
          DO 100 J=1,NtSTPS
          QCOLD=QCOLD-(FLOW(J)+FLOW(J+1))/2.*(HHEL(J,1)+HHEL(J+1,1))*Dt/2.
          ENTRCOLD=ENTRCOLD-(FLOW(J)+FLOW(J+1))/2.*(SHEL(J,1)
        1 +SHEL(J+1,1))*Dt/2.
          QHOT=QHOT-(FLOW(J)+FLOW(J+1))/2.*(HHEL(J,NSEG+1)
        1 +HHEL(J+1,NSEG+1))*Dt/2.
          ENTRHOT=ENTRHOT-(FLOW(J)+FLOW(J+1))/2.*(SHEL(J,NSEG+1)
        1 +SHEL(J+1,NSEG+1))*Dt/2.
  100     CONTINUE
C
C*************************************************************************
C
C   PROCESS 2:  ADIABATIC MAGNETIZATION
C
C*************************************************************************
C
C  IF IENTRAIN=1 THEN ENTRAINED HELIUM EFFECTS ARE CONSIDERED, OTHERWISE
C  ENTRAINED HELIUM IS NEGLECTED.
C
          uoHSTART=uoH(NTSTPS+1)
          IF (K .EQ. 1) t=10.45
          IF (K .EQ. 2) t=20.95
          IF (K .EQ. 3) t=31.45
          IF (K .EQ. 4) GOTO 210
          uoHEND=FLD(t)
          FLOWEND=dmdt(t)
          DO 110 N=1,NSEG
          TYPE *, 'ADMAG N=',N
          TSTART=TSALT(N)
          CALL TSDATA(1,TSALT(N),SSALT(N),uoHEND,dSdT(N),dSduoH(N))
          IF (IENTRAIN .EQ. 1) THEN
            CALL HEPROP(TSTART,RHOHE,HHE,SHE,CPHE,CONDHE,IERR)
            IF (IERR .EQ. 1) GOTO 210
            SSEG=DMSEG*SSALT(N)+POR*VSEG*RHOHE*SHE
C
C  USE BISECTION METHOD TO FIND SOLUTION
C
            TENDA=TSTART
            TENDB=TSALT(N)
            DIFF=1.
            ILOOP=0
            DO WHILE (ABS(DIFF/SSEG) .GT. 0.001)
              ILOOP=ILOOP+1
              IF (ILOOP .EQ. 200) GOTO 210
              TENDM=(TENDA+TENDB)/2.
              CALL TSDATA(0,TENDM,SSALTM,uoHEND,dSdTM,dSduoHM)
              CALL HEPROP(TENDM,RHOHEM,HHEM,SHEM,CPHEM,CONDHEM,IERR)
              IF (IERR .EQ. 1) GOTO 210
              SSEGM=DMSEG*SSALTM+POR*VSEG*RHOHE*SHEM
              DIFF=SSEGM-SSEG
              IF (DIFF .GT. 0.) THEN
                TENDB=TENDM
              ELSE
                TENDA=TENDM
              END IF
            END DO
            TSALT(N)=TENDM
            SSALT(N)=SSALTM
            dSdT(N)=dSdTM
            dSduoH(N)=dSduoHM
          END IF
  110     CONTINUE
```

```
        THEL(1,1)=TEMPC(t)
        CALL HEPROP(THEL(1,1),RHOHEL(1,1),HHEL(1,1),SHEL(1,1),CPHEL(1,1),
     1  CONDHEL(1,1),IERR)
        DO 120 N=1,NSEG
        IF (INFHTC .EQ. 1) THEN
          EXPON=0.
        ELSE
          HTC=3.8*CONDHEL(1,N)/D
          EXPON=EXP(-HTC*P*DL/(FLOWEND*CPHEL(1,N)))
        END IF
        THEL(1,N+1)=TSALT(N)+(THEL(1,N)-TSALT(N))*EXPON
        CALL HEPROP(THEL(1,N+1),RHOHEL(1,N+1),HHEL(1,N+1),
     1  SHEL(1,N+1),CPHEL(1,N+1),CONDHEL(1,N+1),IERR)
        IF (IERR .EQ. 1) GOTO 210
  120   CONTINUE
C
C*****************************************************************************
C
C   PROCESS 3:  MAGNETIZATION WITH FLOW FROM THE COLD TO HOT RESERVOIR.
C
C*****************************************************************************
C
        IF (K .EQ. 1) THEN
          t=10.45
          Dt=(14.85-10.45)/NTSTPS
        ELSE IF (K .EQ. 2) THEN
          t=20.95
          Dt=(24.25-20.95)/NTSTPS
        ELSE IF (K .EQ. 3) THEN
          t=31.45
          Dt=(34.45-31.45)/NTSTPS
        ELSE IF (K .EQ. 4) THEN
          t=36.85
          Dt=(39.55-36.85)/NTSTPS
        END IF
        DO 130 J=1,NTSTPS+1
        THEL(J,1)=TEMPC(t)
        TEXPHDT(J)=TEMPH(t)
        CALL HEPROP(THEL(J,1),RHOHEL(J,1),HHEL(J,1),SHEL(J,1),
     1  CPHEL(J,1),CONDHEL(J,1),IERR)
        uoH(J)=FLD(t)
        duoHdt(J)=FLDDERIV(t)
        FLOW(J)=dmdt(t)
        t=t+Dt
  130   CONTINUE
        DO 150 N=1,NSEG
        TYPE *, 'CYCLE',K,'  P3   N=',N
        DO 140 J=1,NTSTPS
        DERIV1=-(FLOW(J)*(HHEL(J,N+1)-HHEL(J,N))+DMSEG*TSALT(N)*
     1  dSduoH(N)*duoHdt(J))/(POR*VSEG*RHOHEL(J,N+1)*CV(THEL(J,N+1))+
     2  DMSEG*TSALT(N)*dSdT(N))
        TSALTINT=TSALT(N)+Dt/2.*DERIV1
        uoHINT=(uoH(J)+uoH(J+1))/2.
        duoHdtINT=(duoHdt(J)+duoHdt(J+1))/2.
        CALL TSDATA(0,TSALTINT,SSALTINT,uoHINT,dSdTINT,dSduoHINT)
        TININT=(THEL(J,N)+THEL(J+1,N))/2.
        CALL HEPROP(TININT,RHOININT,HININT,SININT,CPININT,CONINNT,IERR)
        FLOWINT=(FLOW(J)+FLOW(J+1))/2.
        IF (INFHTC .EQ. 1) THEN
          EXPON=0.
        ELSE
          HTC=3.8*CONINNT/D
          EXPON=EXP(-HTC*P*DL/(FLOWINT*CPININT))
        END IF
        TOUTINT=TSALTINT+(TININT-TSALTINT)*EXPON
        CALL HEPROP(TOUTINT,RHOOUTINT,HOUTINT,SOUTINT,CPOUTINT,CONOUTINT,
     1  IERR)
        DERIV2=-(FLOWINT*(HOUTINT-HININT)+DMSEG*TSALTINT*
     1  dSduoHINT*duoHdtINT)/(POR*VSEG*RHOOUTINT*CV(TOUTINT)+
     2  DMSEG*TSALTINT*dSdTINT)
        TSALT(N)=TSALT(N)+Dt*DERIV2
        IF (INFHTC .EQ. 1) THEN
          EXPON=0.
        ELSE
          HTC=3.8*CONDHEL(J+1,N)/D
          EXPON=EXP(-HTC*P*DL/(FLOW(J+1)*CPHEL(J+1,N)))
        END IF
        THEL(J+1,N+1)=TSALT(N)+(THEL(J+1,N)-TSALT(N))*EXPON
        CALL HEPROP(THEL(J+1,N+1),RHOHEL(J+1,N+1),HHEL(J+1,N+1),
     1  SHEL(J+1,N+1),CPHEL(J+1,N+1),CONDHEL(J+1,N+1),IERR)
        IF (IERR .EQ. 1) GOTO 210
        CALL TSDATA(0,TSALT(N),SSALT(N),uoH(J+1),dSdT(N),dSduoH(N))
        IF (N .EQ. NSEG) TYPE *, 'J=',J+1,'  THEL=',THEL(J+1,NSEG+1)
```

```
  140   CONTINUE
  150   CONTINUE
        WRITE(4,4170) K
        DO 160 J=1,NtSTPS+1
        WRITE (4,4140) J,THEL(J,NSEG+1),THEL(J,1),TEXPHOT(J),
     1  FLOW(J),uoH(J)
  160   CONTINUE
C
C  CALCULATE HEAT AND ENTROPY FLUXES TO HOT END
C
        DO 170 J=1,NtSTPS+1
        QCOLD=QCOLD+(FLOW(J)+FLOW(J+1))/2.*(HHEL(J,1)+
     1  HHEL(J+1,1))*Dt/2.
        ENTRCOLD=ENTRCOLD+(FLOW(J)+FLOW(J+1))/2.*(SHEL(J,1)+
     1  SHEL(J+1,1))*Dt/2.
        QHOT=QHOT+(FLOW(J)+FLOW(J+1))/2.*(HHEL(J,NSEG+1)+
     1  HHEL(J+1,NSEG+1))*Dt/2.
        ENTRHOT=ENTRHOT+(FLOW(J)+FLOW(J+1))/2.*(SHEL(J,NSEG+1)+
     1  SHEL(J+1,NSEG+1))*Dt/2.
  170   CONTINUE
        QCOLD=QCOLD/10.3
        ENTRCOLD=ENTRCOLD/10.3
        QHOT=QHOT/10.3
        ENTRHOT=ENTRHOT/10.3
        TYPE *, ' QCOLD = ',QCOLD
        TYPE *, ' QHOT=',QHOT
        TYPE *, ' SCOLD=',ENTRCOLD
        TYPE *, ' SHOT=',ENTRHOT
        WRITE(4,4150) QCOLD
        WRITE(4,4160) ENTRCOLD
        WRITE(4,4190) QHOT
        WRITE(4,4200) ENTRHOT
C
C*****************************************************************
C
C   PROCESS 4:  ADIABATIC DEMAGNETIZATION
C
C*****************************************************************
C
C  IF IENTRAIN=1 THEN ENTRAINED HELIUM EFFECTS ARE CONSIDERED, OTHERWISE
C  ENTRAINED HELIUM IS NEGLECTED.
C
        uoHSTART=uoH(NTSTPS+1)
        IF (K .EQ. 1) t=15.85
        IF (K .EQ. 2) t=26.35
        IF (K .EQ. 3) t=36.85
        uoHEND=FLD(t)
        FLOWEND=dmdt(t)
        DO 180 N=1,NSEG
        TYPE *, 'ADDEM N=',N
        TSTART=TSALT(N)
        CALL TSDATA(1,TSALT(N),SSALT(N),uoHEND,dSdT(N),dSduoH(N))
        IF (IENTRAIN .EQ. 1) THEN
          CALL HEPROP(TSTART,RHOHE,HHE,SHE,CPHE,CONDHE,IERR)
          IF (IERR .EQ. 1) GOTO 210
          SSEG=DMSEG*SSALT(N)+POR*VSEG*RHOHE*SHE
C
C  USE BISECTION METHOD TO FIND SOLUTION
C
          TENDA=TSTART
          TENDB=TSALT(N)
          DIFF=1.
          ILOOP=0
          DO WHILE (ABS(DIFF/SSEG) .GT. 0.001)
            ILOOP=ILOOP+1
            IF (ILOOP .EQ. 200) GOTO 210
            TENDM=(TENDA+TENDB)/2.
            CALL TSDATA(0,TENDM,SSALTM,uoHEND,dSdTM,dSduoHM)
            CALL HEPROP(TENDM,RHOHEM,HHEM,SHEM,CPHEM,CONDHEM,IERR)
            IF (IERR .EQ. 1) GOTO 210
            SSEGM=DMSEG*SSALTM+POR*VSEG*RHOHE*SHEM
            DIFF=SSEGM-SSEG
            IF (DIFF .LT. 0.) THEN
              TENDB=TENDM
            ELSE
              TENDA=TENDM
            END IF
          END DO
          TSALT(N)=TENDM
          SSALT(N)=SSALTM
          dSdT(N)=dSdTM
          dSduoH(N)=dSduoHM
        END IF
```

```
 180   CONTINUE
       THEL(1,NSEG+1)=TEMPH(t)
       CALL HEPROP(THEL(1,NSEG+1),RHOHEL(1,NSEG+1),HHEL(1,NSEG+1),
     1 SHEL(1,NSEG+1),CPHEL(1,NSEG+1),CONDHEL(1,NSEG+1),IERR)
       DO 190 N=NSEG,1,-1
       IF (IENTRAIN .EQ. 1) THEN
         EXPON=0.
       ELSE
         HTC=3.8*CONDHEL(1,N+1)/D
         EXPON=EXP(-HTC*P*DL/(FLOWEND*CPHEL(1,N+1)))
       END IF
       THEL(1,N)=TSALT(N)+(THEL(1,N+1)-TSALT(N))*EXPON
       CALL HEPROP(THEL(1,N),RHOHEL(1,N),HHEL(1,N),SHEL(1,N),
     1 CPHEL(1,N),CONDHEL(1,N),IERR)
       IF (IERR .EQ. 1) GOTO 210
 190   CONTINUE
 200   CONTINUE
 210   STOP
4000   FORMAT(' Results of active thermal regenerator simulation:'/
     1' ------------------------------------------------')
4010   FORMAT(' Cold reservoir temp = ',PE11.4,' K.'/
     1' Hot reservoir temp = ',PE11.4,' K.')
4020   FORMAT(' Initial GGG temp is linear from ',PE11.4,' K to ',
     1 PE11.4,' K.')
4030   FORMAT(' Initial GGG temp is ',PE11.4,' K throughout the core.')
4040   FORMAT(' He mass flow during magnetization = ',PE11.4,
     1' * uoH **',PE11.4,' g/s.'
     2/' He mass flow during demagnetization flow process = ',PE11.4,
     3' * uoH **',PE11.4,' g/s.')
4060   FORMAT(' No. of GGG segments = ',I3)
4070   FORMAT(' Length of a single segment = ',PE11.4,' cm.')
4080   FORMAT(' Duration of a magnetization flow process = ',PE11.4,
     1' s.'/' Duration of a demagnetization flow process = ',PE11.4,
     2' s.')
4090   FORMAT(' Duration of an adiabatic magnetization process = ',
     1PE11.4,' s.'/' Duration of an adiabatic demagnetization process
     2 =',PE11.4,' s.')
4100   FORMAT(' The lowest field is ',PE11.4,' T.'/' The highest field
     1 is ',PE11.4,' T.'/' The field ramps up and down at ',PE11.4,
     2' T/s.')
4120   FORMAT(' No. of time steps = ',I3,'.')
4121   FORMAT(' Hot reservoir at ',PE12.4,'  Cold reservoir at ',PE12.4)
4122   FORMAT(' Helium mass flow rate = ',PE12.4)
4130   FORMAT(//' Cycle ',I2,' Demagnetization Flow Process')
4140   FORMAT(I4,6(PE12.4))
4150   FORMAT(' QCOLD = ',PE11.4,' W')
4160   FORMAT(' SCOLD = ',PE11.4,' W/K')
4170   FORMAT(/' Cycle ',I2,' Magnetization Flow Process')
4180   FORMAT(' THEL(',I3,',',I3,') = ',PE11.4)
4190   FORMAT(' QHOT = ',PE11.4,' W')
4200   FORMAT(' SHOT = ',PE11.4,' W/K')
       END



C
C   SUBROUTINES
C
       SUBROUTINE HEPROP(T,DENS,ENTH,ENTR,CP,COND,IERR)
C
C  THIS SUBROUTINE CALCULATES HELIUM DENSITY, ENTHALPY, ENTROPY, SPECIFIC
C  HEAT AT CONSTANT PRESSURE, AND THERMAL CONDUCTIVITY AT 3 ATM OF PRESSURE
C  AND AT TEMPERATURES BETWEEN 2.15 AND 20 K.  THE PROPERTIES ARE INTERPOLATED
C  FROM A TABLE USING CUBIC SPLINES.
C
       COMMON HETEMP(594),HEDENS(594),CURVDENS(594),HEENTH(594),
     1 CURVENTH(594),HEENTR(594),CURVENTR(594),HECP(594),CURVCP(594),
     2 HECOND(594),CURVCOND(594),uoHH(200),TH(200),TC(200),DM(200),
     3 CURVuoH(200),CURVTH(200),CURVTC(200),CURVM(200),T1(200),T2(200),
     4 T3(200),T4(200)
       IERR=0
       IF (T .LT. 2.15) THEN
         IERR=1
         TYPE *, 'HELIUM TEMP TOO LOW TO CALCULATE DENSITY'
         RETURN
       END IF
       IF (T .GT. 20.) THEN
         IERR=1
         TYPE *, 'HELIUM TEMP TOO HIGH TO CALCULATE DENSITY'
         RETURN
       END IF
       IF (T .GT. 10.) THEN
```

```
          IT=394+(T-10.)/0.05
        ELSE
          IT=1+(T-2.14)/0.02
        END IF
        TA=HETEMP(IT)
        TB=HETEMP(IT+1)
        DTEMPI=TB-TA
        DENS=CURVDENS(IT)/6.*((TB-T)**3/DTEMPI-DTEMPI*(TB-T))+
     1  CURVDENS(IT+1)/6.*((T-TA)**3/DTEMPI-DTEMPI*(T-TA))+HEDENS(IT)
     2  *(TB-T)/DTEMPI+HEDENS(IT+1)*(T-TA)/DTEMPI
        DENS=DENS/1000.
        ENTH=CURVENTH(IT)/6.*((TB-T)**3/DTEMPI-DTEMPI*(TB-T))+
     1  CURVENTH(IT+1)/6.*((T-TA)**3/DTEMPI-DTEMPI*(T-TA))+HEENTH(IT)
     2  *(TB-T)/DTEMPI+HEENTH(IT+1)*(T-TA)/DTEMPI
        ENTR=CURVENTR(IT)/6.*((TB-T)**3/DTEMPI-DTEMPI*(TB-T))
     1  +CURVENTR(IT+1)/6.*((T-TA)**3/DTEMPI-DTEMPI*(T-TA))+HEENTR(IT)
     2  *(TB-T)/DTEMPI+HEENTR(IT+1)*(T-TA)/DTEMPI
        CP=CURVCP(IT)/6.*((TB-T)**3/DTEMPI-DTEMPI*(TB-T))
     1  +CURVCP(IT+1)/6.*((T-TA)**3/DTEMPI-DTEMPI*(T-TA))+HECP(IT)
     2  *(TB-T)/DTEMPI+HECP(IT+1)*(T-TA)/DTEMPI
        COND=CURVCOND(IT)/6.*((TB-T)**3/DTEMPI-DTEMPI*(TB-T))
     1  +CURVCOND(IT+1)/6.*((T-TA)**3/DTEMPI-DTEMPI*(T-TA))+HECOND(IT)
     2  *(TB-T)/DTEMPI+HECOND(IT+1)*(T-TA)/DTEMPI
        COND=COND/1000.
        RETURN
        END


        SUBROUTINE TSDATA(IFLAG,T,S,uoH,DSDT,DSDuoH)
C
C  IF IFLAG=0, TEMPERATURE IS GIVEN.  IF IFLAG=1, ENTROPY IS GIVEN.
C
        IF (IFLAG .EQ. 0) THEN
          CALL GGGPROP(T,uoH,DSDuoH,S,DSDT)
        ELSE IF (IFLAG .EQ. 1) THEN
          TA=2.0
          CALL GGGPROP(TA,uoH,DSDuoHA,SA,DSDTA)
          TB=20.
          CALL GGGPROP(TB,uoH,DSDuoHB,SB,DSDTB)
          IF ((S-SA)*(S-SB) .GE. 0.) THEN
            TYPE *,' ENTROPY IS OUT OF RANGE OF THE AVAILABLE DATA.'
            RETURN
          END IF
          RES=1.
          DO WHILE (RES .GT. 0.0001)
            TM=(TA+TB)/2.
            CALL GGGPROP(TM,uoH,DSDuoHM,SM,DSDTM)
            IF ((S-SM)*(S-SB) .LT. 0.) THEN
              TA=TM
            ELSE
              TB=TM
              SB=SM
            END IF
            RES=(TB-TA)
          END DO
          T=TM
          DSDuoH=DSDuoHM
          S=SM
          DSDT=DSDTM
        END IF
        RETURN
        END


        SUBROUTINE GGGPROP(T,uoH,dsduoH,s,dsdT)
C
C    Given temperature in Kelvin and uoH in Tesla, entropy s and its
C  derivatives ds/duoH (equivalent to vdM/dT) and ds/dT are calculated.
C  The units are J/(g K) for s, J/(g K T) for ds/duoH, and J/(g K^2)
C  for ds/dT.
C
C    Calculation of ds/duoH is exact from the curvefitted magnetization.
C  Calculation of s and ds/dT is done with the use of Gauss-Legendre
C  Quadrature.
C
C    W and ETA are used in the quadrature method.
C
        DIMENSION W(6),ETA(6)
        DATA ETA/0.1252334085,0.3678314990,0.5873179543,0.7699026742,
     1  0.9041172564,0.9815606342/
        DATA W/0.2491470458,0.2334925365,0.2031674267,0.1600783285,
     1  0.1069393260,0.0471753364/
C
```

```
C     Calculation of ds/duoH:
C
      CALL DERIV(T,uoH,dsduoH,vd2MdT2)
C
C     Calculation of s and dsdT:  s0 is the entropy at uoH=0, and
C   ds0dT is the derivative of entropy with respect to temperature at
C   uoH=0.  s and dsdT are calculated using Gauss-Legendre Quadrature.
C
      s0=2.3E-07*T**3-3.1925E-02/T**2+1.699E-02/T**3-
     1  (2.3E-07-3.1925E-02+1.699E-02)
      ds0dt=6.9E-07*T**2+6.385E-02/T**3-5.096E-02/T**4
      sSUM=0.
      dsdTSUM=0.
      DO 10 I=1,6
      x1=uoH/2.*(1+ETA(I))
      x2=uoH/2.*(1-ETA(I))
      CALL DERIV(T,x1,vdMdT1,vd2MdT21)
      CALL DERIV(T,x2,vdMdT2,vd2MdT22)
      sSUM=sSUM+W(I)*(vdMdT1+vdMdT2)
      dsdTSUM=dsdTSUM+W(I)*(vd2MdT21+vd2MdT22)
   10 CONTINUE
      s=s0+uoH/2.*sSUM
      dsdT=ds0dT+uoH/2.*dsdTSUM
      RETURN
      END


      SUBROUTINE DERIV(T,uoH,vdMdT,vd2MdT2)
C
C     This subroutine calculates vdM/dT and vd2M/dT2 given T and uoH.
C   T is in Kelvin, uoH is in Tesla, vdM/dT is in J/(g K T), and
C   vd2M/dT2 is in J/(g K T^2).
C
C
C     Calculation of functions C0,C1,C2,C3, and C4 and their derivatives
C   with respect to temperature:
C
      C0=13.67388+2.718523*T+0.1278728*T**2-2.5072373E-03*T**3
      C1=-2.988799+0.9144735*T-7.3461875E-02*T**2+1.1088194E-03*
     1  T**3+9.8684995E-06*T**4
      C2=3.166695-0.6364962*T+4.8334930E-02*T**2-1.0840200E-03*
     1  T**3+4.3787923E-06*T**4
      C3=-0.3461423+9.0944469E-02*T-6.9979527E-03*T**2+
     1  1.3868879E-04*T**3
      C4=1.3560383E-02-4.1968897E-03*T+3.3840450E-04*T**2-
     1  6.8436516E-06*T**3
      dC0dT=2.718523+2.*0.1278728*T-3.*2.5072373E-03*T**2
      dC1dT=0.9144735-2.*7.3461875E-02*T+3.*1.1088194E-03*
     1  T**2+4.*9.8684995E-06*T**3
      dC2dT=-0.6364962+2.*4.8334930E-02*T-3.*1.0840200E-03*
     1  T**2+4.*4.3787923E-06*T**3
      dC3dT=9.0944469E-02-2.*6.9979527E-03*T+3.*1.3868879E-04*T**2
      dC4dT=-4.1968897E-03+2.*3.3840450E-04*T-3.*6.8436516E-06*T**2
      d2C0dT2=2.*0.1278728-6.*2.5072373E-03*T
      d2C1dT2=-2.*7.3461875E-02+6.*1.1088194E-03*T+
     1  12.*9.8684995E-06*T**2
      d2C2dT2=2.*4.8334930E-02-6.*1.0840200E-03*T+
     1  12.*4.3787923E-06*T**2
      d2C3dT2=-2.*6.9979527E-03+6.*1.3868879E-04*T
      d2C4dT2=2.*3.3840450E-04-6.*6.8436516E-06*T
C
C     Calculation of vdMdT and vd2MdT2:
C
      DEN=C0+C1*uoH+C2*uoH**2+C3*uoH**3+C4*uoH**4
      dDENdT=dc0dT+dC1dT*uoH+dC2dT*uoH**2+dC3dT*uoH**3+dC4dT*uoH**4
      d2DENdT2=d2c0dT2+d2C1dT2*uoH+d2C2dT2*uoH**2+d2C3dT2*uoH**3+
     1  d2C4dT2*uoH**4
      vdMdT=-uoH*dDENdT/DEN**2
      vd2MdT2=uoH*(2.*dDENdT**2-DEN*d2DENdT2)/DEN**3
      RETURN
      END


      REAL FUNCTION CV(T)
C
C   This subroutine interpolates the specific heat capacity at
C   at constant pressure for 3-atm supercritical helium.  Linear
C   interpolation is performed from NBS tabulated data.
C
      REAL CVHE(29)
      DATA CVHE/1.773,1.880,2.064,2.217,2.397,2.639,2.699,2.748,
     1  2.765,2.827,2.929,3.098,3.204,3.227,3.225,3.217,3.168,3.137,
     2  3.127,3.112,3.105,3.107,3.107,3.108,3.109,3.112,3.115,3.117,
```

```
     3  3.119/
        IF (T .LE. 2.5) THEN
          CV=CVHE(1)
        ELSE IF (T .LE. 5.) THEN
          I=(T-2.5)/0.5+1
          CV=CVHE(I)+(T-(2.+0.5*I))/0.5*(CVHE(I+1)-CVHE(I))
        ELSE IF (T .LE. 6.) THEN
          I=(T-5.)/0.1+6
          CV=CVHE(I)+(T-(4.4+0.1*I))/0.1*(CVHE(I+1)-CVHE(I))
        ELSE IF (T .LE. 10.) THEN
          I=(T-6.)/0.5+16
          CV=CVHE(I)+(T-(-2.+0.5*I))/0.5*(CVHE(I+1)-CVHE(I))
        ELSE IF (T .LE. 15.) THEN
          I=(T-10.)+24
          CV=CVHE(I)+(T-(-14.+I))*(CVHE(I+1)-CVHE(I))
        ELSE IF (T .GT. 15) THEN
          TYPE *, 'CV CANNOT BE CALCULATED.'
        END IF
        RETURN
        END

        REAL FUNCTION FLD(TT)
C
C   This function reproduces experimental field values in Tesla as a
C   function of time for several cycles using cubic splines.
C
        COMMON HETEMP(594),HEDENS(594),CURVDENS(594),HEENTH(594),
     1  CURVENTH(594),HEENTR(594),CURVENTR(594),HECP(594),CURVCP(594),
     2  HECOND(594),CURVCOND(594),uoHH(200),TH(200),TC(200),DM(200),
     3  CURVuoH(200),CURVTH(200),CURVTC(200),CURVM(200),T1(200),T2(200),
     4  T3(200),T4(200)
        I=TT/0.3+1
        DT=0.3
        IF (I .NE. 132) THEN
          FLD=CURVuoH(I)/6.*((T1(I+1)-tt)**3/Dt-Dt*(T1(I+1)-tt))
     1  +CURVuoH(I+1)/6.*((tt-T1(I))**3/Dt-Dt*(tt-T1(I)))
     2  +uoHH(I)*(T1(I+1)-tt)/Dt+uoHH(I+1)*(tt-T1(I))/Dt
        ELSE
          FLD=uoHH(132)
        END IF
        RETURN
        END

        REAL FUNCTION FLDDERIV(TT)
C
C   This function reproduces experimental values of uodHdt in T/s as a
C   function of time for several cycles using cubic splines.
C
        COMMON HETEMP(594),HEDENS(594),CURVDENS(594),HEENTH(594),
     1  CURVENTH(594),HEENTR(594),CURVENTR(594),HECP(594),CURVCP(594),
     2  HECOND(594),CURVCOND(594),uoHH(200),TH(200),TC(200),DM(200),
     3  CURVuoH(200),CURVTH(200),CURVTC(200),CURVM(200),T1(200),T2(200),
     4  T3(200),T4(200)
        I=TT/0.3+1
        DT=0.3
        IF (I .NE. 132) THEN
          FLDDERIV=CURVuoH(I)/6.*(-3.*(T1(I+1)-tt)**2/Dt+Dt)+
     1  CURVuoH(I+1)/6.*(3.*(tt-T1(I))**2/Dt-Dt)-uoHH(I)/Dt+
     2  uoHH(I+1)/Dt
        ELSE
          FLDDERIV=CURVuoH(I-1)*Dt+CURVuoH(I)*2.*Dt-uoHH(I-1)/Dt+
     2  uoHH(I)/Dt
        END IF
        RETURN
        END

        REAL FUNCTION TEMPH(TT)
C
C   This function reproduces experimental hot reservoir temperatures as
C   a function of time for several cycles using cubic splines.
C
        COMMON HETEMP(594),HEDENS(594),CURVDENS(594),HEENTH(594),
     1  CURVENTH(594),HEENTR(594),CURVENTR(594),HECP(594),CURVCP(594),
     2  HECOND(594),CURVCOND(594),uoHH(200),TH(200),TC(200),DM(200),
     3  CURVuoH(200),CURVTH(200),CURVTC(200),CURVM(200),T1(200),T2(200),
     4  T3(200),T4(200)
        I=(TT-0.05)/0.3+1
        DT=0.3
        IF (I .NE. 132) THEN
          TEMPH=CURVTH(I)/6.*((T2(I+1)-tt)**3/Dt-Dt*(T2(I+1)-tt))
     1  +CURVTH(I+1)/6.*((tt-T2(I))**3/Dt-Dt*(tt-T2(I)))
     2  +TH(I)*(T2(I+1)-tt)/Dt+TH(I+1)*(tt-T2(I))/Dt
        ELSE
```

```
          TEMPH=TH(132)
        END IF
        RETURN
        END

        REAL FUNCTION TEMPC(TT)
C
C   This function reproduces experimental cold reservoir temperature as
C   a function of time for several cycles using cubic splines.
C
        COMMON HETEMP(594),HEDENS(594),CURVDENS(594),HEENTH(594),
     1  CURVENTH(594),HEENTR(594),CURVENTR(594),HECP(594),CURVCP(594),
     2  HECOND(594),CURVCOND(594),uoHH(200),TH(200),TC(200),DM(200),
     3  CURVuoH(200),CURVTH(200),CURVTC(200),CURVM(200),T1(200),T2(200),
     4  T3(200),T4(200)
        I=(TT-0.1)/0.3+1
        DT=0.3
        IF (I .NE. 132) THEN
          TEMPC=CURVTC(I)/6.*((T3(I+1)-tt)**3/Dt-Dt*(T3(I+1)-tt))
     1  +CURVTC(I+1)/6.*((tt-T3(I))**3/Dt-Dt*(tt-T3(I)))
     2  +TC(I)*(T3(I+1)-tt)/Dt+TC(I+1)*(tt-T3(I))/Dt
        ELSE
          TEMPC=TC(132)
        END IF
        RETURN
        END

        REAL FUNCTION HEMASS(tt)
C
C   This function reproduces experimental values of the He mass in the
C   displacer cylinder in grams as a function of time for several
C   cycles using cubic splines.
C
        COMMON HETEMP(594),HEDENS(594),CURVDENS(594),HEENTH(594),
     1  CURVENTH(594),HEENTR(594),CURVENTR(594),HECP(594),CURVCP(594),
     2  HECOND(594),CURVCOND(594),uoHH(200),TH(200),TC(200),DM(200),
     3  CURVuoH(200),CURVTH(200),CURVTC(200),CURVM(200),T1(200),T2(200),
     4  T3(200),T4(200)
        I=(tt-0.25)/0.3+1
        Dt=0.3
        IF (I .NE. 132) THEN
          HEMASS=CURVM(I)/6.*((T4(I+1)-tt)**3/Dt-Dt*(T4(I+1)-tt))
     1  +CURVM(I+1)/6.*((tt-T4(I))**3/Dt-Dt*(tt-T4(I)))
     2  +DM(I)*(T4(I+1)-tt)/Dt+DM(I+1)*(tt-T4(I))/Dt
        ELSE
          HEMASS=DM(132)
        END IF
        RETURN
        END

        REAL FUNCTION dmdt(TT)
C
C   This function reproduces experimental values of the mass flow rate
C   in g/s as a function of time for several cycles using cubic splines.
C
        COMMON HETEMP(594),HEDENS(594),CURVDENS(594),HEENTH(594),
     1  CURVENTH(594),HEENTR(594),CURVENTR(594),HECP(594),CURVCP(594),
     2  HECOND(594),CURVCOND(594),uoHH(200),TH(200),TC(200),DM(200),
     3  CURVuoH(200),CURVTH(200),CURVTC(200),CURVM(200),T1(200),T2(200),
     4  T3(200),T4(200)
        I=(TT-0.25)/0.3+1
        DT=0.3
        IF (I .NE. 132) THEN
          dmdt=CURVM(I)/6.*(-3.*(T4(I+1)-tt)**2/Dt+Dt)
     1  +CURVM(I+1)/6.*(3.*(tt-T4(I))**2/Dt-Dt)
     2  -DM(I)/Dt+DM(I+1)/Dt
        ELSE
          dmdt=CURVM(I-1)*Dt+CURVM(I)*2.*Dt-DM(I-1)/Dt+DM(I)/Dt
        END IF
        RETURN
        END
```

```
C
C   Single-shot Magnetization Flow Program
C
C
C       This program is a numerical simulation of a magnetically active
C   regenerator, based on the differential equations derived in chapter
C   3 and the GGG thermodynamic properties derived in chapter 5.  It
C   uses the Second Order Runge Kutta method to solve the differential
C   equations.
C
C
      PROGRAM MAGFLOW
      DIMENSION TSALT(120),SSALT(120),dSdT(120),dSduoH(120),THEL(401,121),
     1  RHOHEL(401,121),HHEL(401,121),SHEL(401,121),CPHEL(401,121),
     2  CONDHEL(401,121)
      COMMON HETEMP(594),HEDENS(594),CURVDENS(594),HEENTH(594),
     1  CURVENTH(594),HEENTR(594),CURVENTR(594),HECP(594),CURVCP(594),
     2  HECOND(594),CURVCOND(594)
      DATA DL/0.254/,D/0.01016/,A/8.488/,RHO/7.14/,POR/0.044/,
     1  VSEG/2.156/,P/69.17/,DMSEG/15.39/
      OPEN(UNIT=2,FILE='[TAUSSIG.MAGFRIG]HEPROP.DAT',TYPE='OLD')
      OPEN(UNIT=3,FILE='[TAUSSIG.MAGFRIG]HECURV.DAT',TYPE='OLD')
      OPEN(UNIT=7,FILE='MAG.DAT',TYPE='OLD')
      OPEN(UNIT=4,FILE='MAG.OUT',TYPE='NEW')
C
C   READ INPUT DATA FROM 'MAG.DAT'.
C
      READ(7,*) NtSTPS,NSEG
      READ(7,*) TINITIAL,TCOLD
      READ(7,*) INFHTC,HEFLOW,FLTIME
      READ(7,*) uoHINIT,duoHdt
C
C   READ HELIUM PROPERTY DATA FROM 'HEPROP.DAT' AND 'HECURV.DAT'
C
      DO 10 I=1,394
      HETEMP(I)=2.12+I*0.02
      READ(2,*) HEDENS(I),HEENTH(I),HEENTR(I),HECP(I),HECOND(I)
      READ(3,*) CURVDENS(I),CURVENTH(I),CURVENTR(I),CURVCP(I),
     1  CURVCOND(I)
   10 CONTINUE
      DO 20 I=395,594
      HETEMP(I)=10.+(I-394)*0.05
      READ(2,*) HEDENS(I),HEENTH(I),HEENTR(I),HECP(I),HECOND(I)
      READ(3,*) CURVDENS(I),CURVENTH(I),CURVENTR(I),CURVCP(I),
     1  CURVCOND(I)
   20 CONTINUE
C
C   SETUP -- GEOMETRY IS CALCULATED.
C
      WRITE(4,4000)
      WRITE(4,4030) TINITIAL
      WRITE(4,4060) NSEG
      WRITE(4,4070) DL
      WRITE(4,4120) NtSTPS
C
C   INITIALIZE GGG AND HELIUM TEMPS BY ESTABLISHING A TEMPERATURE GRADIENT
C
      CALL HEPROP(TCOLD,RHOCOLD,HCOLD,SCOLD,CPCOLD,CONDCOLD,IERR)
      THEL(1,1)=TCOLD
      HHEL(1,1)=HCOLD
      CPHEL(1,1)=CPCOLD
      CONDHEL(1,1)=CONDCOLD
      CALL TSDATA(0,TINITIAL,SINITIAL,uoHINIT,dSdTINIT,dSduoHINIT)
      DO 30 N=1,NSEG
      TSALT(N)=TINITIAL
      SSALT(N)=SINITIAL
      dSdT(N)=dSdTINIT
      dSduoH(N)=dSduoHINIT
      IF (INFHTC .EQ. 1) THEN
        EXPON=0.
      ELSE
        HTC=3.6*CONDHEL(1,N)/D
        EXPON=EXP(-HTC*P*DL/(HEFLOW*CPHEL(1,N)))
      END IF
      THEL(1,N+1)=TSALT(N)+(THEL(1,N)-TSALT(N))*EXPON
      CALL HEPROP(THEL(1,N+1),RHOHEL(1,N+1),HHEL(1,N+1),SHEL(1,N+1),
     1  CPHEL(1,N+1),CONDHEL(1,N+1),IERR)
   30 CONTINUE
C
C*****************************************************************
C
C   MAGNETIZATION WITH FLOW FROM THE COLD TO HOT RESERVOIR.
C
```

```
C*****************************************************************
C
      DO 40 J=1,NTSTPS+1
      THEL(J,1)=TCOLD
      RHOHEL(J,1)=RHOCOLD
      HHEL(J,1)=HCOLD
      SHEL(J,1)=SCOLD
      CPHEL(J,1)=CPCOLD
      CONDHEL(J,1)=CONDCOLD
   40 CONTINUE
      DO 60 N=1,NSEG
      TYPE *, 'N=',N
      DO 50 J=1,NtSTPS
      Dt=FLTIME/NTSTPS
      uoH=(J-1.)*FLTIME*duoHdT/NTSTPS
      DERIV1=-(HEFLOW*(HHEL(J,N+1)-HHEL(J,N))+DMSEG*TSALT(N)*
     1 dSduoH(N)*duoHdt)/(POR*VSEG*RHOHEL(J,N+1)*CV(THEL(J,N+1))+
     2 DMSEG*TSALT(N)*dSdT(N))
      TSALTINT=TSALT(N)+Dt/2.*DERIV1
      CALL TSDATA(0,TSALTINT,SSALTINT,uoH+duoHdt*Dt/2.,dSdTINT,dSduoHINT)
      TININT=(THEL(J,N)+THEL(J+1,N))/2.
      CALL HEPROP(TININT,RHOININT,HININT,SININT,CPININT,CONININT,IERR)
      IF (INFHTC .EQ. 1) THEN
        EXPON=0.
      ELSE
        HTC=3.8*CONININT/D
        EXPON=EXP(-HTC*P*DL/(HEFLOW*CPININT))
      END IF
      TOUTINT=TSALTINT+(TININT-TSALTINT)*EXPON
      CALL HEPROP(TOUTINT,RHOOUTINT,HOUTINT,SOUTINT,CPOUTINT,CONOUTINT,
     1 IERR)
      DERIV2=-(HEFLOW*(HOUTINT-HININT)+DMSEG*TSALTINT*
     1 dSduoHINT*duoHdt)/(POR*VSEG*RHOOUTINT*CV(TOUTINT)+
     2 DMSEG*TSALTINT*dSdTINT)
      TSALT(N)=TSALT(N)+Dt*DERIV2
      IF (INFHTC .EQ. 1) THEN
        EXPON=0.
      ELSE
        HTC=3.8*CONDHEL(J+1,N)/D
        EXPON=EXP(-HTC*P*DL/(HEFLOW*CPHEL(J+1,N)))
      END IF
      THEL(J+1,N+1)=TSALT(N)+(THEL(J+1,N)-TSALT(N))*EXPON
      CALL HEPROP(THEL(J+1,N+1),RHOHEL(J+1,N+1),HHEL(J+1,N+1),
     1 SHEL(J+1,N+1),CPHEL(J+1,N+1),CONDHEL(J+1,N+1),IERR)
      IF (IERR .EQ. 1) GOTO 80
      CALL TSDATA(0,TSALT(N),SSALT(N),uoH+duoHdt*Dt,dSdT(N),dSduoH(N))
      IF (N .EQ. NSEG) TYPE *, 'J=',J+1,'  THEL=',THEL(J+1,NSEG+1)
   50 CONTINUE
   60 CONTINUE
      DO 70 J=1,NtSTPS+1
      WRITE (4,4140) J,THEL(J,NSEG+1)
   70 CONTINUE
   80 STOP
 4000 FORMAT(' Results of active thermal regenerator simulation:'/
     1' ------------------------------------------------------')
 4010 FORMAT(' Cold reservoir temp = ',PE11.4,' K.'/
     1' Hot reservoir temp = ',PE11.4,' K.')
 4020 FORMAT(' Initial GGG temp is linear from ',PE11.4,' K to ',
     1 PE11.4,' K.')
 4030 FORMAT(' Initial GGG temp is ',PE11.4,' K throughout the core.')
 4040 FORMAT(' He mass flow during magnetization = ',PE11.4,
     1' * uoH **',PE11.4,' g/s.'
     2/' He mass flow during demagnetization flow process = ',PE11.4,
     3' * uoH **',PE11.4,' g/s.')
 4060 FORMAT(' No. of GGG segments = ',I3)
 4070 FORMAT(' Length of a single segment = ',PE11.4,' cm.')
 4080 FORMAT(' Duration of a magnetization flow process = ',PE11.4,
     1' s.'/' Duration of a demagnetization flow process = ',PE11.4,
     2' s.')
 4090 FORMAT(' Duration of an adiabatic magnetization process = ',
     1PE11.4,' s.'/' Duration of an adiabatic demagnetization process
     2 =',PE11.4,' s.')
 4100 FORMAT(' The lowest field is ',PE11.4,' T.'/' The highest field
     1 is ',PE11.4,' T.'/' The field ramps up and down at ',PE11.4,
     2' T/s.')
 4120 FORMAT(' No. of time steps = ',I3,'.')
 4121 FORMAT(' Hot reservoir at ',PE12.4,'  Cold reservoir at ',PE12.4)
 4122 FORMAT(' Helium mass flow rate = ',PE12.4)
 4130 FORMAT(//' Cycle ',I2,' Demagnetization Flow Process')
 4140 FORMAT(I4,6(PE12.4))
 4150 FORMAT(' QCOLD = ',PE11.4,' W')
 4160 FORMAT(' SCOLD = ',PE11.4,' W/K')
 4170 FORMAT(/' Cycle ',I2,' Magnetization Flow Process')
```

```
 4180   FORMAT(' THEL(',I3,',',I3,') = ',PE11.4)
 4190   FORMAT(' QHOT = ',PE11.4,' W')
 4200   FORMAT(' SHOT = ',PE11.4,' W/K')
        END


C
C   SUBROUTINES
C
        SUBROUTINE HEPROP(T,DENS,ENTH,ENTR,CP,COND,IERR)
C
C  THIS SUBROUTINE CALCULATES HELIUM DENSITY, ENTHALPY, ENTROPY, SPECIFIC
C  HEAT AT CONSTANT PRESSURE, AND THERMAL CONDUCTIVITY AT 3 ATM OF PRESSURE
C  AND AT TEMPERATURES BETWEEN 2.15 AND 20 K.  THE PROPERTIES ARE INTERPOLATED
C  FROM A TABLE USING CUBIC SPLINES.
C
        COMMON HETEMP(594),HEDENS(594),CURVDENS(594),HEENTH(594),
     1  CURVENTH(594),HEENTR(594),CURVENTR(594),HECP(594),CURVCP(594),
     2  HECOND(594),CURVCOND(594),uoHH(200),TH(200),TC(200),DM(200),
     3  CURVuoH(200),CURVTH(200),CURVTC(200),CURVM(200),T1(200),T2(200),
     4  T3(200),T4(200)
        IERR=0
        IF (T .LT. 2.15) THEN
          IERR=1
          TYPE *, 'HELIUM TEMP TOO LOW TO CALCULATE DENSITY'
          RETURN
        END IF
        IF (T .GT. 20.) THEN
          IERR=1
          TYPE *, 'HELIUM TEMP TOO HIGH TO CALCULATE DENSITY'
          RETURN
        END IF
        IF (T .GT. 10.) THEN
          IT=394+(T-10.)/0.05
        ELSE
          IT=1+(T-2.14)/0.02
        END IF
        TA=HETEMP(IT)
        TB=HETEMP(IT+1)
        DTEMPI=TB-TA
        DENS=CURVDENS(IT)/6.*((TB-T)**3/DTEMPI-DTEMPI*(TB-T))+
     1  CURVDENS(IT+1)/6.*((T-TA)**3/DTEMPI-DTEMPI*(T-TA))+HEDENS(IT)
     2  *(TB-T)/DTEMPI+HEDENS(IT+1)*(T-TA)/DTEMPI
        DENS=DENS/1000.
        ENTH=CURVENTH(IT)/6.*((TB-T)**3/DTEMPI-DTEMPI*(TB-T))+
     1  CURVENTH(IT+1)/6.*((T-TA)**3/DTEMPI-DTEMPI*(T-TA))+HEENTH(IT)
     2  *(TB-T)/DTEMPI+HEENTH(IT+1)*(T-TA)/DTEMPI
        ENTR=CURVENTR(IT)/6.*((TB-T)**3/DTEMPI-DTEMPI*(TB-T))
     1  +CURVENTR(IT+1)/6.*((T-TA)**3/DTEMPI-DTEMPI*(T-TA))+HEENTR(IT)
     2  *(TB-T)/DTEMPI+HEENTR(IT+1)*(T-TA)/DTEMPI
        CP=CURVCP(IT)/6.*((TB-T)**3/DTEMPI-DTEMPI*(TB-T))
     1  +CURVCP(IT+1)/6.*((T-TA)**3/DTEMPI-DTEMPI*(T-TA))+HECP(IT)
     2  *(TB-T)/DTEMPI+HECP(IT+1)*(T-TA)/DTEMPI
        COND=CURVCOND(IT)/6.*((TB-T)**3/DTEMPI-DTEMPI*(TB-T))
     1  +CURVCOND(IT+1)/6.*((T-TA)**3/DTEMPI-DTEMPI*(T-TA))+HECOND(IT)
     2  *(TB-T)/DTEMPI+HECOND(IT+1)*(T-TA)/DTEMPI
        COND=COND/1000.
        RETURN
        END


        SUBROUTINE TSDATA(IFLAG,T,S,uoH,DSDT,DSDuoH)
C
C  IF IFLAG=0, TEMPERATURE IS GIVEN.  IF IFLAG=1, ENTROPY IS GIVEN.
C
        IF (IFLAG .EQ. 0) THEN
          CALL GGGPROP(T,uoH,DSDuoH,S,DSDT)
        ELSE IF (IFLAG .EQ. 1) THEN
          TA=2.0
          CALL GGGPROP(TA,uoH,DSDuoHA,SA,DSDTA)
          TB=20.
          CALL GGGPROP(TB,uoH,DSDuoHB,SB,DSDTB)
          IF ((S-SA)*(S-SB) .GE. 0.) THEN
            TYPE *,' ENTROPY IS OUT OF RANGE OF THE AVAILABLE DATA.'
            RETURN
          END IF
          RES=1.
          DO WHILE (RES .GT. 0.0001)
            TM=(TA+TB)/2.
            CALL GGGPROP(TM,uoH,DSDuoHM,SM,DSDTM)
            IF ((S-SM)*(S-SB) .LT. 0.) THEN
              TA=TM
```

```
            ELSE
              TB=TM
              SB=SM
            END IF
            RES=(TB-TA)
          END DO
          T=TM
          DSDuoH=DSDuoHM
          S=SM
          DSDT=DSDTM
        END IF
        RETURN
        END


        SUBROUTINE GGGPROP(T,uoH,dsduoH,s,dsdT)
C
C     Given temperature in Kelvin and uoH in Tesla, entropy s and its
C   derivatives ds/duoH (equivalent to vdM/dT) and ds/dT are calculated.
C   The units are J/(g K) for s, J/(g K T) for ds/duoH, and J/(g K*2)
C   for ds/dT.
C
C     Calculation of ds/duoH is exact from the curvefitted magnetization.
C   Calculation of s and ds/dT is done with the use of Gauss-Legendre
C   Quadrature.
C
C     W and ETA are used in the quadrature method.
C
        DIMENSION W(6),ETA(6)
        DATA ETA/0.1252334085,0.3678314990,0.5873179543,0.7699026742,
     1  0.9041172564,0.9815606342/
        DATA W/0.2491470458,0.2334925365,0.2031674267,0.1600783285,
     1  0.1069393260,0.0471753364/
C
C     Calculation of ds/duoH:
C
        CALL DERIV(T,uoH,dsduoH,vd2MdT2)
C
C     Calculation of s and dsdT:  s0 is the entropy at uoH=0, and
C   ds0dT is the derivative of entropy with respect to temperature at
C   uoH=0.  s and dsdT are calculated using Gauss-Legendre Quadrature.
C
        s0=2.3E-07*T**3-3.1925E-02/T**2+1.699E-02/T**3-
     1  (2.3E-07-3.1925E-02+1.699E-02)
        ds0dt=6.9E-07*T**2+6.385E-02/T**3-5.096E-02/T**4
        sSUM=0.
        dsdTSUM=0.
        DO 10 I=1,6
        x1=uoH/2.*(1+ETA(I))
        x2=uoH/2.*(1-ETA(I))
        CALL DERIV(T,x1,vdMdT1,vd2MdT21)
        CALL DERIV(T,x2,vdMdT2,vd2MdT22)
        sSUM=sSUM+W(I)*(vdMdT1+vdMdT2)
        dsdTSUM=dsdTSUM+W(I)*(vd2MdT21+vd2MdT22)
   10   CONTINUE
        s=s0+uoH/2.*sSUM
        dsdT=ds0dT+uoH/2.*dsdTSUM
        RETURN
        END


        SUBROUTINE DERIV(T,uoH,vdMdT,vd2MdT2)
C
C     This subroutine calculates vdM/dT and vd2M/dT2 given T and uoH.
C   T is in Kelvin, uoH is in Tesla, vdM/dT is in J/(g K T), and
C   vd2M/dT2 is in J/(g K T*2).
C
C
C     Calculation of functions C0,C1,C2,C3, and C4 and their derivatives
C   with respect to temperature:
C
        C0=13.67388+2.718523*T+0.1278728*T**2-2.5072373E-03*T**3
        C1=-2.980799+0.9144735*T-7.3461875E-02*T**2+1.1088194E-03*
     1  T**3+9.8684995E-06*T**4
        C2=3.166695-0.6364962*T+4.8334930E-02*T**2-1.0840200E-03*
     1  T**3+4.3787923E-06*T**4
        C3=-0.3461423+9.0944469E-02*T-6.9979527E-03*T**2+
     1  1.3868879E-04*T**3
        C4=1.3560383E-02-4.1968897E-03*T+3.3840450E-04*T**2-
     1  6.8436516E-06*T**3
        dC0dT=2.718523+2.*0.1278728*T-3.*2.5072373E-03*T**2
        dC1dT=0.9144735-2.*7.3461875E-02*T+3.*1.1088194E-03*
     1  T**2+4.*9.8684995E-06*T**3
```

```
      dC2dT=-0.6364962+2.*4.8334930E-02*T-3.*1.0840200E-03*
     1  T**2+4.*4.3787923E-06*T**3
      dC3dT=9.0944469E-02-2.*6.9979527E-03*T+3.*1.3868879E-04*T**2
      dC4dT=-4.1968897E-03+2.*3.3840450E-04*T-3.*6.8436516E-06*T**2
      d2C0dT2=2.*0.1278728-6.*2.5072373E-03*T
      d2C1dT2=-2.*7.3461875E-02+6.*1.1088194E-03*T+
     1  12.*9.8684995E-06*T**2
      d2C2dT2=2.*4.8334930E-02-6.*1.0840200E-03*T+
     1  12.*4.3787923E-06*T**2
      d2C3dT2=-2.*6.9979527E-03+6.*1.3868879E-04*T
      d2C4dT2=2.*3.3840450E-04-6.*6.8436516E-06*T
C
C     Calculation of vdMdT and vd2MdT2:
C
      DEN=C0+C1*uoH+C2*uoH**2+C3*uoH**3+C4*uoH**4
      dDENdT=dc0dT+dC1dT*uoH+dC2dT*uoH**2+dC3dT*uoH**3+dC4dT*uoH**4
      d2DENdT2=d2c0dT2+d2C1dT2*uoH+d2C2dT2*uoH**2+d2C3dT2*uoH**3+
     1  d2C4dT2*uoH**4
      vdMdT=-uoH*dDENdT/DEN**2
      vd2MdT2=uoH*(2.*dDENdT**2-DEN*d2DENdT2)/DEN**3
      RETURN
      END


      REAL FUNCTION CV(T)
      REAL CVHE(29)
      DATA CVHE/1.773,1.880,2.064,2.217,2.397,2.639,2.699,2.748,
     1  2.765,2.827,2.929,3.098,3.204,3.227,3.225,3.217,3.168,3.137,
     2  3.127,3.112,3.108,3.107,3.107,3.108,3.109,3.112,3.115,3.117,
     3  3.119/
      IF (T .LE. 2.5) THEN
        CV=CVHE(1)
      ELSE IF (T .LE. 5.) THEN
        I=(T-2.5)/0.5+1
        CV=CVHE(I)+(T-(2.+0.5*I))/0.5*(CVHE(I+1)-CVHE(I))
      ELSE IF (T .LE. 6.) THEN
        I=(T-5.)/0.1+6
        CV=CVHE(I)+(T-(4.4+0.1*I))/0.1*(CVHE(I+1)-CVHE(I))
      ELSE IF (T .LE. 10.) THEN
        I=(T-6.)/0.5+16
        CV=CVHE(I)+(T-(-2.+0.5*I))/0.5*(CVHE(I+1)-CVHE(I))
      ELSE IF (T .LE. 15.) THEN
        I=(T-10.)+24
        CV=CVHE(I)+(T-(-14.+I))*(CVHE(I+1)-CVHE(I))
      ELSE IF (T .GT. 15) THEN
        TYPE *, 'CV CANNOT BE CALCULATED.'
      END IF
      RETURN
      END
```

```
C
C   Single-shot Demagnetization Flow Program
C
C
C       This program is a numerical simulation of a magnetically active
C   regenerator, based on the differential equations derived in chapter
C   3 and the GGG thermodynamic properties derived in chapter 5.  It
C   uses the Second Order Runge Kutta method to solve the differential
C   equations.
C
C
        PROGRAM DEMFLOW
        DIMENSION TSALT(120),SSALT(120),dSdT(120),dSduoH(120),THEL(401,121),
     1  RHOHEL(401,121),HHEL(401,121),SHEL(401,121),CPHEL(401,121),
     2  CONDHEL(401,121)
        COMMON HETEMP(594),HEDENS(594),CURVDENS(594),HEENTH(594),
     1  CURVENTH(594),HEENTR(594),CURVENTR(594),HECP(594),CURVCP(594),
     2  HECOND(594),CURVCOND(594)
        DATA DL/0.254/,D/0.01016/,A/8.488/,RHO/7.14/,POR/0.044/,
     1  VSEG/2.156/,P/69.17/,DMSEG/15.39/
        OPEN(UNIT=2,FILE='[TAUSSIG.MAGFRIG]HEPROP.DAT',TYPE='OLD')
        OPEN(UNIT=3,FILE='[TAUSSIG.MAGFRIG]HECURV.DAT',TYPE='OLD')
        OPEN(UNIT=7,FILE='DEMAG.DAT',TYPE='OLD')
        OPEN(UNIT=4,FILE='DEMAG.OUT',TYPE='NEW')
C
C   READ INPUT DATA FROM 'MAG.DAT'.
C
        READ(7,*) NtSTPS,NSEG
        READ(7,*) TINITIAL,THOT
        READ(7,*) INFHTC,HEFLOW,FLTIME
        READ(7,*) uoHINIT,duoHdt
C
C   READ HELIUM PROPERTY DATA FROM 'HEPROP.DAT' AND 'HECURV.DAT'
C
        DO 10 I=1,394
        HETEMP(I)=2.12+I*0.02
        READ(2,*) HEDENS(I),HEENTH(I),HEENTR(I),HECP(I),HECOND(I)
        READ(3,*) CURVDENS(I),CURVENTH(I),CURVENTR(I),CURVCP(I),
     1  CURVCOND(I)
   10   CONTINUE
        DO 20 I=395,594
        HETEMP(I)=10.+(I-394)*0.05
        READ(2,*) HEDENS(I),HEENTH(I),HEENTR(I),HECP(I),HECOND(I)
        READ(3,*) CURVDENS(I),CURVENTH(I),CURVENTR(I),CURVCP(I),
     1  CURVCOND(I)
   20   CONTINUE
C
C   SETUP — GEOMETRY IS CALCULATED.
C
        WRITE(4,4000)
        WRITE(4,4030) TINITIAL
        WRITE(4,4060) NSEG
        WRITE(4,4070) DL

        WRITE(4,4120) NtSTPS
C
C   INITIALIZE GGG AND HELIUM TEMPS BY ESTABLISHING A TEMPERATURE GRADIENT
C
        CALL HEPROP(THOT,RHOHOT,HHOT,SHOT,CPHOT,CONDHOT,IERR)
        THEL(1,NSEG+1)=THOT
        HHEL(1,NSEG+1)=HHOT
        CPHEL(1,NSEG+1)=CPHOT
        CONDHEL(1,NSEG+1)=CONDHOT
        CALL TSDATA(0,TINITIAL,SINITIAL,uoHINIT,dSdTINIT,dSduoHINIT)
        DO 30 N=NSEG,1,-1
        TSALT(N)=TINITIAL
        SSALT(N)=SINITIAL
        dSdT(N)=dSdTINIT
        dSduoH(N)=dSduoHINIT
        IF (INFHTC .EQ. 1) THEN
          EXPON=0.
        ELSE
          HTC=3.8*CONDHEL(1,N+1)/D
          EXPON=EXP(-HTC*P*DL/(HEFLOW*CPHEL(1,N+1)))
        END IF
        THEL(1,N)=TSALT(N)+(THEL(1,N+1)-TSALT(N))*EXPON
        CALL HEPROP(THEL(1,N),RHOHEL(1,N),HHEL(1,N),SHEL(1,N),
     1  CPHEL(1,N),CONDHEL(1,N),IERR)
   30   CONTINUE
C
C**************************************************************************
C
C   MAGNETIZATION WITH FLOW FROM THE COLD TO HOT RESERVOIR.
C
```

```
C*************************************************************************
C
      DO 40 J=1,NTSTPS+1
      THEL(J,NSEG+1)=THOT
      RHOHEL(J,NSEG+1)=RHOHOT
      HHEL(J,NSEG+1)=HHOT
      SHEL(J,NSEG+1)=SHOT
      CPHEL(J,NSEG+1)=CPHOT
      CONDHEL(J,NSEG+1)=CONDHOT
   40 CONTINUE
      DO 60 N=NSEG,1,-1
      TYPE *, 'N=',N
      DO 50 J=1,NtSTPS
      Dt=FLTIME/NTSTPS
      uoH=(J-1.)*FLTIME*duoHdT/NTSTPS
      DERIV1=-(HEFLOW*(HHEL(J,N)-HHEL(J,N+1))+DMSEG*TSALT(N)*
     1 dSduoH(N)*(-duoHdt))/(POR*VSEG*RHOHEL(J,N)*CV(THEL(J,N))+
     2 DMSEG*TSALT(N)*dSdT(N))
      TSALTINT=TSALT(N)+Dt/2.*DERIV1
      CALL TSDATA(0,TSALTINT,SSALTINT,uoH+duoHdt*Dt/2.,dSdTINT,dSduoHINT)
      TININT=(THEL(J,N+1)+THEL(J+1,N+1))/2.
      CALL HEPROP(TININT,RHOININT,HININT,SININT,CPININT,CONININT,IERR)
      IF (INFHTC .EQ. 1) THEN
        EXPON=0.
      ELSE
        HTC=3.8*CONININT/D
        EXPON=EXP(-HTC*P*DL/(HEFLOW*CPININT))
      END IF
      TOUTINT=TSALTINT+(TININT-TSALTINT)*EXPON
      CALL HEPROP(TOUTINT,RHOOUTINT,HOUTINT,SOUTINT,CPOUTINT,CONOUTINT,
     1 IERR)
      DERIV2=-(HEFLOW*(HOUTINT-HININT)+DMSEG*TSALTINT*
     1 dSduoHINT*(-duoHdt))/(POR*VSEG*RHOOUTINT*CV(TOUTINT)+
     2 DMSEG*TSALTINT*dSdTINT)
      TSALT(N)=TSALT(N)+Dt*DERIV2
      IF (INFHTC .EQ. 1) THEN
        EXPON=0.
      ELSE
        HTC=3.8*CONDHEL(J+1,N+1)/D
        EXPON=EXP(-HTC*P*DL/(HEFLOW*CPHEL(J+1,N+1)))
      END IF
      THEL(J+1,N)=TSALT(N)+(THEL(J+1,N+1)-TSALT(N))*EXPON
      CALL HEPROP(THEL(J+1,N),RHOHEL(J+1,N),HHEL(J+1,N),
     1 SHEL(J+1,N),CPHEL(J+1,N),CONDHEL(J+1,N),IERR)
      IF (IERR .EQ. 1) GOTO 80
      CALL TSDATA(0,TSALT(N),SSALT(N),uoH+duoHdt*Dt,dSdT(N),dSduoH(N))
      IF (N .EQ. 1) TYPE *, 'J=',J+1,'  THEL=',THEL(J+1,1)
   50 CONTINUE
   60 CONTINUE
      DO 70 J=1,NtSTPS+1
      WRITE (4,4140) J,THEL(J,1)
   70 CONTINUE
   80 STOP
 4000 FORMAT(' Results of active thermal regenerator simulation:'/
     1' ------------------------------------------------')
 4010 FORMAT(' Cold reservoir temp = ',PE11.4,' K.'/
     1' Hot reservoir temp = ',PE11.4,' K.')
 4020 FORMAT(' Initial GGG temp is linear from ',PE11.4,' K to ',
     1 PE11.4,' K.')
 4030 FORMAT(' Initial GGG temp is ',PE11.4,' K throughout the core.')
 4040 FORMAT(' He mass flow during magnetization = ',PE11.4,
     1' * uoH **',PE11.4,' g/s.'
     2/' He mass flow during demagnetization flow process = ',PE11.4,
     3' * uoH **',PE11.4,' g/s.')
 4060 FORMAT(' No. of GGG segments = ',I3)
 4070 FORMAT(' Length of a single segment = ',PE11.4,' cm.')
 4080 FORMAT(' Duration of a magnetization flow process = ',PE11.4,
     1' s.'/' Duration of a demagnetization flow process = ',PE11.4,
     2' s.')
 4090 FORMAT(' Duration of an adiabatic magnetization process = ',
     1PE11.4,' s.'/' Duration of an adiabatic demagnetization process
     2 =',PE11.4,' s.')
 4100 FORMAT(' The lowest field is ',PE11.4,' T.'/' The highest field
     1 is ',PE11.4,' T.'/' The field ramps up and down at ',PE11.4,
     2' T/s.')
 4120 FORMAT(' No. of time steps = ',I3,'.')
 4121 FORMAT(' Hot reservoir at ',PE12.4,'  Cold reservoir at ',PE12.4)
 4122 FORMAT(' Helium mass flow rate = ',PE12.4)
 4130 FORMAT(//' Cycle ',I2,' Demagnetization Flow Process')
 4140 FORMAT(I4,6(PE12.4))
 4150 FORMAT(' QCOLD = ',PE11.4,' W')
 4160 FORMAT(' SCOLD = ',PE11.4,' W/K')
 4170 FORMAT(/' Cycle ',I2,' Magnetization Flow Process')
```

```
 4180   FORMAT(' THEL('.I3.','.I3.') = '.PE11.4)
 4190   FORMAT(' QHOT = '.PE11.4.' W')
 4200   FORMAT(' SHOT = '.PE11.4.' W/K')
        END


C
C   SUBROUTINES
C
        SUBROUTINE HEPROP(T.DENS.ENTH.ENTR.CP.COND.IERR)
C
C  THIS SUBROUTINE CALCULATES HELIUM DENSITY, ENTHALPY, ENTROPY, SPECIFIC
C  HEAT AT CONSTANT PRESSURE, AND THERMAL CONDUCTIVITY AT 3 ATM OF PRESSURE
C  AND AT TEMPERATURES BETWEEN 2.15 AND 20 K.  THE PROPERTIES ARE INTERPOLATED
C  FROM A TABLE USING CUBIC SPLINES.
C
        COMMON HETEMP(594),HEDENS(594),CURVDENS(594),HEENTH(594),
     1  CURVENTH(594),HEENTR(594),CURVENTR(594),HECP(594),CURVCP(594),
     2  HECOND(594),CURVCOND(594),uoHH(200),TH(200),TC(200),DM(200),
     3  CURVuoH(200),CURVTH(200),CURVTC(200),CURVM(200),T1(200),T2(200),
     4  T3(200),T4(200)
        IERR=0
        IF (T .LT. 2.15) THEN
          IERR=1
          TYPE *, 'HELIUM TEMP TOO LOW TO CALCULATE DENSITY'
          RETURN
        END IF
        IF (T .GT. 20.) THEN
          IERR=1
          TYPE *, 'HELIUM TEMP TOO HIGH TO CALCULATE DENSITY'
          RETURN
        END IF
        IF (T .GT. 10.) THEN
          IT=394+(T-10.)/0.05
        ELSE
          IT=1+(T-2.14)/0.02
        END IF
        TA=HETEMP(IT)
        TB=HETEMP(IT+1)
        DTEMPI=TB-TA
        DENS=CURVDENS(IT)/6.*((TB-T)**3/DTEMPI-DTEMPI*(TB-T))+
     1  CURVDENS(IT+1)/6.*((T-TA)**3/DTEMPI-DTEMPI*(T-TA))+HEDENS(IT)
     2  *(TB-T)/DTEMPI+HEDENS(IT+1)*(T-TA)/DTEMPI
        DENS=DENS/1000.
        ENTH=CURVENTH(IT)/6.*((TB-T)**3/DTEMPI-DTEMPI*(TB-T))+
     1  CURVENTH(IT+1)/6.*((T-TA)**3/DTEMPI-DTEMPI*(T-TA))+HEENTH(IT)
     2  *(TB-T)/DTEMPI+HEENTH(IT+1)*(T-TA)/DTEMPI
        ENTR=CURVENTR(IT)/6.*((TB-T)**3/DTEMPI-DTEMPI*(TB-T))
     1  +CURVENTR(IT+1)/6.*((T-TA)**3/DTEMPI-DTEMPI*(T-TA))+HEENTR(IT)
     2  *(TB-T)/DTEMPI+HEENTR(IT+1)*(T-TA)/DTEMPI
        CP=CURVCP(IT)/6.*((TB-T)**3/DTEMPI-DTEMPI*(TB-T))
     1  +CURVCP(IT+1)/6.*((T-TA)**3/DTEMPI-DTEMPI*(T-TA))+HECP(IT)
     2  *(TB-T)/DTEMPI+HECP(IT+1)*(T-TA)/DTEMPI
        COND=CURVCOND(IT)/6.*((TB-T)**3/DTEMPI-DTEMPI*(TB-T))
     1  +CURVCOND(IT+1)/6.*((T-TA)**3/DTEMPI-DTEMPI*(T-TA))+HECOND(IT)
     2  *(TB-T)/DTEMPI+HECOND(IT+1)*(T-TA)/DTEMPI
        COND=COND/1000.
        RETURN
        END


        SUBROUTINE TSDATA(IFLAG,T,S,uoH,DSDT,DSDuoH)
C
C  IF IFLAG=0, TEMPERATURE IS GIVEN.  IF IFLAG=1, ENTROPY IS GIVEN.
C
        IF (IFLAG .EQ. 0) THEN
          CALL GGGPROP(T,uoH,DSDuoH,S,DSDT)
        ELSE IF (IFLAG .EQ. 1) THEN
          TA=2.0
          CALL GGGPROP(TA,uoH,DSDuoHA,SA,DSDTA)
          TB=20.
          CALL GGGPROP(TB,uoH,DSDuoHB,SB,DSDTB)
          IF ((S-SA)*(S-SB) .GE. 0.) THEN
            TYPE *,' ENTROPY IS OUT OF RANGE OF THE AVAILABLE DATA.'
            RETURN
          END IF
          RES=1.
          DO WHILE (RES .GT. 0.0001)
            TM=(TA+TB)/2.
            CALL GGGPROP(TM,uoH,DSDuoHM,SM,DSDTM)
            IF ((S-SM)*(S-SB) .LT. 0.) THEN
              TA=TM
```

```
            ELSE
              TB=TM
              SB=SM
            END IF
            RES=(TB-TA)
          END DO
          T=TM
          DSDuoH=DSDuoHM
          S=SM
          DSDT=DSDTM
        END IF
        RETURN
        END


        SUBROUTINE GGGPROP(T,uoH,dsduoH,s,dsdT)
C
C    Given temperature in Kelvin and uoH in Tesla, entropy s and its
C  derivatives ds/duoH (equivalent to vdM/dT) and ds/dT are calculated.
C  The units are J/(g K) for s, J/(g K T) for ds/duoH, and J/(g K*2)
C  for ds/dT.
C
C    Calculation of ds/duoH is exact from the curvefitted magnetization.
C  Calculation of s and ds/dT is done with the use of Gauss-Legendre
C  Quadrature.
C
C    W and ETA are used in the quadrature method.
C
        DIMENSION W(6),ETA(6)
        DATA ETA/0.1252334085,0.3678314990,0.5873179543,0.7699026742,
     1  0.9041172564,0.9815606342/
        DATA W/0.2491470458,0.2334925365,0.2031674267,0.1600783285,
     1  0.1069393260,0.0471753364/
C
C    Calculation of ds/duoH:
C
        CALL DERIV(T,uoH,dsduoH,vd2MdT2)
C
C    Calculation of s and dsdT:  s0 is the entropy at uoH=0, and
C  ds0dT is the derivative of entropy with respect to temperature at
C  uoH=0.  s and dsdT are calculated using Gauss-Legendre Quadrature.
C
        s0=2.3E-07*T**3-3.1925E-02/T**2+1.699E-02/T**3-
     1  (2.3E-07-3.1925E-02+1.699E-02)
        ds0dt=6.9E-07*T**2+6.385E-02/T**3-5.096E-02/T**4
        sSUM=0.
        dsdTSUM=0.
        DO 10 I=1,6
        x1=uoH/2.*(1+ETA(I))
        x2=uoH/2.*(1-ETA(I))
        CALL DERIV(T,x1,vdMdT1,vd2MdT21)
        CALL DERIV(T,x2,vdMdT2,vd2MdT22)
        sSUM=sSUM+W(I)*(vdMdT1+vdMdT2)
        dsdTSUM=dsdTSUM+W(I)*(vd2MdT21+vd2MdT22)
   10   CONTINUE
        s=s0+uoH/2.*sSUM
        dsdT=ds0dT+uoH/2.*dsdTSUM
        RETURN
        END


        SUBROUTINE DERIV(T,uoH,vdMdT,vd2MdT2)
C
C    This subroutine calculates vdM/dT and vd2M/dT2 given T and uoH.
C  T is in Kelvin, uoH is in Tesla, vdM/dT is in J/(g K T), and
C  vd2M/dT2 is in J/(g K T*2).
C
C
C    Calculation of functions C0,C1,C2,C3, and C4 and their derivatives
C  with respect to temperature:
C
        C0=13.67388+2.718523*T+0.1278728*T**2-2.5072373E-03*T**3
        C1=-2.980799+0.9144735*T-7.3461875E-02*T**2+1.1088194E-03*
     1  T**3+9.8684995E-06*T**4
        C2=3.166695-0.6364962*T+4.8334930E-02*T**2-1.0840200E-03*
     1  T**3+4.3787923E-06*T**4
        C3=-0.34614234+9.0944469E-02*T-6.9979527E-03*T**2+
     1  1.3868879E-04*T**3
        C4=1.3560383E-02-4.1968897E-03*T+3.3840450E-04*T**2-
     1  8.8436516E-06*T**3
        dC0dT=2.718523+2.*0.1278728*T-3.*2.5072373E-03*T**2
        dC1dT=0.9144735-2.*7.3461875E-02*T+3.*1.1088194E-03*
     1  T**2+4.*9.8684995E-06*T**3
```

```
      dC2dT=-0.6364962+2.*4.8334930E-02*T-3.*1.0840200E-03*
     1  T**2+4.*4.3787923E-06*T**3
      dC3dT=9.0944469E-02-2.*6.9979527E-03*T+3.*1.3868879E-04*T**2
      dC4dT=-4.1968897E-03+2.*3.3840450E-04*T-3.*6.8436516E-06*T**2
      d2C0dT2=2.*0.1278728-6.*2.5072373E-03*T
      d2C1dT2=-2.*7.3461875E-02+6.*1.1088194E-03*T+
     1  12.*9.8684995E-06*T**2
      d2C2dT2=2.*4.8334930E-02-6.*1.0840200E-03*T+
     1  12.*4.3787923E-06*T**2
      d2C3dT2=-2.*6.9979527E-03+6.*1.3868879E-04*T
      d2C4dT2=2.*3.3840450E-04-6.*6.8436516E-06*T
C
C     Calculation of vdMdT and vd2MdT2:
C
      DEN=C0+C1*uoH+C2*uoH**2+C3*uoH**3+C4*uoH**4
      dDENdT=dc0dT+dC1dT*uoH+dC2dT*uoH**2+dC3dT*uoH**3+dC4dT*uoH**4
      d2DENdT2=d2c0dT2+d2C1dT2*uoH+d2C2dT2*uoH**2+d2C3dT2*uoH**3+
     1  d2C4dT2*uoH**4
      vdMdT=-uoH*dDENdT/DEN**2
      vd2MdT2=uoH*(2.*dDENdT**2-DEN*d2DENdT2)/DEN**3
      RETURN
      END


      REAL FUNCTION CV(T)
      REAL CVHE(29)
      DATA CVHE/1.773,1.880,2.064,2.217,2.397,2.639,2.699,2.748,
     1  2.765,2.827,2.929,3.098,3.204,3.227,3.225,3.217,3.168,3.137,
     2  3.127,3.112,3.108,3.107,3.107,3.108,3.109,3.112,3.115,3.117,
     3  3.119/
      IF (T .LE. 2.5) THEN
        CV=CVHE(1)
      ELSE IF (T .LE. 5.) THEN
        I=(T-2.5)/0.5+1
        CV=CVHE(I)+(T-(2.+0.5*I))/0.5*(CVHE(I+1)-CVHE(I))
      ELSE IF (T .LE. 6.) THEN
        I=(T-5.)/0.1+6
        CV=CVHE(I)+(T-(4.4+0.1*I))/0.1*(CVHE(I+1)-CVHE(I))
      ELSE IF (T .LE. 10.) THEN
        I=(T-6.)/0.5+16
        CV=CVHE(I)+(T-(-2.+0.5*I))/0.5*(CVHE(I+1)-CVHE(I))
      ELSE IF (T .LE. 15.) THEN
        I=(T-10.)+24
        CV=CVHE(I)+(T-(-14.+I))*(CVHE(I+1)-CVHE(I))
      ELSE IF (T .GT. 15) THEN
        TYPE *, 'CV CANNOT BE CALCULATED.'
      END IF
      RETURN
      END
```

Appendix H Data from an Experimental Run

Figures H1, H2, H3, and H4 present the data gathered from one of the experiments. The last three cycles of the set were used in the numerical simulation.

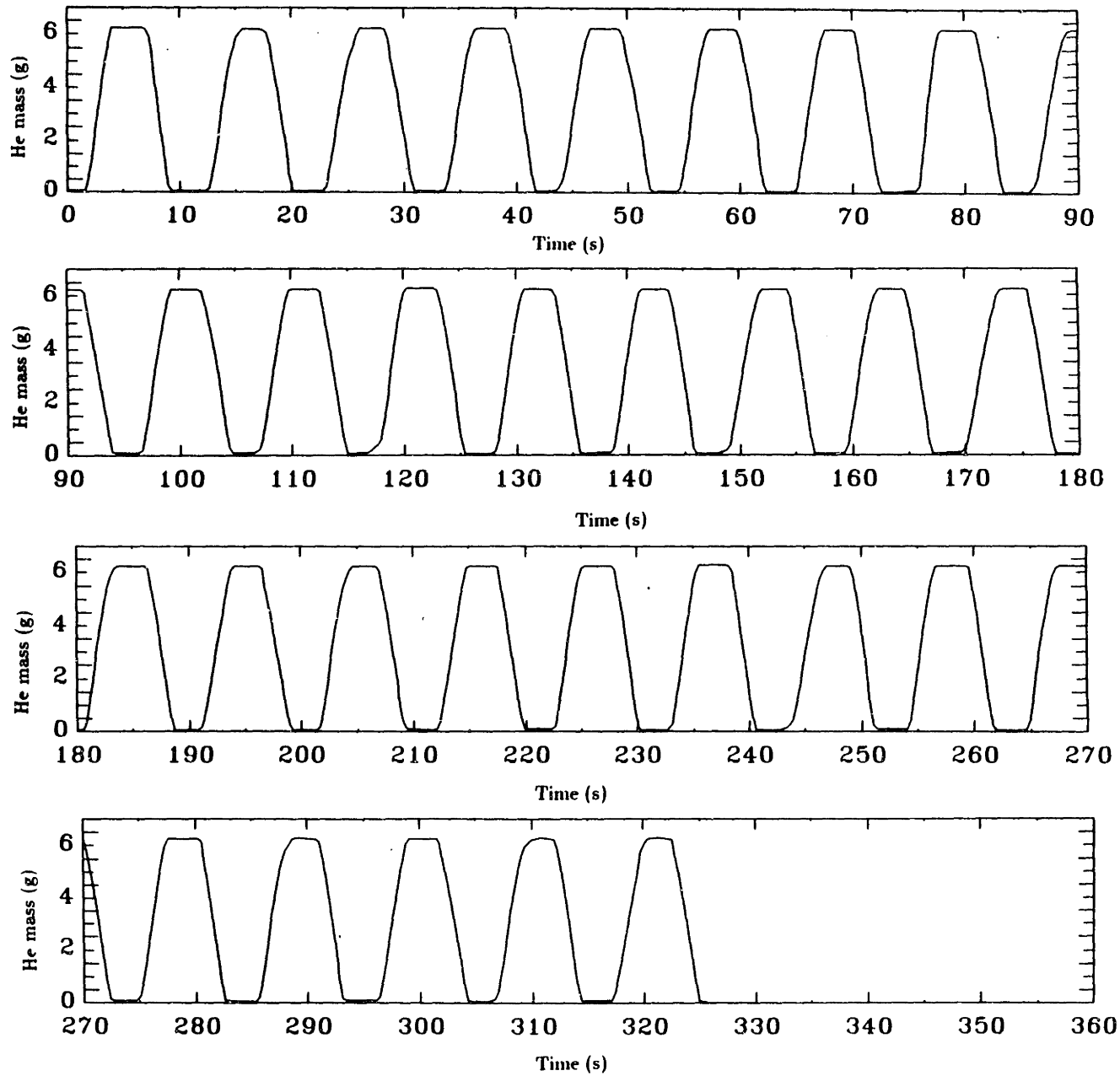

Fig. H1 Helium mass in compensator vs. time.

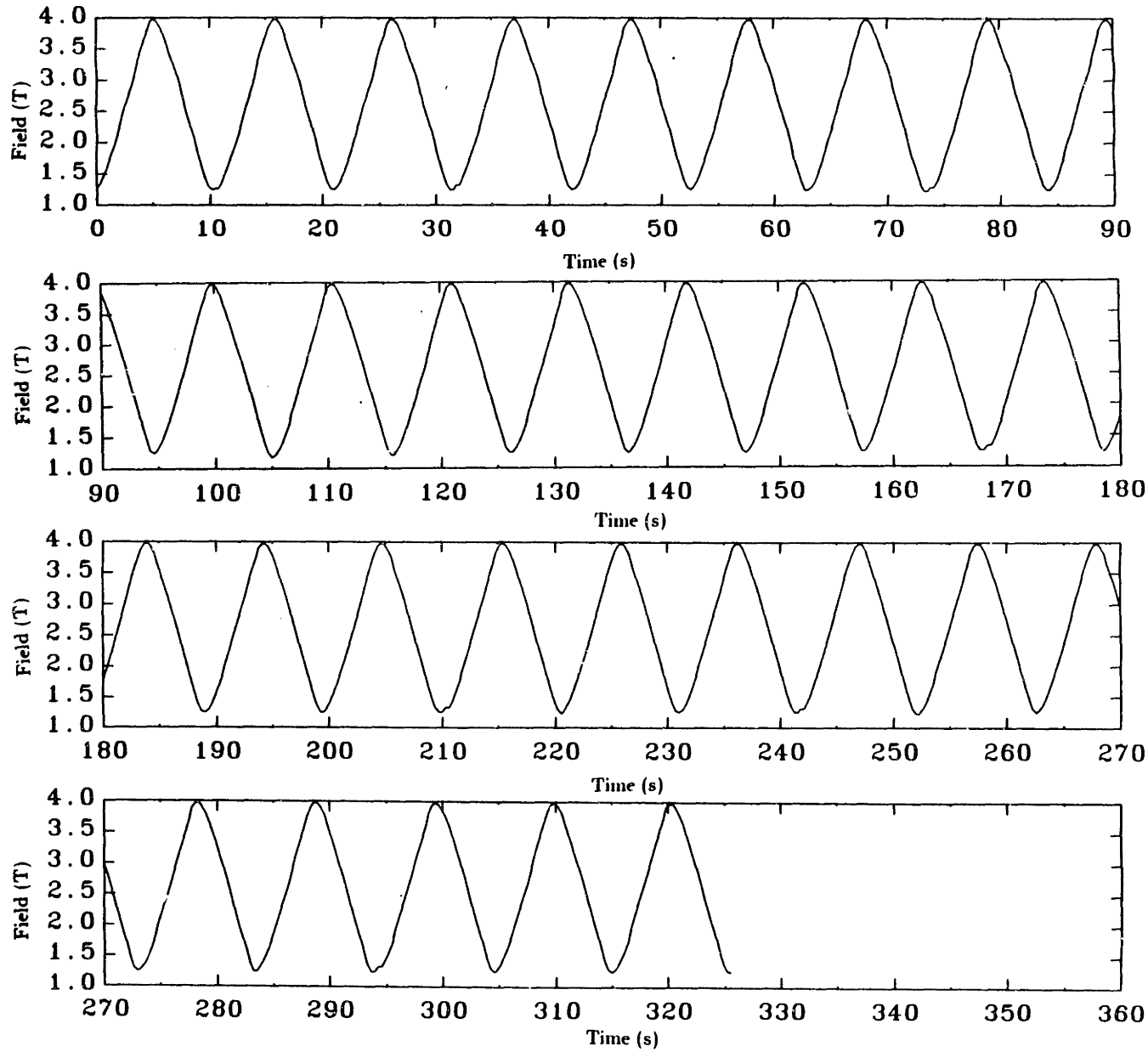

Fig. H2 Field as a function of time.

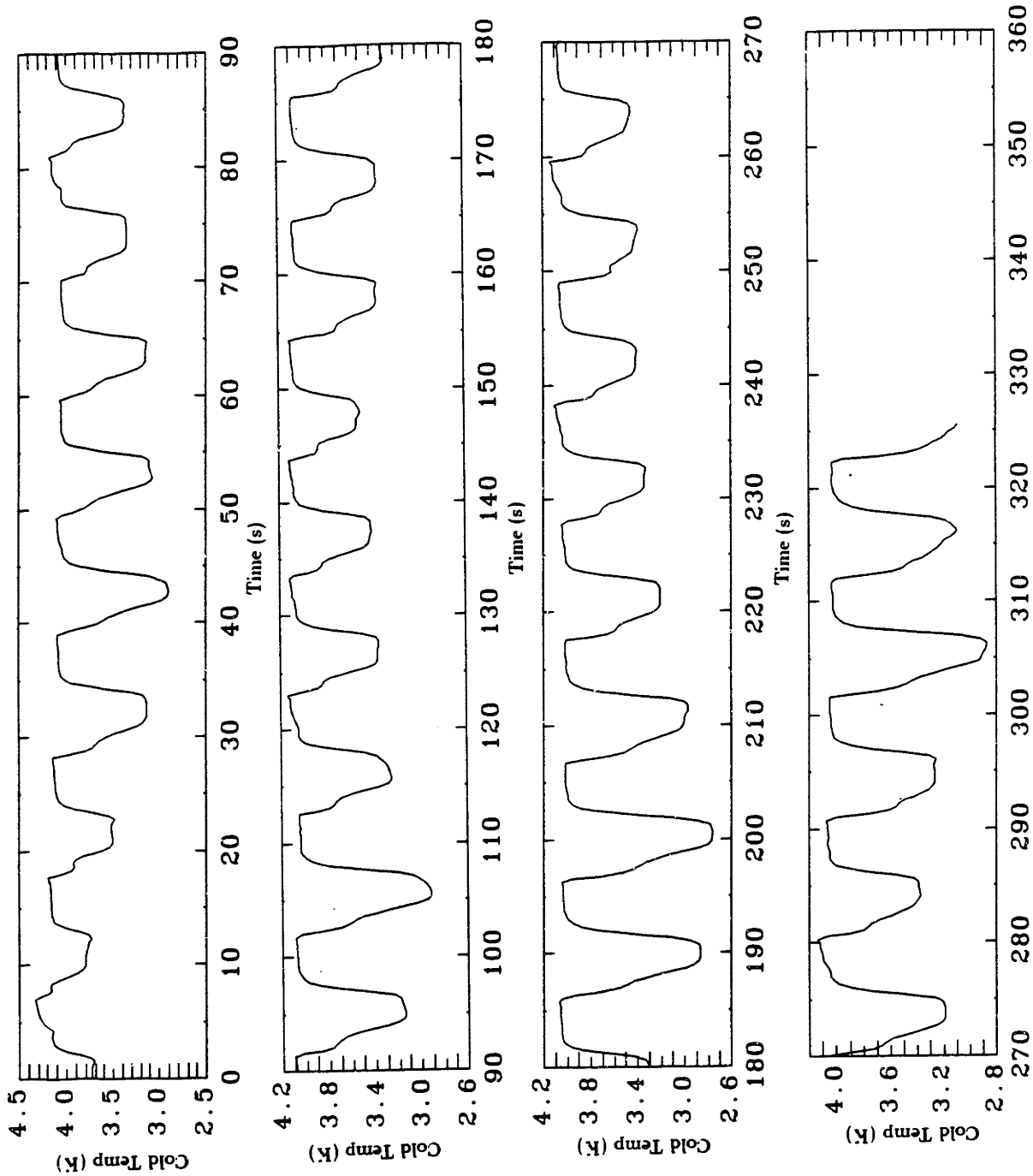

Fig. H3 Cold-end temperature vs. time.

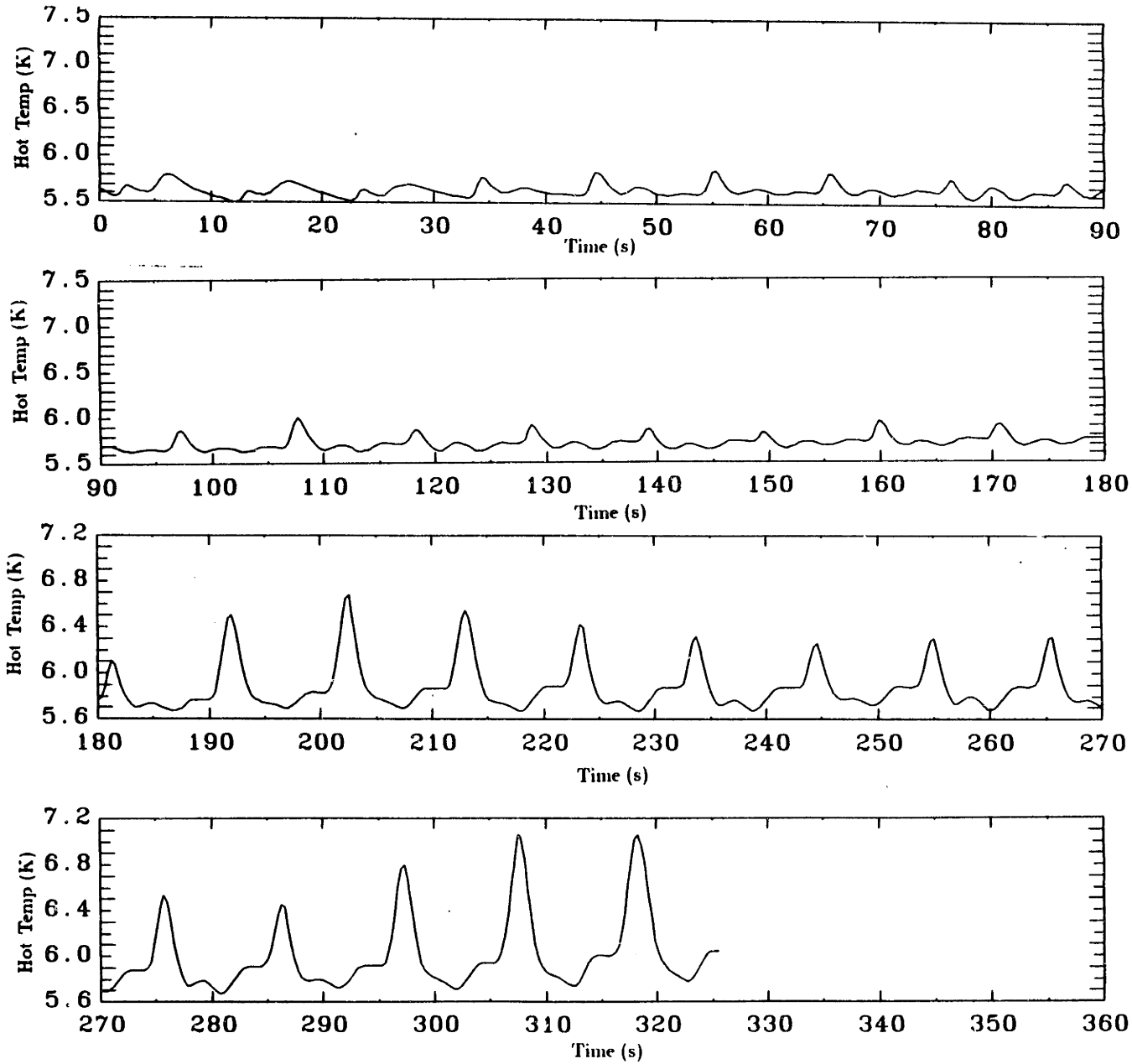

Fig. H4 Hot-end temperature vs. time.

References

1. K. Mendelsshon, *The Quest for Absolute Zero; the meaning of low temperature physics*, Taylor & Francis, Ltd., London (1977), p. 161.

2. W.F. Giauque, and D.P. MacDougall, "Attainment of temperatures below 1° absolute by demagnetization of $Gd_2(SO_4)_3 \cdot 8H_2O$," *Phys. Rev.*, **43**:768, (1933).

3. C.V. Heer, C.B. Barnes, J.G. Daunt, "The design and operation of a magnetic refrigerator for maintaining temperatures below 1° K" *Rev. Sci. Inst.*, **25**:1088, (1954).

4. J.R. Van Geuns, "A Study of a New Magnetic Refrigerating Cycle," *Philips Res. Rept. Suppl.* **6**, (1966).

5. C. Delpeuch, R. Béranger, G. Bon Mardion, G. Claudet, and A.A. Lacaze, "Double acting reciprocating magnetic refrigerator: first experiments," *Cryogenics*, **21**:579–584, (1981).

6. A.F. Lacaze, R. Béranger, G. Bon Mardion, G. Claudet, and A.A. Lacaze, "Efficiency improvements of a double acting reciprocating magnetic refrigerator," *Cryogenics*, **23**:427–436, (1983).

7. J.A. Barclay, W.F. Stewart, W.C. Overton, R.J. Candler, and O.D. Harkleroad, "Experimental results on a low-temperature magnetic refrigerator," *Advances in Cryogenic Engineering*, **31**:743–752, (1985).

8. H. Nakagome, T. Kuriyama, H. Ogiwara, T. Fujita, T. Yazawa, and T. Hashimoto, "Reciprocating magnetic refrigerator for helium liquefaction," *Advances in Cryogenic Engineering*, **31**:753–762, (1985).

9. G.V. Brown, "Magnetic heat pumping near room temperature," *Journal of Applied Physics* **47**:3673–3680, (1976).

10. J.A. Barclay, W.A. Steyert, "Materials for magnetic refrigeration between 2 K and 20 K," *Cryogenics*, **22**:73–80, (1982).

11. W.P. Pratt, Jr., S.S. Rosenblum, W.A. Steyert, and J.A. Barclay, "A continuous demagnetization refrigerator operating near 2 K and a study of magnetic refrigerants." *Cryogenics*, **17**:689–693, (1977).

12. T. Hashimoto, T. Numazawa, Y. Watanabe, A. Sato, H. Nakagome, O. Horigami, S. Takayama, and M. Watanabe, "The magnetic refrigeration characteristics of several magnetic refrigerants below 20 K: I. Magnetocaloric effects," *Proc. 9th Intl. Cryogenic Engineering Conference*, p. 26, (1982).

13. T. Numazawa, Y. Watanabe, T. Hashimoto, A. Sato, H. Nakagome, O. Horigami, S. Takayama, and M. Watanabe, "The magnetic refrigeration characteristics of several magnetic refrigerants below 20 K: II. Thermal properties," *Proc. 9th Intl. Cryogenic Engineering Conference*, p. 30, (1982).

14. Barclay and Steyert, p. 77.

15. Carl P. Taussig, "Magnetically Active Regeneration," MIT Ph.D. Thesis, 1986.

16. Warren M. Rohsenow and Harry Y. Choi, *Heat, Mass, and Momentum Transfer*, Prentice-Hall, Englewood Cliffs, New Jersey, 1975.

17. R.A. Fisher, G.E. Brodale, E.W. Hornung, and W.F. Giauque, "Magnetothermodynamics of gadolinium gallium garnet. I. Heat capacity, entropy, magnetic moment from 0.5 to 4.2 K, with fields to 90 kG along the [100] axis," *J. Chem. Phys.*, **59**:4652 (1972).

18. *Ibid.*

19. E.W. Hornung, R.A. Fisher, G.E. Brodale, and W.F. Giauque, "Magnetothermodynamics of gadolinium gallium garnet. II. Heat capacity, entropy, magnetic moment from 0.5 to 4.2 K, with fields to 90 kG along the [111] axis," *J. Chem. Phys.*, **61**:282 (1974).

20. G.E. Brodale, E.W. Hornung, R.A. Fisher, and W.F. Giaque, "Magnetothermodynamics of gadolinium gallium garnet. III. Heat capacity, entropy, magnetic moment from 0.5 to 4.2 K, with fields to 90 kG along the [110] axis," *J. Chem. Phys.*, **62**:4041 (1975).

21. T. Hashimoto, personal communication to Y. Iwasa from S. Kuriyama of Toshiba Corporation. Data collected by Hashimoto at Tokyo Institute of Technology.

22. W.P. Wolf, M. Ball, M.T. Hutchings, M.J.M. Leask, and A.F.G. Wyatt, "The Magnetic Properties of Rare Earth Ions in Garnets," *Journal of the Physical Society of Japan*, **17**, Supplement B-I (1962).

23. B.I. Bleaney and B. Bleaney, *Electricity and Magnetism*, Oxford University Press, London, 1976.

24. *Ibid.*

25. R.A. Fisher *et al.*

26. J.A. Barclay and W.A. Steyert, "Materials for magnetic refrigeration between 2 K and 20 K, *Cryogenics*, **22**:73 (1982).

27. R.A. Fisher *et al.*

28. Barclay, *et. al.*

29. Robert W. Hornbeck, *Numerical Methods*, Prentice-Hall, Inc., New Jersey, 1975.

30. B. Daudin, R. Lagnier, and B. Salce, "Thermodynamic properties of the gadolinium gallium garnet, $Gd_3Ga_5O_{12}$ between 0.05 and 25 K," *Journal of Magnetism and Magnetic Materials*, **27**:315–322, (1982).

31. Gregg E. Childs, Lewis J. Fricks, and Robert L. Powell, *Thermal Conductivity of Solids at Room Temperature and Below*, National Bureau of Standards, Boulder, CO, 1973.

Bibliography

Angus, S. and K.M. deReuck, eds. *International Thermodynamic Tables of the Fluid State Helium-4*. New York: Pergamon Press, 1977.

Barclay, J.A., W.F. Stewart, W.C. Overton, R.J. Candler, and O.D. Harkleroad. "Experimental results on a low-temperature magnetic refrigerator for helium liquefaction." *Advances in Cryogenic Engineering.* **31**:743–752 (1985).

Barclay, J.A. and W.A. Steyert. "Materials for magnetic refrigeration between 2 K and 20 K. *Cryogenics.* **22**:73 (1982).

Bleaney, B.I. and B. Bleaney, *Electricity and Magnetism.* London: Oxford University Press, 1976.

Brodale, G.E., E.W. Hornung, R.A. Fisher, and W.F. Giauque. "Magnetothermodynamics of gadolinium gallium garnet. III. Heat capacity, entropy, magnetic moment from 0.5 to 4.2 K, with fields to 90 kG along the [110] axis." *J. Chem. Phys.* **62**:4041 (1975).

Brown, G.V. "Magnetic heat pumping near room temperature." *Journal of Applied Physics* **47**:73–80 (1982).

Callaway, Joseph. *Quantum Theory of the Solid State: Part A.* New York: Academic Press, 1974.

Childs, Gregg E., Lewis J. Ericks, and Robert L. Powell. *Thermal Conductivity of Solids at Room Temperature and Below.* Boulder, CO: National Bureau of Standards, 1973.

Daudin, B., R. Lagnier, and B. Salce. "Thermodynamic properties of the gadolinium gallium garnet, $Gd_3Ga_5O_{12}$ between 0.05 and 25 K." *Journal of Magnetism and Magnetic Materials.* **27**:315–322 (1982).

Delpeuch, C., R. Béranger, G. Bon Mardion, G. Claudet, and A.A. Lacaze. "Double acting reciprocating magnetic refrigerator: first experiments." *Cryogenics.* **21**:579–584 (1981).

Fisher, R.A., G.E. Brodale, E.W. Hornung, and W.F. Giauque. "Magnetothermodynamics of gadolinium gallium garnet. I. Heat capacity, entropy, magnetic moment from 0.5 to 4.2 K, with fields to 90 kG along the [100] axis." *J. Chem. Phys.* **59**:4652 (1972).

Giauque, W.F., and D.P. MacDougall. "Attainment of temperatures below 1 ° absolute by demagnetization of $Gd_2(SO_4)_3 \cdot 8H_2O$." *Phys. Rev.* **43**:768 (1933).

Hashimoto, T. Personal communication to Y. Iwasa from S. Kuriyama of Toshiba Corporation. Data collected by Hashimoto at Tokyo Institute of Technology.

Hashimoto, T., T. Numazawa, Y. Watanabe, A. Sato, H. Nakagome, O. Horigami, S. Takayama, and M. Watanabe. "The magnetic refrigeration characteristics

of several magnetic refrigerants below 4 K: I. Magnetocaloric effects." *Proc. 9th Intl. Cryogenic Engineering Conference.* p. 26 (1982).

Heer, C.V., C.B. Barnes, and J.G. Daunt. "The design and operation of a magnetic refrigerator for maintaining temperatures below 1° K." *Rev. Sci. Inst.* **25**:1088 (1954).

Hornbeck, Robert W. *Numerical Methods.* Englewood Cliffs: NJ, 1977.

Hornung, E.W., R.A. Fisher, G.E. Brodale, and W.F. Giauque. "Magnetothermodynamics of gadolinium gallium garnet. II. Heat capacity, entropy, magnetic moment from 0.5 to 4.2 K, with fields to 90 kG along the [111] axis." *J. Chem. Phys.* **61**:282 (1974).

Lacaze, A.F., R. Béranger, G. Bon Mardion, G. Claudet, and A.A. Lacaze. "Efficiency improvements of a double acting reciprocating magnetic refrigerator." *Cryogenics.* **23**:427-436 (1983).

Mendelssohn, K. *The Quest for Absolute Zero; the meaning of low temperature physics.* London: Taylor & Francis, Ltd., 1977.

Nakagome, H., T. Kuriyama, H. Ogiwara, T. Fujita, T. Yazawa, and T. Hashimoto. 'Reciprocating magnetic refrigerator for helium liquefaction." *Advances in Cryogenic Engineering.* **31**:753–762 (1985).

Numazawa, T., Y. Watanabe, T. Hashimoto, A. Sato, H. Nakagome, O. Horigami, S. Takayama, and M. Watanabe. " The magnetic refrigeration characteristics of several magnetic refrigerants below 20 K: II. thermal properties." *Proc. 9th Intl. Cryogenic Engineering Conference.* p. 30 (1982).

Pratt, W.P., Jr., S.S. Rosenblum, W.A. Steyert, and J.A. Barclay. "A continuous demagnetization refrigerator operating near 2 K and a study of magnetic refrigerants." *Cryogenics.* **17**:689–693 (1977).

Rohsenow, Warren M. and Harry Y. Choi. *Heat, Mass, and Momentum Transfer.* Englewood Cliffs, NJ: Prentice-Hall, 1975.

Sears, F.W. *An Introduction to Thermodynamics, The Kinetic Theory of Gases, and Statistical Mechanics.* Reading, MA: Addison-Wesley, 1953.

Taussig, Carl P. "Magnetically Active Regeneration." Massachusetts Institute of Technology, Ph.D. Thesis, 1986.

Van Geuns, J.R. "A Study of a New Magnetic Refrigerating Cycle." *Philips Res. Rept. Suppl.* **6** (1966).

Wolf, W.P., M. Ball, M.T. Hutchings, M.J.M. Leask, and A.F.G. Wyatt. "The Magnetic Properties of Rare Earth Ions in Garnets." *Journal of the Physical Society of Japan.* **17** Supplement B-I (1962).